69-11,022

LEVINE, Stanley R., 1942-

THE THERMODYNAMICS OF REFRACTORY METAL SILICIDES BY AN EMF METHOD.

The City University of New York, Ph.D., 1969
Engineering, chemical

University Microfilms, Inc., Ann Arbor, Michigan

THE THERMODYNAMICS OF REFRACTORY METAL SILICIDES BY AN EMF METHOD

by

STANLEY R. LEVINE

A dissertation submitted to the Graduate Faculty in Engineering in partial fulfillment of the requirements for the degree of Doctor of Philosophy, The City University of New York.

1968

This manuscript has been read and accepted for the Graduate Faculty in Engineering in satisfaction of the dissertation requirement for the degree of Doctor of Philosophy.

November 21, 1968
date

Morris Kolodney
Chairman of Examining Committee

November 21, 1968
date

Executive Officer

R. A. Graff

H. Heideklang

M. Kolodney

J. Morrow

Supervisory Committee

The City University of New York

Acknowledgements

The author gratefully acknowledges and thanks the following people:

The National Aeronautics and Space Administration for their support through NASA Grant 33-013-017 to Professors M. Kolodney and R.A. Graff. The NASA Grant Administrator was Mr. Robert Oldrieve of the Lewis Research Center.

Professor Morris Kolodney of the Department of Chemical Engineering, The City University of New York, who, as my mentor for nearly five years, gave me timely advice and encouragement. Without his guidance this work would have been impossible.

Professor Robert A. Graff of the Department of Chemical Engineering, The City University of New York, for his kind advice.

The entire Shop and Secretarial Staff of the Department of Chemical Engineering, The City University of New York, for their assistance; particularly, Mr. David Marden and Mrs. Norma Cohen.

My colleagues who took an interest in the work and provided a stimulating environment: Mr. George Halbfinger, Mr. Andrew Mueller, Mr. Leon Schwartz and Mr. Frederic Schwettmann.

Abstract

Thoria-yttria electrolytes were employed in solid-state electrochemical cells to obtain free energy of formation data for the tantalum silicides. The cells consisted of a reference electrode, electrolyte and silicide electrode . The cell components were fabricated by cold pressing of powders followed by sintering in vacuum. Reference electrodes were fabricated from metal, metal oxide mixtures having well established thermodynamic properties.

Stable silicide electrodes were selected from the family of possible electrodes by studying their stability at high temperature. The family consists of all reactions of the form:

high silicide → low silicide + silica

low silicide → high silicide + tantala

silicide → tantala + silica

where the tantalum silicides are (highest to lowest): $TaSi_2$, Ta_5Si_3, Ta_2Si, $Ta_{4.5}Si$. The thermal stability study predicted that the following electrodes are stable:

$TaSi_2$, Ta_5Si_3, SiO_2(a) (I)

Ta_5Si_3, Ta_2Si, Ta_2O_5 (II)

Ta_2Si, $Ta_{4.5}Si$, Ta_2O_5 (III)

Ta_5Si_3, SiO_2, Ta_2O_5 (IV)

EMF measurements were made with the following half-cells with respect to an Fe,Fe_xO reference electrode at temperatures ranging from about 800°C to 1100°C:

$$5\ TaSi_2 + 14\ O^{=} = 7\ SiO_2(a) + Ta_5Si_3 + 28e^{-} \quad (V)$$

which corresponds to electrode (I) above,

$$2\ Ta_5Si_3 + 2\ O^{=} = SiO_2(a) + 5\ Ta_2Si + 4e^{-} \qquad (VI)$$

which was predicted to be unstable in the electrode stability study,

$$6\ Ta_2Si + 5\ O^{=} = Ta_2O_5 + 2\ Ta_5Si_3 + 10e^{-} \qquad (VII)$$

which corresponds to electrode (II) above, and

$$4\ Ta_{4.5}Si + 25\ O^{=} = 5\ Ta_2O_5 + 4\ Ta_2Si + 50e^{-} \qquad (VIII)$$

which corresponds to electrode (III) above.

From the data obtained with the above electrodes and corrections for electronic transport (about 1%) the following values for the free energies of formation of the tantalum silicides per gram-atom of silicon at 1300°K were computed:

$$\Delta G_{TaSi_2} = -8.1\ ^{+1.8}_{-3.7}\ \text{kcal.}$$

$$\Delta G_{Ta_5Si_3} = -24 \pm 3\ \text{kcal.}$$

$$\Delta G_{Ta_2Si} = -27.2 \pm 3.1\ \text{kcal.}$$

$$\Delta G_{Ta_{4.5}Si} = -37.3 \pm 7.2\ \text{kcal.}$$

About 45% of the uncertainties listed above are caused by uncertainties in the free energy data for ferrous oxide, tantala and silica. The above data represent a considerable improvement over earlier enthalpy of formation data in terms of accuracy and thermodynamic consistency.

The EMF measurements on the silicide electrodes were difficult because dense silicide electrodes could not be fabricated by cold-pressing and sintering. The resultant electrode porosity coupled with sluggish electrode reactions permitted interference by the inert gas environment in the majority of cells. An improvement in electrode fabrication and the employment of isolated electrodes in future work may result in considerable improvement in the data for the tantalum-silicon and other metal-silicon systems.

Table of Contents

Table of Contents (cont.)

List of Tables

List of Tables (cont.)

List of Figures and Plates

List of Figures and Plates (cont.)

List of Figures and Plates (cont.)

List of Figures and Plates (cont.)

I. INTRODUCTION

At temperatures from 2000°F to 2400°F superalloys are inadequate as structural materials. Therefore, for applications such as high-temperature furnace parts and turbine components for the super-sonic transport, interest focuses on the refractory metals which maintain high strength at these temperatures(1,2). However, this class of materials has one serious deficiency - a high affinity for oxygen and nitrogen and the inability to form a protective oxide film at temperatures as low as 1300°F. Columbium and tantalum also suffer hardening and embrittlement by absorption of oxygen and nitrogen on interstitial lattice sites. Alloying does not provide an adequate solution to these problems. Therefore, protective coatings are required to prevent or sufficiently inhibit the ingress of oxygen and nitrogen to the underlying refractory metal substrate and to thereby make the lifetime of a component long enough for practical employment. The coating protects the substrate via its oxidation behavior, that is, by forming a dense, adherent oxide film with a high resistance to oxygen diffusion. The coating systems showing the most promise are based on silicides or aluminides which oxidize to form silica and alumina respectively - both highly resistant to the diffusion of oxygen. Furthermore, these coatings are potentially self-healing; they act as reservoirs of silicon or aluminum so that perforations in the oxide are sealed by the formation of new oxide. The silicides are of particular interest in this study.

Silicide based protective coatings are applied to the substrate by a number of techniques such as vapor deposition, slurry spraying and pack cementation. From a practical viewpoint the coating application technique is of considerable

importance. Such physical and mechanical properties as melting point, coefficient of thermal expansion and modulus of elasticity need to be considered. In addition, the self-healing ability of the coating and its interaction with the substrate are important.

For silicide coatings the desired protective reaction is of the form:

$$R_xSi_y + O_2 \rightarrow SiO_2 + R_xSi_{y-1} \qquad (1)$$

while reactions of the form:

$$R_xSi_y + (x + y)O_2 \rightarrow xRO_2 + ySiO_2 \qquad (2)$$

are undesirable since the refractory metal oxide generally interferes with the formation of a glassy silica film. However, formation of the refractory metal oxide is tolerable where SiO_2 and RO_2 form a glass or where RO_2 is volatile(3,4). The latter situation occurs with $MoSi_2$(4,5). In order to predict and understand the oxidation behavior of refractory metal silicides accurate free energy of formation data are required for the silicides and their oxidation products. Data for silica and for the refractory metal oxides are available(6). Data for silicides are scanty.

Free energy of formation data are available only for some of the rhenium silicides(7). For most other refractory metal silicides only enthalpies of formation are available. The entropy of formation of Mo_3Si was found to be -0.2eu at 298°K(8). If the Neumann-Kopp rule is invoked we have

$$\Delta C_p \approx 0 \qquad (3)$$

$$\Delta S_f^\circ \approx 0 \qquad (4)$$

and

$$\Delta G_T^\circ \approx \Delta H_{298}^\circ \qquad (5)$$

for the entropy and free energy of formation of the silicides from the pure solid elements. The available enthalpy of formation data are of little use in many instances because of their poor precision. Predictions made with these data are frequently ambiguous as will be evident later. All of the available data have been collected by three classical techniques which will be discussed below with particular emphasis placed on the data for the tantalum silicides.

Brewer and Krikorian(9) determined limits for the stability of some refractory metal silicides by direct reaction of the compounds with carbides and nitrides. The products of the reaction were analyzed by X-ray diffraction and limits on the enthalpy of formation were computed based on the spontaneity of the reactions. This technique can give narrow limits in some cases, but in general the range of enthalpies is large.

Robins and Jenkins(10) determined the heats of formation of some transition metal silicides by directly measuring the heat evolved during formation of the compounds from the elements. A bar composed of the elements in the proper proportions is placed in a calorimeter and heated at one end by a coil to cause ignition. The reaction is self-propagating. In some cases a thermit pellet had to be placed in contact with the bar to cause ignition. The heat of formation of the silicide can be calculated from the measured temperature rise and corrections for the contritutions due to the heater and thermit pellet. The precision of the measurements is about ±3%.

In the third technique, employed by Searcy and coworkers (11,12,13), the dissociation pressure of silicon over the

silicide of interest is measured by the Knudsen effusion method. The vapor pressure data may be analyzed by either a Second or Third Law approach. In the former, the heat of dissociation is determined from a plot of -RlnP vs 1/T. From the slope and the heat of sublimation of silicon one can calculate the enthalpy of formation of the silicide. In the Third Law method the vapor pressure data are combined with the estimated values for $(F^{\circ} - H^{\circ}_{298})/T$ for crystalline and gaseous silicon and with the heat of sublimation of silicon to obtain enthalpies of formation for the silicides.

Data for the tantalum silicides, obtained by the three techniques discussed above, are presented in Table I. The values in column IV are based on an average of the Second and Third Law techniques using a value of -112 Kcal. for the heat of sublimation of silicon at 298°K. The values in column V are based on the same vapor pressures as column IV but an improved value of the heat of sublimation of silicon (-108.4 kcal. at 298°K) was used and the calculations were made using only the Third Law method(14,15). The Third Law method is generally more reliable than the Second Law method. In Table I the "confidence" intervals in columns III, IV, and V range from ±4% to ±40% with ±15% being close to average. Therefore, the classical methods which have been employed in thermodynamic measurements on the refractory metal silicides do not give results that are as good as one might desire.

TABLE I

ENTHALPY OF FORMATION DATA FOR THE TANTALUM SILICIDES

ΔH kcal/g-atom of silicon

I Compound	II Brewer and Krikorian(9) ΔH°_{298}	III Robins and Jenkins(10) ΔH°_{T}	IV Myers and Searcy(11) ΔH°_{298}	V Searcy and Finnie(14) ΔH°_{298}
$TaSi_2$	-12.8 to -32.3	-13.9 ± 1	-11.6 ± 5	-12 ± 3
Ta_5Si_3	-20 to -77.2	-25.3 ± 1	-26.7 ± 5	-24 ± 4
Ta_2Si	-20 to -90.1	---	-29.3 ± 5	-30.2 ± 4
$Ta_{4.5}Si$	<-20	---	-34.4 ± 5	-35.8 ± 4

In this work a fourth method was applied to the determination of the free energy of formation of the tantalum silicides for the first time. This technique employs solid oxide electrolytes to establish the difference in oxygen partial pressure between a silicide electrode and a reference electrode. The reference electrode is fabricated from an intimate mixture of a metal and its oxide with well known thermodynamic properties. The silicide electrode consists of a silicide pair and an oxide. A typical formulation for such a cell might be:

$$Pt/RSi_x, RSi_y, SiO_2//\text{oxide electrolyte}//M, MO/Pt, \quad (6)$$

with the cell reaction:

$$2MO + wRSi_x \rightarrow 2M + SiO_2 + zRSi_y \quad (7)$$

In order to determine individual values for the free energy of formation of all the tantalum silicides four such cells must be examined. The potential accuracy and precision of this method is good and it can be readily extended to other silicide families once its value is established.

II. Application of the EMF Method to the Tantalum-Silicon System.

A. The Tantalum-Silicon System.

Before discussing the EMF method, a survey of the tantalum-silicon system is in order. The available thermodynamic data have already been discussed. Tantalum and silicon form four compounds according to the phase diagram shown in Samsonov(16) and reproduced in Figure 1.

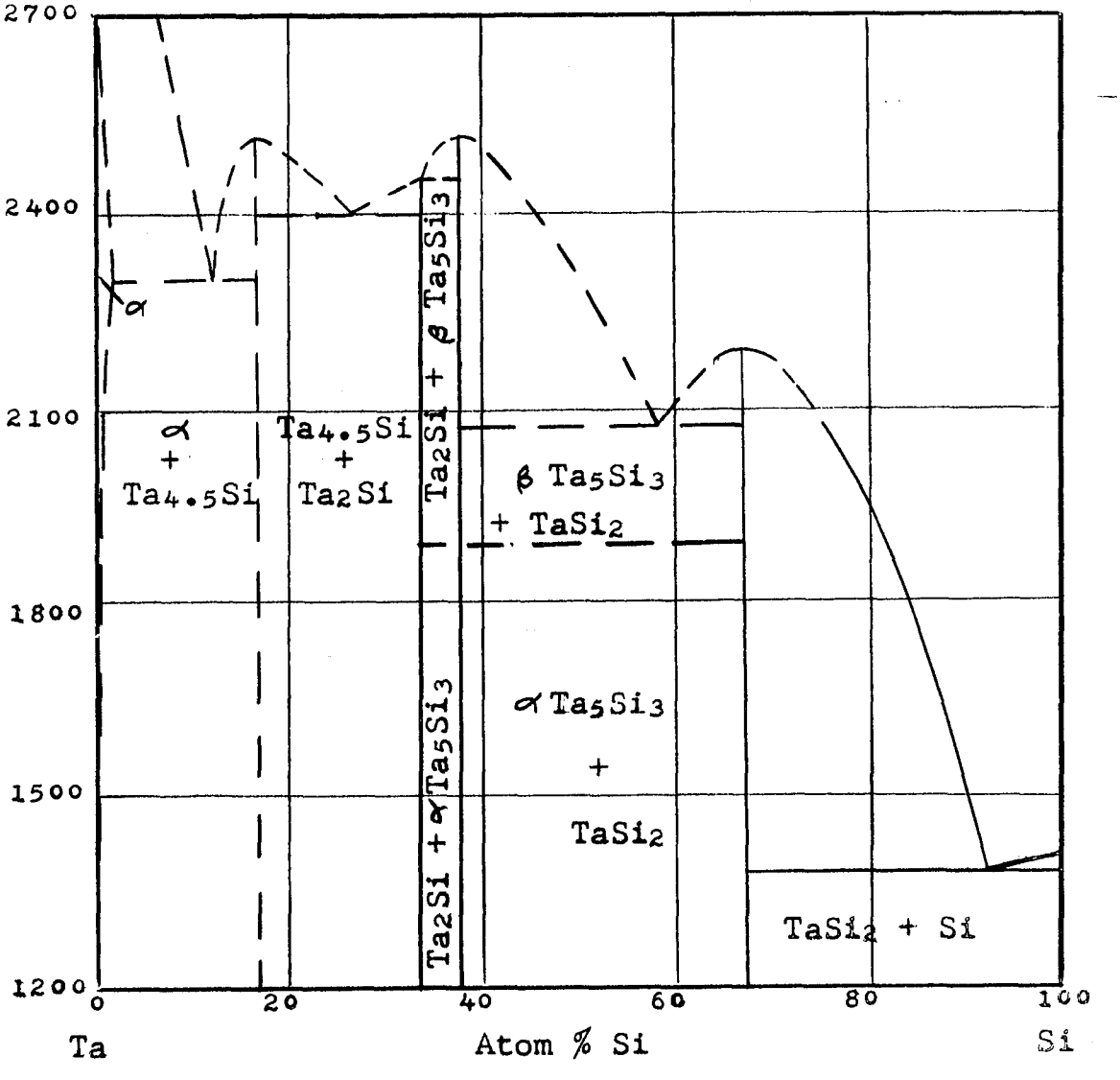

FIGURE 1. Tantalum-silicon System.

Tantalum disilicide was first identified by Honigschmid(17). The other compounds were identified as $Ta_{4.5}Si$, Ta_2Si, and Ta_5Si_3(18,19). Brewer et. al.(18) synthesized the compounds directly from the elements in an argon atmosphere and identified the lower silicides as $TaSi_{0.6}$ $TaSi_{0.4 \pm 1}$, and $TaSi_{0.2 \pm 0.05}$ by X-ray diffraction. Nowotny et. al.(19) identified essentially the same compounds by X-ray diffraction and also by microscopy. A melting point study was conducted by Kiefer et. al.(20) and the results were used to construct the liquidus curve from Ta up to Ta_5Si_3 on the phase diagram of Figure 1. Melting points for the eutectics were determined by Brewer and coworkers(19). The melting points of Ta_5Si_3 and $TaSi_2$ were also determined by Geach and Jones(21) and their results were used in the phase diagram for these compounds and also to modify the results of Kiefer et. al. in the silicon-rich region. Schubert et. al.(22) found a phase with the composition Ta_3Si. Goldschmidt et. al.(23) reported that Ta_3Si is the lowest silicide and that $Ta_{4.5}Si$ and Ta_2Si are impurity stabilized phases. In addition Goldschmidt reported the limits of solubility of silicon in tantalum. The maximum solubility is 2.25 atom % at the eutectic temperature of Ta - "$Ta_{4.5}Si$", 2310°C. Tantalum is not soluble in silicon(24). Homogeneity ranges for the tantalum silicides have not been established. Berezhnoi(24) states that $Ta_{4.5}Si$ exists over the range Ta_5Si to Ta_4Si and that Ta_2Si has a very narrow region of homogeneity. Brewer et. al.(18) found no shifting of the lines from one sample to another in their X-ray studies of the silicides. This indicates that the homogeneity ranges are small. On the other hand, Alyainovskii et. al. (25) report

that Nb_5Si_3 and $NbSi_2$ have large homogeneity ranges. The former exists from $Nb_5Si_{2.9}$ to $Nb_5Si_{3.3}$ while the latter exists from $NbSi_{1.85}$ to $NbSi_{2.2}$. Since there is a great deal of similarity between the niobium-silicon and tantalum-silicon systems, a broad homogeneity range for the higher tantalum silicides should not be ruled out.

X-ray data for the tantalum silicides are reported by Brewer et. al(18), Nowotny et. al.(19), and Wallbaum(26). $TaSi_2$ is reported to be hexagonal by Wallbaum. Nowotny reports that Ta_5Si_3 and $Ta_{4.5}Si$ have hexagonal crystal structures and that Ta_2Si is tetragonal. Knapton(27) and Parthé et. al.(28,29) report that hexagonal Ta_5Si_3 is an impurity-stabilized phase and that Ta_5Si_3 is actually tetragonal as a pure binary phase in the absence of carbon, nitrogen, and oxygen. Parthé reports that Ta_5Si_3 transforms from a low-temperature tetragonal form to a high-temperature tetragonal form.

In conclusion, it is fair to say that at this time there is still controversy about the nature of the lowest silicides and the crystallography of Ta_5Si_3(30). Evidently, in the presence of impurities such as carbon, nitrogen, oxygen, or boron, $Ta_{4.5}Si$, Ta_2Si, and Ta_5Si_3 in a hexagonal and tetragonal modification are formed. In the absence of impurities Ta_3Si may be the lowest silicide with Ta_2Si absent and Ta_5Si_3 existing in only one or two tetragonal modifications.

The tantalum silicides can be synthesized by a number of methods(24,30,31). The most important is direct reaction between the elements in vacuo or an inert atmosphere. Other techniques such as alumino-thermic reduction of the oxides

or reaction between the oxides and carbon tend to give contaminated products. Formation of the silicides by reaction with silane has the disadvantage of being diffusion-limited and offering an unnecessarily complicated procedure for most applications as compared with synthesis by direct reaction of the elements. Electrolysis schemes also offer no advantage over direct reaction. The factors to be considered during synthesis of the silicides directly from the elements are the purity of the reactants, contamination and silicon loss during synthesis, and the homogeneity of the products.

The tantalum silicides are generally inert to reagents except for HF and fused alkalis. Although the higher silicides are resistant to oxidation, the compounds low in silicon are not. The silicides have a metallic luster and are metallic conductors of electricity. However, they are hard, brittle, and melt at high temperatures. The latter properties make this family of materials extremely difficult to fabricate and sinter.

II. B. The EMF Method

The employment of solid electrolytes in the measurement of thermodynamic properties was brought into prominence by Wagner(32), and Schmalzried(33), and others. A typical cell formulation for such a measurement is:

$$A/M,\ MX_m//CX//R,\ RX_n/A \qquad (8)$$

The lead wires are represented by A. M, MX_m is a reference electrode with well established thermodynamic properties and R, RX_n is the electrode under study. CX is an electrolyte which conducts by X^- migration. Anionic conductors are most common although a number of studies have been made with cationic electrolytes. The half-cell reactions are:

$$ne^- + \frac{n}{m} MX_m = \frac{n}{m} M + nX^-$$

$$nX^- + R = RX_n + ne^-$$

and the total reaction is:

$$R + \frac{n}{m} MX_m = \frac{n}{m} M + RX_n \qquad (9)$$

The free energy of the cell reaction is related to the observed voltage by

$$\Delta G_R(T) = -nFE(T) \qquad (10)$$

where $\Delta G_R(T)$ = free energy of reaction at $T^\circ K$, cal.

n = number of equivalents transferred in the reaction

F = the value of the Faraday (23,060 cal/volt-gram-equiv.)

E = observed cell voltage at null current, volts

provided that the following conditions are fulfilled:

The cell reaction is reversible; that is, polarization is zero and current efficiency for the postulated reaction is 100%.

From equations (9) and (10), the free energy of formation of RX_n is:

$$\Delta G^\circ_{RX_n}(T) = \frac{n}{m}\Delta G^\circ_{MX_m}(T) - nFE(T) \qquad (11)$$

The entropy of formation of RX_n is determined from the temperature dependence of the EMF:

$$\Delta S^\circ_{RX_n}(T) = \frac{n}{m}\Delta S^\circ_{MX_m}(T) + nF\frac{\partial E(T)}{\partial T} \qquad (12)$$

Differences in oxygen partial pressure can be conveniently measured with electrochemical cells employing ceramic oxide electrolytes. Oxide electrolytes are binary oxides which conduct essentially only by oxygen ion ($O^{=}$) migration over a given temperature-oxygen partial pressure domain. They will be discussed in detail in a later section. A cell employing an oxide electrolyte may be formulated as:

$$Pt/M, MO//\text{oxide electrolyte}//R, RO/Pt \qquad (13)$$

where the electrode reactions are:

$$R + O^{=} = RO + 2e^-$$

$$2e^- + MO = M + O^{=}$$

The cell reaction is:

$$R + MO = RO + M \qquad (14)$$

and

$$\Delta G(T) = -nFE(T) = \Delta G^{\circ}_{RO}(T) - \Delta G^{\circ}_{MO}(T) \qquad (15)$$

At the electrode-electrolyte interfaces we have equilibrium:

$$G^{\circ}_{RO}(T) - G^{\circ}_{R}(T) - G^{\circ}_{O^{=}}(T) + RT \ln \frac{a_{RO}}{a_R \, a_{O^{=}_{..}}} = 0 \qquad (16)$$

$$G^{\circ}_{M}(T) + G^{\circ}_{O^{=}}(T) - G^{\circ}_{MO}(T) + RT \ln \frac{a_M \, a_{O^{=}_{..}}}{a_{MO}} = 0 \qquad (17)$$

Adding (16) and (17) and combining the appropriate free energies and setting the activities of R, RO, M, MO equal to unity gives:

$$\Delta G^{\circ}_{RO}(T) - \Delta G^{\circ}_{MO}(T) = RT \ln \frac{a_{O^{=}_{..}}}{a_{O^{=}_{.}}} \qquad (18)$$

or

$$E = -\frac{RT}{nF} \ln \frac{a_{O^{=}_{..}}}{a_{O^{=}_{.}}} \qquad (19)$$

For the reaction

$$2e^{-} + \tfrac{1}{2} O_2(g) = O^{=} \qquad (20)$$

one can write

$$-2F\phi + \tfrac{1}{2} G^{\circ}_{O_2}(T) + RT \ln p_{O_2}^{\frac{1}{2}} = -2F\phi + G^{\circ}_{O^{=}}(T) + RT \ln a_{O^{=}} \qquad (21)$$

where $-2F\phi$ is the electrical potential. The electrochemical

potential, $\bar{\mu}$, is the sum of the electrical and chemical potential:

$$\bar{\mu} = qF\phi + \mu$$

Since n = 2, from (21) and (19)

$$E = -\frac{RT}{4F} \ln \frac{p''_{O_2}}{p'_{O_2}} \qquad (22)$$

The object of this study was to determine the free energy of formation of the tantalum silicides by an EMF method employing solid oxide electrolytes. This technique has never been applied to silicides. Furthermore, studies of three phase electrodes $+O_2(g)$ with oxide electrolytes are uncommon. Such electrodes were necessary in this study. The data were obtained by measuring the oxygen partial pressure established at equilibrium over the silicides and their oxidation products. The oxidation products are the oxides of tantalum and silicon. According to Kofstad(34), Ta_2O_5 is the only thermodynamically stable oxide of tantalum. Tantalum pentoxide exists in two configurations: a beta or low temperature form and an alpha or high temperature form. The transition from beta to alpha occurs at about 1320°C. However, the high temperature form has been detected at temperatures as low as 1250°C in oxidation studies(35). Complete thermodynamic data for tantalum pentoxide are available(6). X-ray data can be found in the ASTM file(36). Tantalum pentoxide has a narrow homogeneity range and is an n-type conductor at low oxygen partial pressure(37). The picture for silicon oxide is more complex. First, silicon forms a monoxide, SiO. According to a survey by Toropov and Barzakoskii(38) SiO does not

exist as a solid. Gaseous SiO does not form from Si and SiO_2 below about 1280°C. A silicon sesquioxide has been reported, but satisfactory confirmation has not been obtained. There are no fewer than seventeen crystalline forms of silica and three amorphous forms(39). However, only alpha and beta quartz, tridymite-S and alpha cristobalite are thermodynamically stable at atmospheric pressure. Beta quartz is stable from absolute zero to 573°C. From 573°C to 867°C, alpha quartz is stable. At one atmosphere total pressure, alpha quartz transforms to tridymite-S at 867°C. This phase is stable to 1470°C where alpha cristobalite forms. Alpha cristobalite melts at 1723°C. Tridymite-S has only been produced as the intermediate phase between α-quartz and α-cristobalite in the presence of mineralizers. In the absence of mineralizers α-quartz is stable to 1027°C where it transforms directly to α-cristobalite. The reverse transformations, that is, from α-cristobalite to tridymite-S to α-quartz occur with great difficulty in the absence of mineralizers. Over the temperature range used in this work, the largest difference between the free energies of formation of the stable crystalline forms of silica is 250 calories(6). Amorphous silica is metastable with respect to the crystalline forms (approximately 6 kcal. less stable over the temperature range of interest). However, amorphous silica is almost always the thermal oxidation product of silicon and the silicides. This occurs because the silicon sites in the substrate are more suitably arranged for the formation of an amorphous product, so that geometric considerations prevail. Devitrification is not to be expected at the temperatures used in this study. At 1000°C

crystallization of silica glass proceeds at an inappreciable rate. At 1160°C the process takes about six days while at 1200°C it takes about three days. Alpha cristobalite is usually the product of the devitrification process. Complete thermodynamic data for silica are available(6). X-ray data are found in the ASTM file(36).

As was mentioned earlier, the silicide electrodes are formulated from silicides and the oxidation products. The first step in the development of the method is to list all of the possible half-cell reactions. The two-phase fields in the tantalum-silicon system are, from Figure 1:

$$Si - TaSi_2$$

$$TaSi_2 - Ta_5Si_3$$

$$Ta_5Si_3 - Ta_2Si$$

$$Ta_2Si - Ta_{4.5}Si$$

$$Ta_{4.5}Si - Ta_{\alpha}$$

No useful information can be obtained from the $Si - TaSi_2$ and $Ta_{4.5}Si - Ta_{\alpha}$ phase fields since the oxygen partial pressure in equilibrium with the former is simply the oxygen partial pressure over silica in equilibrium with silicon while the oxygen partial pressure over the latter is essentially equal to the oxygen partial pressure over tantalum in equilibrium with its oxide. The remaining reactions fall into three categories:

(A) electrodes where SiO_2(a) is the oxidation product,

(B) electrodes where $\beta - Ta_2O_5$ is the oxidation product, and

(C) electrodes where the silicide is completely oxidized to SiO_2(a) and $\beta - Ta_2O_5$.

Table II lists all of the possible half-cell reactions. The last two columns show the cell voltages expected if the electrodes of interest are run against an iron, wustite reference electrode. Data for the oxides are from Wicks and Block(6) and enthalpy of formation data for the silicides are taken from Searcy and Finnie(14).

A number of observations about the half-cells in Table II can be made. First, as we proceed from the Ta-rich to the Si-rich end of the phase diagram (Figure 1) the activity of tantalum decreases monotonically and the activity of silicon increases monotonically. The following equations apply to the oxygen partial pressures:

over group A electrodes,

$$-\Delta G^{o}_{SiO_2(a)}(T) = RT \ln \frac{a_{SiO_2(a)}}{a_{Si}\, p_{O_2}} \qquad (23)$$

over group B electrodes,

$$-\Delta G^{o}_{Ta_2O_5}(T) = RT \ln \frac{a_{Ta_2O_5}}{a^2_{Ta}\, p^{5/2}_{O_2}} \qquad (24)$$

In equations (23) and (24) the free energies of formation are fixed and the oxides are at unit activity. Therefore, as we proceed from the Ta-rich to the Si-rich silicides the oxygen partial pressure decreases in group A electrodes where SiO_2(a) is the oxidation product and increases in group B electrodes where β-Ta_2O_5 is the oxidation product.

TABLE II

POSSIBLE HALF-CELL REACTIONS AND EXPECTED VALUES

WITH RESPECT TO Fe - Fe_xO at 1000°K and 1300°K

HALF-CELL REACTIONS	(millivolts) EXPECTED VALUES	
	1000°K	1300°K
A. SiO_2(a) IS THE OXIDATION PRODUCT:		
(1) $5\ TaSi_2 + 14\ O^{=} = 7\ SiO_2(a) + Ta_5Si_3 + 28e^-$	634 ±65	613 ±65
(2) $2\ Ta_5Si_3 + 2\ O^{=} = SiO_2(a) + 5\ Ta_2Si + 4e^-$	895 ±477	870 ±477
(3) $9\ Ta_2Si + 10\ O^{=} = 5\ SiO_2(a) + 4\ Ta_{4.5}Si + 20e^-$	433 ±113	409 ±113
B. β-Ta_2O_5 IS THE OXIDATION PRODUCT:		
(4) $4\ Ta_5Si_3 + 35\ O^{=} = 7\ Ta_2O_5 + 6\ TaSi_2 + 70e^-$	548 ±52	528 ±52
(5) $6\ Ta_2Si + 5\ O^{=} = Ta_2O_5 + 2\ Ta_5Si_3 + 10e^-$	475 ±208	457 ±208
(6) $4\ Ta_{4.5}Si + 25\ O^{=} = 5\ Ta_2O_5 + 4\ Ta_2Si + 50e^-$	617 ±28	598 ±28
(C) COMPLETE OXIDATION TO SiO_2(a) AND β-Ta_2O_5:		
(7) $2\ TaSi_2 + 13\ O^{=} = Ta_2O_5 + 4\ SiO_2(a) + 26e^-$	603 ±20	580 ±20
(8) $2\ Ta_5Si_3 + 37\ O^{=} = 5\ Ta_2O_5 + 6\ SiO_2(a) + 74e^-$	577 ±14	556 ±14
(9) $Ta_2Si + 7\ O^{=} = Ta_2O_5 + SiO_2(a) + 14e^-$	565 ±13	543 ±13
(10) $4\ Ta_{4.5}Si + 53\ O^{=} = 9\ Ta_2O_5 + 4\ SiO_2 + 106e^-$	590 ±7	570 ±7

Since the oxygen partial pressure over Fe, Fe_xO is fixed at a given temperature one can conclude, in the light of equation (22), that within group A in Table II the observed EMFs must be in the order

$$E(TaSi_2,Ta_5Si_3,SiO_2(a)) > E(Ta_5Si_3,Ta_2Si,SiO_2(a)) > E(Ta_2Si,Ta_{4.5}Si,SiO_2(a)) \quad (25)$$

Similarly the EMFs observed for group B must be in the order

$$E(TaSi_2Ta_5Si_3,Ta_2O_5) < E(Ta_5Si_3,Ta_2Si,Ta_2O_5) < E(Ta_2Si,Ta_{4.5}Si,Ta_2O_5) \quad (26)$$

Examination of Table II and the above inequalities, (25) and (26), clearly shows the shortcomings of the available data.

Under ideal conditions, reaction kinetics should play no role in the EMF measurements. Hence, reaction (6) should occur to the exclusion of reaction (3). Also, reaction (1) should occur in preference to reaction (4) and reaction (2) should occur in preference to reaction (5). The prediction for the first pair can be confirmed and the picture for the latter pairs can be more clearly established by determining the thermal stability of the various electrodes. This can be accomplished by bringing a silicide pair and the appropriate oxides to equilibrium at an elevated temperature and determining the phases present by X-ray diffraction. The detection of SiO_2 by X-ray diffraction is difficult in the presence of the silicides. However, changes in the quantity of the silicides and Ta_2O_5 can be detected and it is on this

basis that the results of the electrode stability studies were evaluated. Further details of the electrode stability studies will be presented in a later section. The calculated free energies of reaction at 1700°K for this study are presented in Table III. These calculations are based on the enthalpy of formation data of Searcy and Finnie(14). Data for the oxides were taken from Wicks and Block(6). Based on the available data the only electrode which is clearly stable is Ta_2Si, $Ta_{4.5}Si$, Ta_2O_5. The experimental electrode stability study confirmed this and also showed that $TaSi_2$, Ta_5Si_3, SiO_2(a) is a stable electrode. The thermal stability study also showed that Ta_5Si_3, Ta_2Si, Ta_2O_5 is a stable electrode. At this point, half-cells (2), (3), and (4) in Table II may be eliminated as possibilities.

In category C of Table II, complete oxidation reactions, only one of the reactions can occur. This can be shown by again considering equations (23) and (24). Since only one oxygen partial pressure is permitted over an electrode, p_{O_2} can be eliminated between the equations and the required relationship between Ta and Si activity can be computed:

$$\ln \frac{a_{Si}}{a_{Ta}^{4/5}} = \frac{\Delta G^\circ_{Si\,O_2(a)}(T) - \frac{2}{5}\Delta G^\circ_{Ta_2O_5}(T)}{RT} \qquad (27)$$

At 1300°K

$$\ln \frac{a_{Si}}{a_{Ta}^{4/5}} = -2.49 \qquad (28)$$

TABLE III

CALCULATIONS OF ELECTRODE STABILITY

	REACTION	ΔG (kcal)
$\frac{37}{7}$	$TaSi_2 + 2\ Ta_2O_5 = 5\ SiO_2(a) + \frac{13}{7}\ Ta_5Si_3$	-33 ± 54
14	$Ta_5Si_3 + 2\ Ta_2O_5 = 5\ SiO_2(a) + 37\ Ta_2Si$	-136 ± 316
$\frac{53}{5}$	$Ta_2Si + 2\ Ta_2O_5 = 5\ SiO_2(a) + \frac{28}{5}\ Ta_{4.5}Si$	$+94 \pm 64$

or

$$\frac{a_{Si}}{a_{Ta}^{4/5}} = 0.083 \qquad (29)$$

This can be true for only one silicide. The electrode stability study showed that Ta_2Si, $Ta_{4.5}Si$, β-Ta_2O_5; Ta_5Si_3, Ta_2Si; β-Ta_2O_5 and $TaSi_2$, Ta_5Si_3, SiO_2(a) are stable electrodes (i.e. the oxidation of $TaSi_2$ yields Ta_5Si_3 and SiO_2(a); the oxidation of Ta_2Si yields Ta_5Si_3 and Ta_2O_5, and the oxidation of $Ta_{4.5}Si$ yields Ta_2Si and Ta_2O_5). Therefore, the complete oxidation reaction should be possible only for Ta_5Si_3. Half-cells (7), (9), and (10) of Table II are eliminated.

At this point, an examination of a plot of enthalpy of formation per gram-atom of silicon against composition is instructive. The graph, Figure 2, indicates that there is an inconsistency in the data for Ta_2Si, Ta_5Si_3, and $TaSi_2$ based on mean values. The mean for Ta_5Si_3 should fall below the line connecting the mean for Ta_2Si and $TaSi_2$. It does not. From the graph, "activities" of silicon and tantalum were calculated and they were used to compute a_{Si}/a_{Ta} 4/5. For the $Ta_{4.5}Si$ - Ta_2Si phase field this ratio attains a possible maximum value of 0.0183. For the Ta_5Si_3 - $TaSi_2$ phase field the ratio ranges from 0.027 to 114 with a mean of 1.68. These values are to be compared to the calculated value of 0.083 for the complete oxidation reaction at 1300°K. This lends support to the observations made in the electrode stability study. Further calculations were not worth while in view of the inconsistent data.

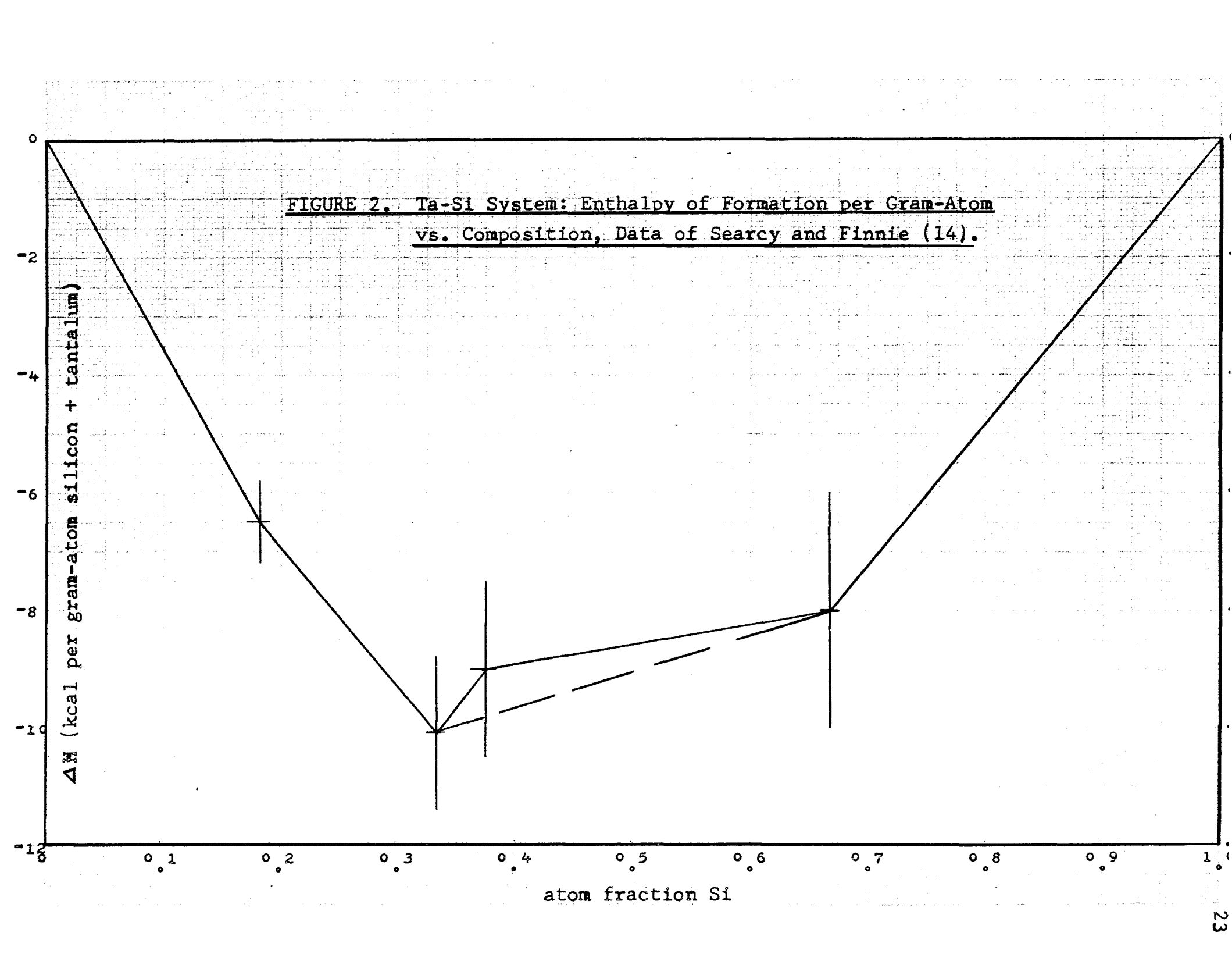

FIGURE 2. Ta-Si System: Enthalpy of Formation per Gram-Atom vs. Composition, Data of Searcy and Finnie (14).

In summary, the following electrodes provide possible reactions:

	Designation in Table II
$TaSi_2$, Ta_5Si_3, SiO_2(a)	(1)
Ta_5Si_3, Ta_2Si, SiO_2(a)	(2)
and/or	
Ta_5Si_3, Ta_2Si, β-Ta_2O_5	(5)
Ta_2Si, $Ta_{4.5}Si$, β-Ta_2O_5	(6)
Ta_5Si_3, SiO_2(a), β-Ta_2O_5	(8)

Electrodes (2) and (5) are mutually exclusive under ideal conditions. However, ideal behavior will not necessarily be observed. If the EMF difference between electrodes (2) and (5) is small, then kinetic influences can be expected to determine which reaction occurs.

It will now be shown that the above electrodes can yield the individual free energies of formation of the tantalum silicides. First, only one degree of freedom exists, so that the oxygen partial pressure over each electrode is fixed at constant temperature. This follows from application of the phase rule. The electrolyte may be

regarded as a source of oxygen at the equilibrium partial pressure. Then, in each case in Table II there are three solid phases and one gas phase. There are also four chemical species and one independent reaction; that is, the electrode reaction with $\frac{1}{2}O_2(g)$ substituted for $O^=$ and e^- eliminated. Then, from the phase rule, the number of degrees of freedom, f, is one.

$$f = N - R - P + 2 \qquad (30)$$

$$f = 4 - 1 - 4 + 2 = 1$$

With one degree of freedom, the temperature may be selected and the oxygen partial pressure will thereby be fixed.

For each of the possible electrodes the following equations relate the free energies of formation of the compounds involved to the observed voltages. EMFs are labeled according to the reaction as designated in Table II.

$$5\Delta G^\circ_{TaSi_2}(T) - \Delta G^\circ_{Ta_5Si_3}(T) = n_1 F E_1(T) + 7\Delta G^\circ_{Si O_2(s)}(T) - 14\Delta G^\circ_{FeO}(T) \quad (1)$$

$$2\Delta G^\circ_{Ta_5Si_3}(T) - 5\Delta G^\circ_{Ta_2Si}(T) = n_2 F E_2(T) + \Delta G^\circ_{Si O_2(s)}(T) - 2\Delta G^\circ_{FeO}(T) \quad (2)$$

$$6\Delta G^\circ_{Ta_2Si}(T) - 2\Delta G^\circ_{Ta_5Si_3}(T) = n_5 F E_5(T) + \Delta G^\circ_{Ta_2O_5}(T) - 5\Delta G^\circ_{FeO}(T) \quad (5)$$

$$4\Delta G^\circ_{Ta_{4.5}Si}(T) - 4\Delta G^\circ_{Ta_2Si}(T) = n_6 F E_6(T) + 5\Delta G^\circ_{Ta_2O_5} - 25\Delta G^\circ_{FeO}(T) \quad (6)$$

$$2\Delta G^{\circ}_{Ta_5Si_3}(T) = n_8 F E_8(T) + 5\Delta G^{\circ}_{Ta_2O_5}(T) + 6\Delta G^{\circ}_{SiO_{2(c)}}(T) - 37\Delta G^{\circ}_{FeO}(T) \quad (8)$$

In writing the above equations it was assumed that the homogeneity range for each silicide is exceedingly narrow in which case the free energies of formation of the silicides do not vary appreciably from one extreme of the homogeneity range to the other. From the left side of the above equations one can see that successful measurements on reactions (1), (6), (2), and (5), or (1), (6), (2) or (5), and (8) are required to determine all four free energies of formation.

II. C. Oxide Electrolytes

During the past dozen years the literature on solid electrolytes and their employment in thermodynamic measurements and other applications has grown at a rapid pace under the stimulus of an early paper by Kiukkola and Wagner(32). A complete survey will not be presented here, but rather a comprehensive examination of oxide electrolytes, their properties and some of the EMF measurements performed will be presented.

The subject of oxide electrolytes pre-dates Wagner. In 1902 Reynolds(40) investigated the electrolyte 90% ZrO_2 - 10% MgO. Treadwell et. al., 1916(41) employed porcelain as an electrolyte. In 1940 Hauffe(42) used glass as an electrolyte. Wagner(43) gave a correct explanation for the transport mechanism in doped zirconia in 1943. However, it was not until 1956 that Kiukkola and Wagner(32) showed the way by demonstrating that zirconia-15 mole % calcia was an essentially pure ionic conductor over an extended oxygen partial pressure range, and that it could be applied with great success to a variety of thermodynamic investigations. They also found that thoria based electrolytes exhibited electronic conduction at high oxygen partial pressures. Since this work, other oxide electrolytes have been developed. Peters and Mann(44) showed that ThO_2 based electrolytes can be employed in thermodynamic measurements. Dixon et. al.(45) found that ZrO_2-Y_2O_3 was a good electrolyte. Strickler and Carlson(46) investigated ZrO_2 doped with Sc_2O_3, Yb_2O_3, Y_2O_3, Sm_2O_3 and Gd_2O_3. HfO_2-CaO was studied by Johansen and Cleary(47). Steele and Alcock(48) demonstrated that ThO_2-Y_2O_3, ThO_2-La_2O_3 and ThO_2-CaO formed good electrolytes. CeO_2-La_2O_3 was investigated as an electrolyte for fuel cells by Singman(49).

Oxide electrolytes have been fabricated in two ways. The first starts with the aqueous metal nitrates. They are mixed together in the proper proportions and coprecipitated as the oxalates in an ice bath. This is followed by filtration, washing, dehydration and calcination at 900°C for several hours. From this point the first and second methods are the same. In the second method the starting materials are the oxide powders mixed together in the proper proportions. The powder is pressed into the desired shape and fired at 1700 to 2300°C. Starting with the nitrates offers no advantage over fabricating directly from the oxides in terms of purity of the final product. Where the oxides and nitrates are both available at comparable purity starting with the oxides is preferable. The sintered electrolytes can be produced with densities approaching 100% of theoretical. Density is an important consideration since the electrolytes must be gas-tight. The color of sintered thoria-yttria electrolytes varies from a reddish-brown to white. Zirconia-calcia electrolytes can be produced in colors ranging from tan to white. The color of the electrolytes depends upon the oxygen content of the sintering atmosphere. Electrolytes are white in the stoichiometric condition. Electrolytes that are hyperstoichiometric with respect to oxygen are colored. This occurs by dissolution of excess oxygen with the creation of electron holes. Coloring can also be produced by gamma radiation. The radiation damage process is reversible. However it is undesirable because the defects produced cause electronic conduction.

All of the oxide electrolyte systems are similar in several respects. The pure oxides ZrO_2, ThO_2, HfO_2, and CeO_2

are refractory oxides with extremely large free energies of formation. As pure materials they are mixed conductors of electricity(48). The principal conducting species are either positive holes or excess electrons and oxygen ions depending on the oxygen partial pressure. The ionic transport numbers (the fraction of the conductivity attributable to ions) are relatively small except perhaps over a limited intermediate oxygen partial pressure domain(50). The addition of aliovalent cations such as Ca^{+2} or Y^{+3} greatly enhances the ionic conductivity and has little or no effect on p and n-type conduction. The net effect is an essentially pure ionic conductor. It has been shown by lattice parameter, density and X-ray diffraction intensity measurements(51) that for ZrO_2-CaO the Ca^{+2} substitute for Zr^{+4}. To maintain electroneutrality an equivalent number of oxygen lattice sites are left vacant. The same substitution of the dopant cation for the host occurs in the other oxide electrolyte systems. The electrolytes all have the cubic fluorite crystal structure. In hafnia and zirconia this structure is produced by the aliovalent addition. A minimum addition for each dopant is required before a solid solution with the fluorite structure is formed. ThO_2 has the fluorite structure to begin with. The partial phase diagrams, Figure 3, illustrate the ThO_2-Y_2O_3 and ZrO_2-CaO systems.

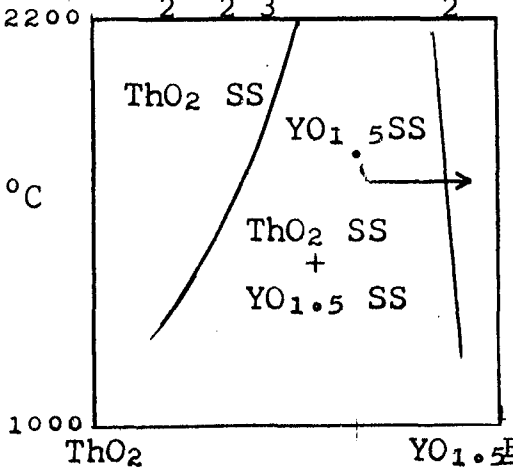

PHASE DIAGRAM, $ThO_2.Y_2O_3$(52)

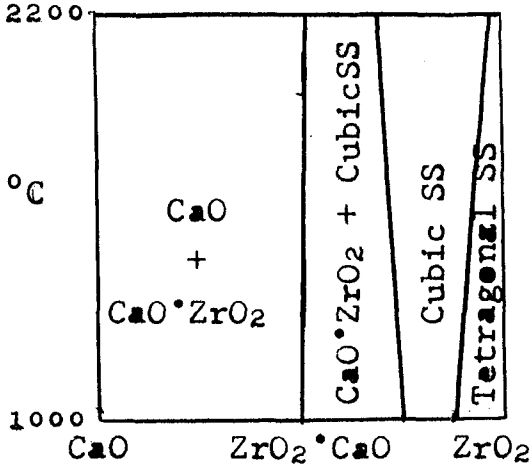

PHASE DIAGRAM, $ZrO_2.CaO$(53)

Figure 3

The effect of doping was clearly demonstrated by Kiukkola and Wagner(32). The conductivity of a particular species σ_i, is given by

$$\sigma_i = C_i q_i \mu_i \tag{31}$$

and the total conductivity σ_T is

$$\sigma_T = \sum_i \sigma_i \tag{32}$$

The terms in the above equations are defined as follows:

σ_i is the conductivity due to the i^{th} species, mho-cm^{-1}

C_i is the concentration of the i^{th} species, particles/cm^3

q_i is the charge on the i^{th} species, coulombs/particle

μ_i is the mobility of the i^{th} species, cm^2/volt-sec.

The concentration of oxygen vacancies, $V_O^=$, is governed by the concentration of the dopant cation. The concentrations of the other conducting species are governed by equilibria between oxygen gas and the electrolyte. At low oxygen partial pressure, oxygen ions on lattice sites, $O^=$, are lost to the gas phase with the creation of oxygen vacancies, $V_O^=$, and excess electrons, Θ,:

$$2O^=(lattice) = O_2(g) + 4\Theta + 2V_O^= \tag{33}$$

with

$$K_1' = \frac{(C_{O^=})^2}{P_{O_2}(C_\Theta)^4 (C_{V_O^=})^2} \tag{34}$$

At high oxygen partial pressure oxygen gas dissolves in the electrolyte. The dissolved oxygen occupies vacant oxygen lattice sites, $V_O^=$, and positive holes, $\oplus$, are created:

$$O_2(g) + 2V_O^{=} = 2O^{=}(lattice) + 4\oplus \qquad (35)$$

with

$$K_2' = \frac{(C_{O^{=}})^2 (C_\oplus)^4}{p_{O_2} (C_{V_O^{=}})^2} \qquad (36)$$

Kiukkola and Wagner argued that $C_{O^{=}}$ is essentially constant. Also, as a result of the doping with calcia which introduces one mole of vacant oxygen sites for each mole of Ca^{+2}, $C_{V_O^{=}}$, the concentration of vacant oxygen sites, is also constant. Equations (34) and (36) can therefore be simplified and solved for $C_\ominus$ and $C_\oplus$ respectively:

$$C_\ominus = K_1 p_{O_2}^{-\frac{1}{4}} \qquad (37)$$

$$C_\oplus = K_2 p_{O_2}^{\frac{1}{4}} \qquad (38)$$

and therefore, since $q_i \mu_i$ is constant in equation (31) at constant temperature, the total conductivity equation may be written as:

$$\sigma_T = K_n p_{O_2}^{-\frac{1}{4}} + \sigma_{O^{=}} + K_p p_{O_2}^{\frac{1}{4}} \qquad (39)$$

where subscripts p and n represent the positive hole and excess electron contributions respectively.

An ionic conductor should have a constant value of σ_T at a given temperature independent of oxygen partial pressure since $\sigma_{O^{=}}$ is the largest item on the right hand side of equation (39). Kiukkola and Wagner measured the total

conductivity of ZrO_2-CaO electrolytes with alternating current at 870°C in atmospheres ranging from pure oxygen at one atmosphere to hydrogen at one atmosphere saturated with water at 0°C ($P_{O_2} = 4 \times 10^{-22}$ atm) and found that electronic conduction was insignificant over this range of oxygen partial pressures.

Further evidence in support of the doping mechanism has been accumulated. Independent measurements of oxygen ion diffusivity have shown that it accounts for the observed conductivity(54-5). The diffusivity is related to the conductivity through the Einstein Equation:

$$D_i = \frac{\sigma_T t_i k T}{C_i q_i^2 e^2} \qquad (40)$$

where σ_T = total conductivity, mho-cm^{-1}

t_i = transport number for the i^{th} species

k = Boltzmann constant, erg/°K

T = absolute temperature, °K

e = electronic charge

q_i = charge on the i^{th} species

C_i = concentration of the i^{th} species, particles/cm^3

D_i = diffusivity of the i^{th} species, cm^2/sec

Rhodes and Carter(56) determined that Zr^{+4} and Ca^{+2} diffusion were negligible in ZrO_2-CaO electrolytes.

For equal vacancy concentrations the ionic conductivity is determined by the host lattice(48). A secondary effect is played by the dopant cation. The ionic conductivity varies inversely as the size of the dopant cation at equivalent

vacancy concentration in a particular host lattice(46). The temperature dependence of the conductivity of all species can be adequately represented by Arrhenius-type equations.

The effect of dopant concentration on the ionic conductivity does not follow the simple proportionality of equation (31). In electrolytes based on ZrO_2 and HfO_2, a conductivity maximum occurs at the minimum dopant level required to stabilize the fluorite phase(45). In thoria-based electrolytes the conductivity is directly proportional to the dopant concentration for small additions. The conductivity reaches a maximum for thoria-yttria at 15 mole % $YO_{1.5}$ and for thoria-calcia the maximum occurs at about 8 Mole % CaO(48). Further additions cause the anionic conductivity to diminish. At the ionic conductivity maximum the electronic contributions are at a minimum(48).

Transport numbers for oxide electrolytes are defined as the fraction of total current carried by a particular species. Then, the ionic transport number is:

$$t_{O^=} = \frac{\sigma_{O^=}}{\sigma_T} = \frac{\sigma_{O^=}}{K_p p_{O_2}^{\frac{1}{4}} + \sigma_{O^=} + K_n p_{O_2}^{-\frac{1}{4}}} \qquad (41)$$

By definition:

$$t_{O^=} + t_{\oplus} + t_{\ominus} = 1 \qquad (42)$$

where $t_{O^=}$ is the ionic transport number

$t_{\oplus}$ is the transport number for positive holes

$t_{\ominus}$ is the transport number for excess electrons.

For the electrolyte to be considered a true ionic conductor, $\sigma_{O^=}$ must be equal to σ_T. However, $\sigma_{O^=} = 0.99\ \sigma_T$ is

considered adequate. The oxygen partial pressure limits for this condition may be determined in a number of ways. The most elementary is the method used by Kiukkola and Wagner(32) where the total conductivity is determined as a function of oxygen partial pressure. A second method is to measure the EMFs of cells with known free energies of reaction. One electrode should be in the ionic region and the other electrode is varied. Deviations from the expected values indicate that electronic conduction is occurring. This method was used by Steele and Alcock(48) on thoria-based electrolytes. For the dopants Y_2O_3, La_2O_3 and CaO they found that the region where $t_i > 0.99$ extends from about $P_{O_2} = 10^{-7}$ atm. to about $P_{O_2} = 10^{-24}$ atm. at 1000°C. For zirconia-based electrolytes Steele and Alcock report that $t_i > 0.99$ at 1000°C from $P_{O_2} = 1$ atm. to about $P_{O_2} = 10^{-17}$ atm.

Other techniques for determining the T, P_{O_2} domain where an oxide electrolyte may be considered a pure ionic conductor are based on polarization schemes. In the technique used by Danforth and Bodine(57) and Vest and Tallan(58) the electrolyte is placed between inert blocking electrodes in various oxygen atmospheres. The blocking electrodes prevent the passage of $O^=$ between the electrolyte and the leads. A small constant current is applied to the electrolyte and the voltage-time behavior is measured. The electronic transport number is determined from the voltage across the specimen at zero and infinite time from:

$$t_e = \frac{E(0)}{E(\infty)} \qquad (43)$$

In the method of Hebb(59) and Wagner(60) one inert blocking electrode and one metal, metal oxide electrode are used.

The metal, metal oxide electrode fixes the oxygen partial pressure. An EMF below the decomposition potential of the electrolyte is impressed upon the cell. The blocking electrode is made negative so that anions migrate to the metal, metal oxide electrode. The current at infinite time is related to the EMF by

$$I_\infty = \frac{RT}{FL}\left[\sigma_\oplus\left(1-e^{-\frac{EF}{RT}}\right) + \sigma_\ominus\left(e^{\frac{EF}{RT}}-1\right)\right] \qquad (44)$$

where I_∞ is the current at infinite time, amp

L is the thickness of the electrolyte, cm

$\sigma_\oplus$ is the positive hole conductivity, mho-cm^{-1}

$\sigma_\ominus$ is the excess electron conductivity, mho-cm^{-1}

and the other terms have been defined earlier.

In the limiting cases where $\sigma_\oplus \gg \sigma_\ominus$ or $\sigma_\ominus \gg \sigma_\oplus$ the equation may be readily solved. Patterson, Bogren, and Rapp(61) rearranged the equation to read:

$$\frac{I_\infty}{1-e^{-\frac{EF}{RT}}} = \frac{RT}{FL}\left[\sigma_\oplus + \sigma_\ominus\, e^{\frac{EF}{RT}}\right] \qquad (45)$$

A plot of $I_\infty/(e^{EF/RT}-1)$ against $e^{-EF/RT}$ gives a straight line of slope $RT/FL\,\sigma_\oplus$ and intercept $RT/FL\,\sigma_\ominus$. Rapp(51) reports, from the data of Patterson et. al(61), that ThO_2-7.5 mol % Y_2O_3 has $t_i > 0.99$ at $P_{O_2} = 10^{-34.3}$ atm. at 1000°C. At this low oxygen partial pressure thermionic shunting occurs and obscures true electronic conduction via the electrolyte. The value of P_{O_2} where $t_i > 0.99$ reported by Rapp is considerably different from the value reported by Steele and Alcock(48) - about ten orders of magnitude.

There is better agreement on the oxygen partial pressure limit where $t_i > 0.99$ for ZrO_2-15 mol % CaO. Steele and Alcock(48) and Schmalzried(33) report a value of about 10^{-17} atm. at 1000°C.

The oxygen partial pressures to be measured in the present investigation were estimated to be about 10^{-24} atmospheres at 1000°C. The thoria-yttria system appears more promising as an electrolyte than zirconia-calcia because the former remains an ionic conductor down to pressures of about 10^{-24} atmospheres or less whereas the latter fails at about 10^{-17} atmospheres. Another advantage of the thoria-yttria electrolytes is their higher resistivity as compared to zirconia-calcia electrolytes (about two orders of magnitude higher). If electronic conduction is occurring in the electrolyte, then the exchange current is limited to a maximum value by the resistence of the electrolyte. The lower the exchange current, the closer the cell approaches reversibility. For these reasons, the thoria-yttria electrolyte system was used in the present work.

All EMF measurements where the ionic transport number is not equal to unity are made under irreversible conditions. The EMF of the cell is not related to ΔG_R by

$$\Delta G_R = -nFE \tag{10}$$

in cells where electronic conduction is occurring in the electrolyte. Wagner(62) showed that for $t_i < 1$

$$E_m = -\frac{1}{4F}\int_{\mu_{O_2}''}^{\mu_{O_2}'} t_i \, d\mu_{O_2} \tag{46}$$

for oxide electrolytes. E_m is the observed EMF in the presence of electronic conduction. From this equation Schmalzried(33) derived the following equation for the case where n-type electronic conduction develops at low oxygen partial pressure. He defined P_Θ as the oxygen partial pressure where

$$\sigma_i = \sigma_\Theta = K_n p_\Theta^{-\frac{1}{m}} \tag{47}$$

Then,

$$t_i = \left[1 + \left(\frac{p_{O_2}}{p_\Theta}\right)^{-\frac{1}{m}}\right]^{-1} \tag{48}$$

Substituting equation (48) in equation (46) and integrating gives:

$$E_m = -\frac{mRT}{4F}\left[\ln \frac{p_\Theta^{\frac{1}{m}} + p_{O_2}^{\cdot\cdot\,\frac{1}{m}}}{p_\Theta^{\frac{1}{m}} + p_{O_2}^{\cdot\,\frac{1}{m}}}\right] \tag{49}$$

Further simplification of the above equation can be achieved for the case where $P_{O_2}^{\cdot} \gg P_\Theta$. Such is the case for Fe, Fe_xO with respect to p_Θ for thoria-yttria electrolytes. The equation under these conditions becomes:

$$E_m = -\frac{mRT}{4F}\left[\ln \frac{p_\Theta^{\frac{1}{m}} + p_{O_2}^{\cdot\cdot\,\frac{1}{m}}}{p_{O_2}^{\cdot\,\frac{1}{m}}}\right] \tag{50}$$

The effective transport number, $\bar{t}_i$, is defined as:

$$\bar{t}_i = \frac{E_m}{E} \tag{51}$$

The value of m from theoretical considerations is 4 as was shown earlier in the discussion of Wagner's development of

equation (39). Measurement of E_m for a cell with known E enables one to calculate p_θ using equations (22) and (49). With p_θ in hand one can calculate E_m vs P''_{O_2} with respect to P'_{O_2}. E can also be calculated using equation (22). Then, E may be plotted against E_m for a particular temperature and electrolyte.

A plot of $\Delta G^\circ(T)$ per mole of O_2 against temperature for a wide variety of oxides results in a family of essentially parallel lines(63). Since p_θ is a hypothetical oxygen partial pressure derived from the partial reduction of a stable oxide, $RT \ln p_\theta$ vs T should exhibit the same slope as does $\Delta G^\circ(T)$ vs T for most other oxides. Then, $\bar{t}_i$ should not be strongly dependent upon temperature for a particular cell. This observation was made by Schmalzried(33). It is a very important observation since it provides a criterion for evaluating cell performance in the presence of electronic conduction. Under non-equilibrium conditions, measurements may be considered to be of some value if the temperature dependence of the EMF is of the same magnitude and sign as one would expect in the absence of electronic conduction. If it is not, then some kinetic effect is interfering with the measurement. Some of the possible kinetic effects are: polarization of one or both electrodes; gas leakage at one or both electrodes; unaccounted for reaction at one or both electrodes. Gas leakage at the electrodes was expected to give some difficulty. To minimize this effect, dense gas-tight electrodes which make a good seal against the electrolyte are required. This is readily accomplished with deformable electrodes such as low melting metal, metal oxide electrodes. Silicide electrodes which are

sintered with difficulty, are not deformable, and are in equilibrium with oxygen at extremely low oxygen partial pressure are most susceptible to leakage.

To conclude this section on the oxide electrolytes a brief description of some of the measurements made by other workers will be presented. Kiukkola and Wagner(32) studied the following cells:

$$Fe, Fe_xO \,||\, ZrO_2 + 15 \text{ mol \% } CaO \,||\, Fe_yO, Fe_3O_4$$

$$Fe, Fe_xO \,||\, \text{"} \,||\, Co, CoO$$

$$Fe, Fe_xO \,||\, \text{"} \,||\, Ni, NiO$$

$$Fe, Fe_xO \,||\, \text{"} \,||\, Cu, Cu_2O$$

$$Fe_yO, Fe_3O_4 \,||\, \text{"} \,||\, Cu, Co_2O$$

Steele and Alcock(48), in addition to replicating some of the cells investigated by Kiukkola and Wagner, studied the following systems:

$$Ir/Cu,Cu_2O//ZrO_2 + CaO//Pb(l), PbO/Ir$$

$$Ir/Pb(l), PbO//ZrO_2 + CaO//Ni, NiO/Ir$$

as well as the electrodes Nb, NbO; NbO, NbO_2, and NbO_2, Nb_2O_5 with respect to Fe, Fe_xO, and Ni, NiO and with respect to each other. They used zirconia and thoria-based electrolytes.

Rapp(64) determined the free energy of formation of MoO_2 from the following cells:

$$Pt/Mo,MoO_2//ZrO_2 + 15 \text{ mol \% } CaO//\begin{matrix} Fe, Fe_xO \\ \text{or} \\ Ni, NiO \end{matrix}// Pt$$

Rapp in collaboration with Maak(65) investigated the thermodynamic properties of solid copper-nickel alloys using the

cell:

$$Pt/Ni,NiO//ZrO_2 + 15 \text{ mol \% } CaO//Cu\text{-}Ni \text{ alloy, } NiO/NiO/Pt$$

Weissbart and Ruka(66) applied solid state electrolytes to oxygen pressure measurements through the cell:

$$O_2^{\bullet}, Pt//ZrO_2 + 15 \text{ mol \% } CaO//Pt, O_2^{\bullet\bullet}$$

Matsushita and Goto(67) used zirconia-calcia to replicate some former work and added SnO, PbO, CaO and Ta_2O_5 to the list of oxides studied. The results for Ta_2O_5 were not in agreement with thermal data. Worrell(68) investigated the stabilities of tantalum and niobium oxides using thoria-yttria and thoria-calcia electrolytes. Worrell's data for Ta_2O_5 were in agreement with thermal data.

Fitterer(69) used ZrO_2 + 15 mol % CaO to determine the oxygen content of liquid steels. Schwerdtfeger(70) used oxide electrolytes to measure oxygen activity in iron, iron-silicon, manganese and iron-manganese melts. In the iron-silicon melt the oxidation product is SiO_2(a). It is one of the few cases where a cell in which silica is a participant has been studied.

Wilder(71) used an oxide electrolyte to determine the activity of oxygen in liquid copper. Thermodynamic data for plutonium oxides were determined by Markin and Rand(72) with the cell:

$$PuO_{2-x}//ThO_2+Y_2O_3//ZrO_2 + CaO//ThO_2+Y_2O_3//Ni, NiO$$

One can see from the above survey that most of the cells studied to date have employed binary <u>two</u> phase $+O_2$ or ternary <u>two</u> phase $+O_2$ electrodes. A more complex case is the ternary three phase $+O_2$ electrode. Very little work has been done for this case with oxide electrolytes. Taylor

and Schmalzried(73) examined the cells

$$\text{Pt} \left| \begin{array}{c} \text{Co, } \text{CoTiO}_3, \text{TiO}_2 \\ \text{or} \\ \text{Co, } \text{Co}_2\text{TiO}_4, \text{CoTiO}_3 \end{array} \right\| \text{ZrO}_2 \text{ (+CaO, MgO)} // \text{Co, CoO/Pt}$$

to determine the free energy of formation of Co_2TiO_4 and $CoTiO_3$.

The work done here represents an extension of free energy measurements employing solid oxide electrolytes to a second family of three phase $+O_2$, three component electrodes derived from the Ta-Si system. Because successful measurements on at least four electrodes are required to completely determine the free energies of formation of the individual silicides, the problem is a particularly difficult one.

III. EXPERIMENTAL

A. Preparation of Materials

The tantalum silicides were prepared by direct reaction of the elements. The tantalum used in the synthesis was -120 mesh powder secured from Fansteel Metallurgical Corp. The minimum purity was 99.9%. The silicon was -325 mesh powder of 99.99% purity and was obtained from United Mineral and Chemical Corp. The tantalum and silicon were weighed out in the desired proportions on an analytical balance. They were mixed together in plastic vials for a minimum of twenty minutes in a Spex Grinder using plastic balls. The Spex Grinder has a vibrating action which approaches the shape of a figure 8 drawn on the surface of a sphere. The machine can be used for the mixing, grinding, or sieving of powdered materials. The powder was then pressed into 1/2" diameter pellets weighing approximately three grams. A pressure of 40,000 psi was used. The unreacted pellets were placed in a one inch diameter alumina crucible which contained a tantalum susceptor. The crucible was covered with a tantalum sheet and inserted in an induction heated vertical tube furnace connected to a vacuum system. Temperatures were measured through a quartz window at the top of the furnace by sighting an optical pyrometer at an opening in the crucible cover. From three to six pellets were reacted at one time. The pellets were brought up to the reaction temperature slowly in order to maintain the pressure in the system below about 10^{-2} Torr. This outgassing process generally required about ten minutes. The pellets reacted spontaneously at about 1125^{o}C with visible evolution of heat. The reaction lasted less than one minute. The rapid evolution of

the heat of reaction brought the temperature up to about 1400°C. During the reaction period the pressure rose above 10^{-2} Torr. due to silicon evolution. Samples weighed before and after reaction showed that the weight loss per gram of silicide was proportional to the silicon content in weight per cent. Less than 0.01% of the silicon was lost by sublimation during the reaction.

The reacted pellets were crushed to a powder with a mortar and pestle and ground in plastic vials with tungsten carbide ends and a tungsten carbide ball with a Spex Grinder for a minimum of twenty minutes. X-ray examination of the reacted materials showed that equilibrium was not obtained. However, the expected products were the major constituents.

The synthesized silicides were used in a phase study, an electrode stability study and in the cell electrodes. The phase study was performed to identify the lower silicides. Compositions were selected so that one could determine whether the lowest silicides produced in the synthesis and subsequent sintering were Ta_3Si or "$Ta_{4.5}Si$" and Ta_2Si. Compositions were also selected to determine the nature of "$Ta_{4.5}Si$". After the reaction and grinding steps the silicides were pressed into 2.5 gram pellets in a 1/2 inch diameter die. A pressure of about 40,000 psi was used. Because the silicides are extremely hard and brittle a binder is necessary to provide strength for handling the green pellets. A one per cent solution of polymethyl-methacrylate (PMMA) in methyl ethyl ketone was used as the binder solution. Approximately equal volumes of binder solution and silicide powder were used so that the dry powder contained about 0.2% (PMMA) by weight. The pellets were presintered in vacuum to remove the binder

by depolymerization to methyl methacrylate. The presintering was done in a wire-wound pot furnace. Power input was controlled by a carbon pile and the temperature was measured with a chromel-alumel thermocouple. The furnace was heated to about 550°C over a three hour period. The power was shut off at this point and the furnace cooled slowly to room temperature. The temperature was over 500°C for about one hour. The presintered pellets were then sintered on alumina trays in vacuum at about 1625°C for ten minutes. A tantalum resistance furnace manufactured by Brew was used. The furnace was coupled to a 4" NRC pumping station. The system pressure was maintained below 10^{-5} Torr. during the sintering operation. The temperature was measured with a Leeds and Northrup optical pyrometer. A +50C° correction was made to compensate for absorption by the glass window and for the grey body source. Identical pelletizing, presintering, and sintering procedures were used in the electrode stability study and in the fabrication of the silicide electrodes.

The silicide pellets in the phase study did not show appreciable densification after sintering. Since the pellet surfaces lost silicon by sublimation during sintering, the surface layer was removed from the pellets to permit a center section to be X-rayed on a Norelco diffractometer. A scan from $2\theta = 18^{\circ}$ to $2\theta = 72^{\circ}$ was made in each case. The scanning rate was one degree per minute. The full scale counting rate was set at 1000 counts per second and a time constant of 0.5 reciprocal seconds was used. The diffraction patterns were indexed with the aid of the ASTM file(36).

For the electrode stability study the reacted tantalum and silicon was first heat treated in the same manner as

pellets used in the phase study. The heat treated material was crushed with a mortar and pestle and was ground for twenty minutes in the Spex Grinder. Then, tantalum oxide, silica and 0.07 wt % nickel were added. The nickel was added as a sintering aid. The tantalum oxide was a purified grade obtained from Fisher Scientific Co. Technical grade silica, in the form of alpha quartz, was also obtained from Fisher Scientific Co. The powders were ground together for twenty minutes in the Spex Grinder. The powder was mixed with PMMA binder and pressed into 1/2" diameter pellets under a pressure of 40,000 psi. The pellets were X-rayed. They were then presintered and sintered in the usual manner. The surface layer was removed and the pellets were X-rayed again and indexed. Comparison of the X-ray diffraction patterns before and after sintering facilitated interpretation of the electrode stability study.

Silicide electrodes for cell measurements were fabricated from "as reacted" silicide powder or from reacted and heat treated material. The appropriate oxides and Ni sintering aid were added. The powders were ground together for twenty minutes, pelletized with PMMA binder, presintered and sintered. With the exception of $TaSi_2$, Ta_5Si_3, SiO_2 electrodes containing little or no silica, the electrodes sintered poorly. The $TaSi_2$, Ta_5Si_3, SiO_2 electrodes which sintered well were ground and polished to a bright metallic finish. Plates VIII, XII, and XIV show three such electrodes before they were used in an electrochemical cell. The electrode shown in plate VIII has the most silica; the electrode shown in plate XIV has the least. All three electrodes contain many large holes. However, the holes appear to be isolated so that the effective porosity for gas flow is zero.

The lower-silicide electrodes did not sinter well. They powdered when ground on emery paper. In order to present a dense surface to the electrolyte these lower-silicide electrodes had to be used in the as-sintered conditon. However, because of silicon losses their surfaces within a particular batch of electrodes showed considerable variation in composition. Therefore, suitable electrodes for use in the cells were selected by X-ray diffraction. All surfaces were screened by examining the diffraction pattern between 35° and 41° (2θ). This permitted a determination of the relative amounts of the lower silicides present. Plates XVI through XX show some surfaces of the lower-silicide electrodes as they appeared after use in a cell. The photographs were taken using the same lighting as was used in Plates VIII, XII, and XIV. The irregularity of the surfaces of the lower silicide electrodes and the many connected pores are apparent in the photographs.

Reference electrodes for the EMF measurements were prepared from the appropriate metal and metal oxide powders by powder metallurgical techniques. Copper, cuprous oxide electrodes were prepared from equimolar amounts of electrolytic copper powder (>99.9% pure) obtained from U.S. Metals Refining Co. and cuprous oxide powder of greater than 96% purity which was obtained from Fisher Scientific Co. The powders were mixed together with a Spex Grinder for thirty minutes and pressed into 1/2" diameter pellets weighing 2 grams under a pressure of 30,000 psi. The pellets were sintered in vacuum at 950°C for ten minutes. Nickel, nickel oxide electrodes were prepared from approximately equimolar amounts of nickel and nickel(ous) oxide. Nickel powder of 99.9% purity was

obtained from Cerac, Inc. Green nickel(ous) oxide of 99.8% purity was obtained from the Fisher Scientific Co. The powders were mixed together for approximately twenty minutes with a Spex Grinder and pressed into 1/2" diameter pellets weighing from 2 to 4 grams under a pressure of 30,000 psi. The pellets were sintered in vacuo for ten minutes at 1200°C. Iron, ferrous oxide(Wustite) electrodes were prepared from 97.1% pure iron powder obtained from the J.T. Baker Chemical Co. The iron was oxidized in air at about 500°C. The powder was mixed periodically during the oxidation. The powder was weighed and oxidation was stopped when one-third of the oxygen required to oxidize all of the iron to FeO had been gained. The powder was then pressed into two-gram pellets in a 1/2" diameter die at a pressure of 30,000 psi. These wafers were sintered in vacuo at 1250°C for fifteen minutes. Tantalum, ditantalum pentoxide electrodes were fabricated from 99.9% pure tantalum powder obtained from Fansteel Metallurgical Corp. and purified grade Ta_2O_5 obtained from Fisher Scientific Co. Three batches of electrodes were prepared by mixing the powders for twenty minutes with a Spex Grinder, pressing into 1/2" diameter pellets weighing 2.5 grams and sintering in vacuo. The first batch was composed of 3 grams of tantalum per gram of Ta_2O_5 and was sintered at 1500°C for ten minutes. The second and third batches were composed of 4 grams of tantalum per gram of Ta_2O_5. The second batch was sintered at 1650°C for 15 minutes and the third was sintered for 15 minutes at 1700°C.

All reference electrodes were ground flat on emery papers down to 3/0 grit. The iron, wustite and Ta, Ta_2O_5 electrodes from batches two and three were of sufficient quality to

permit final polishing on a napless nylon cloth with 5 micron levigated alumina. A photomicrograph of an iron, wustite electrode is given in Plate I. The electrode is free of pores and contains approximately equal volumes of metal and oxide. A photomicrograph of a Ta, Ta_2O_5 electrode from the first batch is shown in Plate II. The porosity is evident. Plate III is a photomicrograph of a Ta, Ta_2O_5 electrode from batch three. It is pore-free. Ta, Ta_2O_5 electrodes from batch two were similar to those of batch three.

Thoria-yttria electrolytes were fabricated from 99.9% pure thoria powder and 99.99% pure yttria powder. Both materials were obtained from A.D. Mackay, Inc. The powders were weighed out in the desired proportions and mixed for either twenty minutes in plastic vials with the Spex Grinder or for 60 hours in a conventional ball mill. The mixed powder was pressed into 1/2" diameter pellets weighing from three to six grams. The pellets were sintered in a Brew Furnace for 3 to 36 hours at temperatures from 1900°C to 2200°C. In some cases small amounts of silica were added in an effort to improve the finished density of the sintered product. Also, since silica happens to be a contaminant in commercially produced ThO_2-Y_2O_3 electrolytes the addition of silica in controlled amounts provides a means of assessing its effect upon the electrical properties of commercial electrolytes at low oxygen partial pressure. X-ray diffraction analyses of a ThO_2-6 wt % Y_2O_3 pellet before sintering and after sintering at 2000°C for three hours clearly showed that the Y_2O_3 dissolved. The Y_2O_3 peak which was present before sintering was absent in the sintered material and the ThO_2 peaks shifted by the amount expected from the data of Subbarao et. al. (52).

The sintered pellets were cut on a 15 micron diamond wheel to remove the surface layer and any fractured areas. Opposite faces were maintained parallel to within 0.002". The electrolytes were final-polished on a napless nylon cloth with 5 micron levigated alumina abrasive. The density was measured by water displacement. Some results are presented in Table IV. Theoretical densities were calculated from X-ray data in the ASTM file(36) and in Subbarao(52). For ThO_2-1 wt % Y_2O_3 the theoretical density is 9.95 gm/cc. For ThO_2-6 wt % Y_2O_3 the theoretical density is 9.37 gm/cc. As can be seen from table IV, sintering time, temperature, silica content, and milling all have an effect upon the sintered density. The effect of temperature and silica content for 6 wt % Y_2O_3 electrolytes fabricated from ThO_2 and Y_2O_3 that were mixed for twenty minutes is shown in Figure 4. The value of SiO_2 as a sintering aid is clearly demonstrated. The silica probably acts as a complex melt containing ThO_2 and Y_2O_3. The diffusivity at the surface of the particles is thereby greatly increased and the sintering process is accelerated. Since silica is thermodynamically less stable than ThO_2 and Y_2O_3 one might expect electrolytes in which silica was used as a sintering aid to be inferior to pure thoria-yttria electrolytes at low oxygen partial pressure. Some EMF measurements were conducted to compare pure electrolytes with electrolytes containing SiO_2. The small amounts of SiO_2 used has no appreciable effect upon the transport number. Details of these EMF measurements will be presented in a later section.

Photomicrographs of some electrolytes are given in Plates IV through VI. Plate IV is a photomicrograph of

TABLE IV

DENSITY OF THORIA-YTTRIA ELECTROLYTES

I. Materials Mixed for Twenty Minutes with Spex Ball Mill:

A. ThO_2 - 6 wt % Y_2O_3

Temperature ^oK	Time (hrs)	Density as % of Theoretical
1900	3	84.3
1900	3	84.9
2000	3	86.5
2000	3	86.7
2000	28	90.7
2000	28	90.9
2100	3	88.2
2100	3	89.0
2200	36	92.0

B. ThO_2 - 6 wt % Y_2O_3 - 0.1 wt % SiO_2

1900	3	90.7
1900	3	94.4
2000	3	96.4
2000	3	95.4
2100	3	97.1
2100	3	96.8

C. ThO_2 - 6 wt % Y_2O_3 - 0.2 wt % SiO_2

1900	3	94.0
1900	3	95.7
2000	3	98.1
2000	3	96.9
2100	3	97.2
2100	3	100

TABLE IV (cont.)

D. ThO_2 - 1 wt % Y_2O_3

Temperature ^oK	Time (hrs.)	Density as % of Theoretical
2000	3	95.0
2000	3	92.0

E. ThO_2 - 1 wt % Y_2O_3 - 0.1 wt % SiO_2

2000	3	92.2
2000	3	92.6

II. ThO_2 - 6 wt % Y_2O_3 mixed for 60 hours in a conventional ball mill.

2000	3	96.6
2000	3	95.7
2000	3	93.0
2000	3	93.1
2000	3	96.0

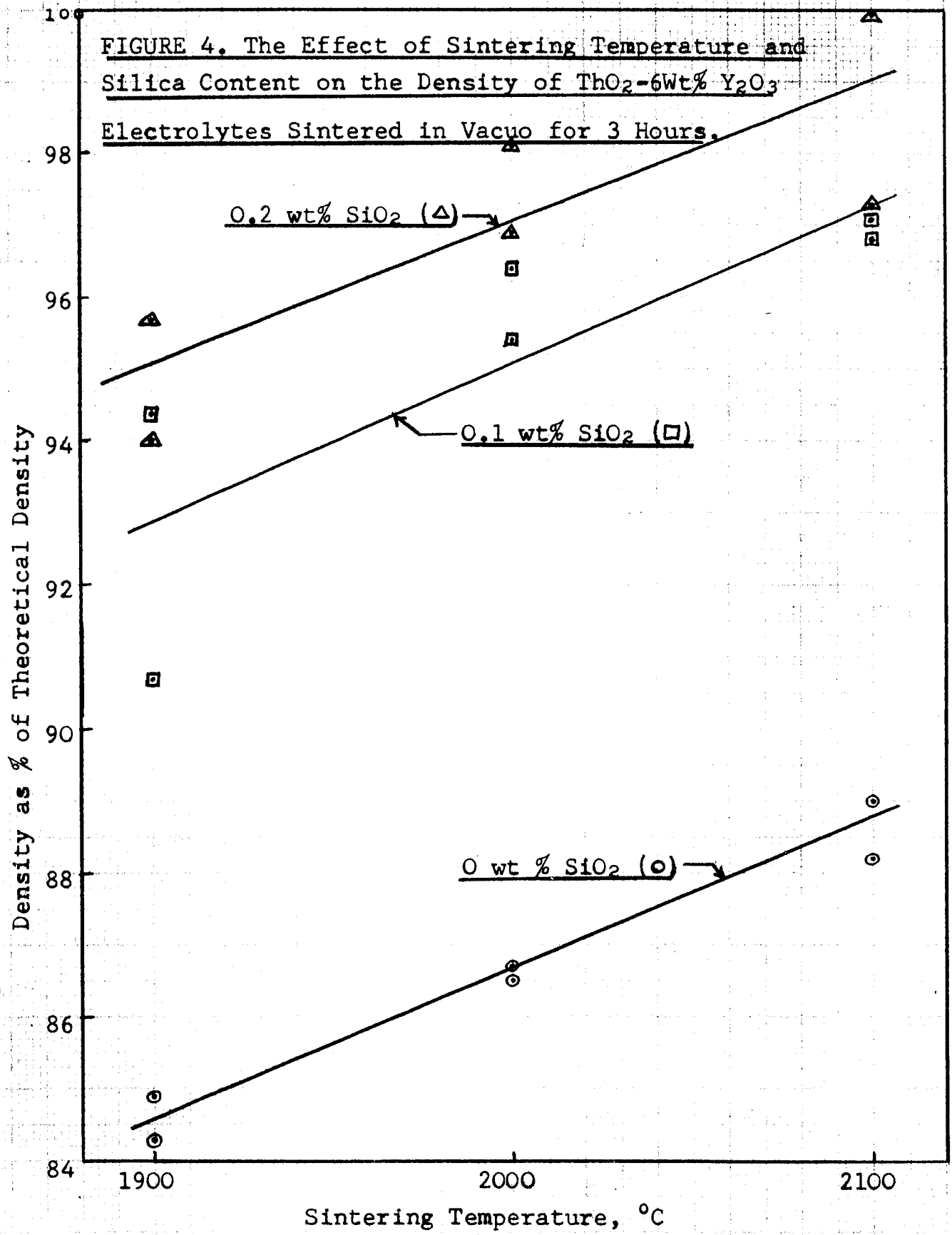

FIGURE 4. The Effect of Sintering Temperature and Silica Content on the Density of ThO_2-6Wt% Y_2O_3 Electrolytes Sintered in Vacuo for 3 Hours.

a commercially produced ThO_2 – 7.5 mol % Y_2O_3 electrolyte. Such electrolytes were obtained from the Zirconium Corp. of America (Zircoa) and were used in some of the early EMF measurements. The three electrolytes shown appear to have closed pores only. The microstructure of the electrolytes was revealed by etching in concentrated sulfuric acid for forty-five minutes at 175°C. A second phase appears to be present at the boundaries of some grains in the Zircoa material. The electrolytes produced in this work appear to be single phase. The greater density of the electrolyte where silica was used as a sintering aid as compared with the pure thoria-yttria electrolyte is apparent (compare plates V and VI).

Both thoria and yttria are white or colorless in the stoichiometric condition. Their stoichiometric solid solutions are also white. When the oxygen content departs from the stoichiometric value, positive holes or negative electrons are trapped in the lattice and impart a color to the ceramic. Pure thoria in the hyperstoichiometric condition is red. Zircoa electrolytes are reddish-brown in the hyperstoichiometric condition. They can be reduced to the stoichiometric white condition by heating in a reducing atmosphere at elevated temperature. The oxygen partial pressure established in the carbon-carbon monoxide equilibrium above about 800°C is sufficiently reducing. Irradiation in a cobalt 60 gamma ray source or heating in air restores the brown color. The silica-free electrolytes prepared in the present work were dark green with a reddish-brown skin. The interior varied from light green to very dark green depending on sintering temperature and composition. Pellets of lower yttria content

were a lighter shade of green than pellets of higher yttria content. Also, pellets sintered at higher temperatures were a slightly darker green than pellets sintered at lower temperature. Electrolytes containing silica were brownish-green in the as-sintered condition. The electrolytes turned white after use in the electrochemical cells where the oxygen partial pressure is low. Also, decolorization occurred upon heating in air above about 200°C. At 200°C the process took several hours. At 300°C the process was complete in two hours and at 400°C the process was complete in twenty minutes. Heating at 1400°C in air also produced a color change from green to white. After being held at 1400°C in air for three days a tan layer appeared on the surface of the electrolyte. Electrolytes containing SiO_2 were transluscent whereas pure electrolytes were opaque in the decolorized condition. Pure electrolytes were not affected by gamma irradiation. The green color could be restored by reheating in vacuum in the Brew Furnace for 15 minutes at 2000°C. Pure unsintered material that was heated in an oxidizing flame of an oxy-acetylene torch at 2400°C remained white except for the surface in the colder part of the flame which became brown. Electrolytes containing silica were affected by gamma irradiation; as-sintered material became browner. Decolorized material turned transluscent green. The decolored electrolytes containing SiO_2 were observed to be fluorescent.

A complete explanation for these observations can not be given since insufficient evidence has been accumulated. However, it appears that the brown color of Zircoa electrolytes and the red color of pure thoria in the hyperstoichiometric condition are due to excess oxygen dissolution with the

production of an electrochemical equivalent number of positive holes. Radiation damage produces the same color change via the creation of positive holes with an equivalent number of electrons being trapped at vacant oxygen lattice sites. The brown skin observed on silica free electrolytes in the as-sintered condition as well as on materials heat treated in air at elevated temperature is probably due to excess oxygen dissolved in the lattice. Since pure thoria-yttria electrolytes were not susceptible to Co^{60} gamma radiation damage whereas the Zircoa material and the thoria-yttria-silica electrolytes were, it is fair to say that impurities play a key role in the damage mechanism; perhaps holding electrons at high enough energy levels to be displaced by gamma rays and trapped. The low temperature decolorization phenomenon seems to indicate that non-massive particles (electrons or holes) are migrating. However, the fact that the electrolytes emerge from the sintering process with a green color is contradictory to this mechanism. Further evidence is required to clarify all of the observed phenomena and to provide mechanistic explanations. Fluorescence spectra, EPR spectra, and correlation of color with transport number, stoichiometry and purity are necessary.

III. B. EMF Apparatus

Preliminary EMF measurements were made with ZrO_2-15 mol % CaO and ThO_2-7.5 mol % Y_2O_3 electrolytes in crucible form. The electrolytes were obtained from Zircoa and were used in a crude apparatus to establish the feasibility of the method. The anode material in the powdered condition was tamped into the crucible along with a platinum foil and lead wire. The cathode, in pellet form, was placed in contact with the base of the crucible. The other face of the cathode was placed in contact with a platinum foil which was spot welded to the positive platinum lead wire. The lead wires were insulated with quartz tubing. The cell was enclosed between a pair of alumina discs and then between a pair of nickel discs. The lower nickel disc was fixed to the top cloture of the furnace tube by a pair of alumel wires. The upper nickel disc was free to slide along these suspension wires and, under the impetus of a small load suspended by alumel wires, exerted a small compressive force upon the cell. The insulated platinum lead wires were fed through center holes in the alumina and nickel discs. The cell assembly was suspended halfway down a 30" long vertical fused quartz tube with a 3/4" inside diameter. The tube was heated by a wire wound resistance tube furnace. The furnace chamber was 1" in diameter and 13 inches long. The heating element was about 12 inches long. The tube was located symmetrically in the furnace since a traverse of the furnace showed that the temperature profile was symmetrical about the mid-point over the central 10 inches to within $5C^{o}$. The constant temperature zone was 2 inches long. The fused quartz tube was closed off by rubber stoppers. The platinum lead wires were fed through the center of the stoppers in the

earlier experiments and through teflon sleeves that were placed in the stoppers in later experiments. A chromel-alumel control thermocouple and a gas outlet tube penetrated the top stopper. A calibrated chromel-alumel thermocouple for temperature measurements and a gas inlet tube were inserted through the bottom stopper. Both thermocouples were housed in Vycor thermocouples wells. Argon of 99.995% purity (Matheson Co. prepurified grade) was used as an inert atmosphere. The gas flow rate was measured with a rotameter. A slight positive pressure was maintained by a bubbler on the gas outlet line.

Temperature control was provided by a West Gardsman JEP proportional controller. The power supply consisted of a Variac with a maximum output of 7.5 amperes at 120 volts. The Variac was connected to a rheostat in series with the furnace windings. The West controller was used to close a normally open mercury relay. In the normally open position the relay placed the rheostat in series with the furnace windings. In the closed position the rheostat was shunted. Thus, two levels of power input were provided to the furnace; power was measured with an ammeter and voltmeter. The measuring thermocouple with an ice bath cold junction was connected to a DPDT switch. This permitted the thermocouple voltage to be measured with a Leeds and Northrup Millivolt Potentiometer or continuously recorded with a Varian Model G-11A Strip-Chart Recorder with a T2 thermocouple input chassis. The cell EMF was measured with a Keithley Model 610B Electrometer with a 10^{14} ohm input impedance on the volt scale. Part or all of the cell voltage was normally bucked out by a Leeds and Northrup Potentiometer in series with the electrometer. The electrometer had a 0-3 volt output signal proportional to the input but of opposite

sign. This output was recorded with a potentiometric Varian Model G-11A Strip-Chart Recorder with a B1 input chassis.

EMF measurements were made over the interval from 600°C to 800°C with the anodic electrode maintained at ground potential. The runs were started by purging the system with argon for several minutes and then heating to the operating temperature. The argon flow was maintained at about 1 CFH during the run. Because EMF measurements with this simple apparatus showed some promise of future success a second unit was constructed.

The second unit was designed with the following considerations in mind: A gas purification system was needed to remove water and oxygen from the argon since the oxygen partial pressure over the silicide electrodes is extremely low. A means for maintaining the cell under a substantial compressive load to insure good contact at electrode-electrolyte interfaces was desired. The system should be capable of maintaining a hard vacuum at elevated temperatures so that vacuum operation will be possible and also so that leakage will be minimal when an inert atmosphere is used. Finally, the system should be designed to permit future modifications such as separate electrode compartments or operation at higher temperatures.

The second apparatus is illustrated in Figure 5. The cell is drawn approximately to scale. The associated control and measuring systems and the gas purification train are indicated schematically. The cell is assembled between fused quartz rods. The lower rod is fixed in the brass supporting stand which is part of the lower brass flange. The upper rod is free to travel through a Veeco Quick Coupling at the center of the upper brass flange. The platinum lead wires were initially

Figure 5. SECOND APPARATUS USED FOR EMF MEASUREMENTS

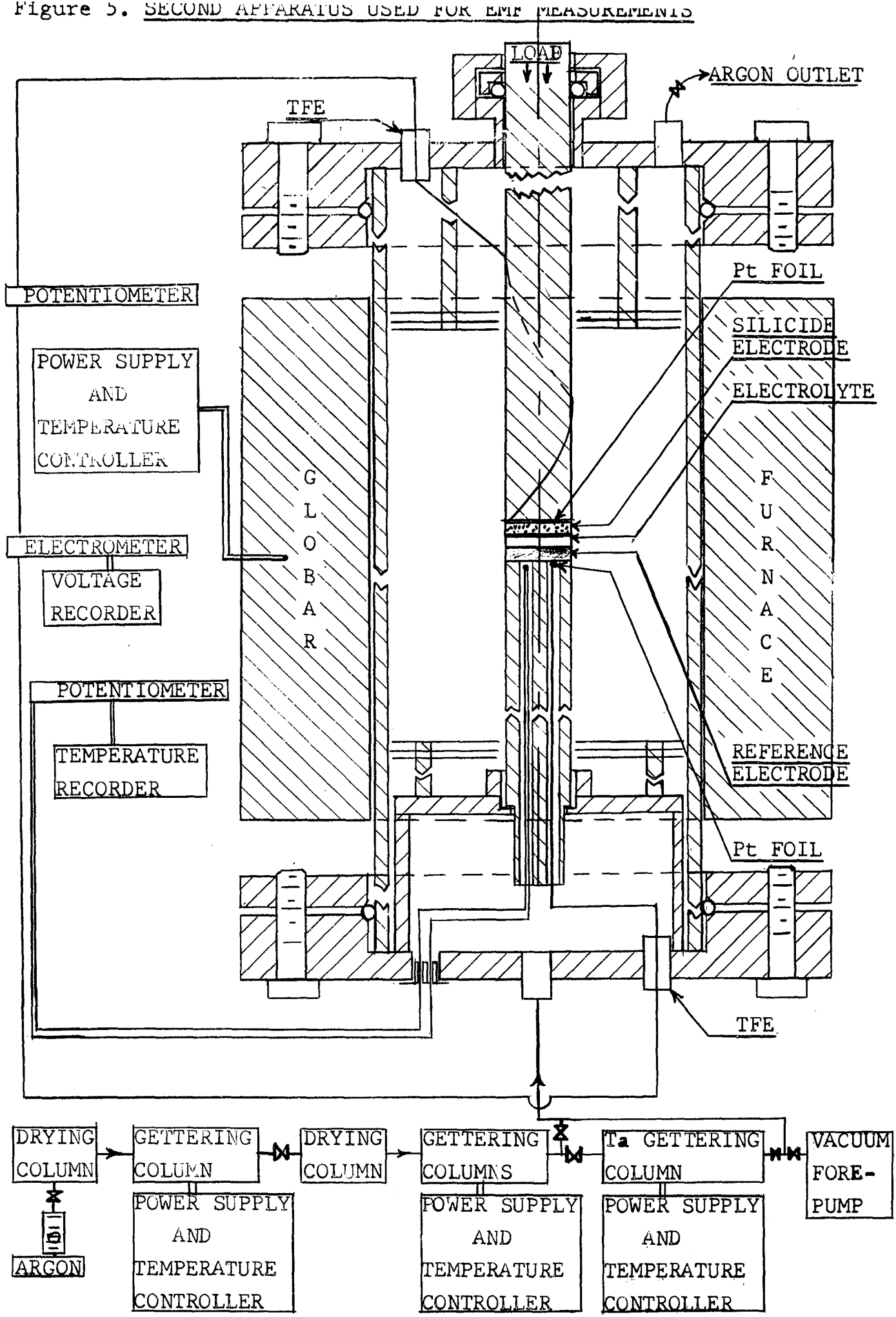

brought through the flanges with ceramic vacuum lead-throughs. These were later replaced by teflon lead-throughs. The chromel-alumel thermocouple used for measuring the cell temperature was brought through the lower flange via a ceramic vacuum lead-through. The thermocouple was calibrated at the melting point of silver. The equipment used for measuring and recording the cell EMF and cell temperature are the same as described earlier. The cell was enclosed in a Vycor tube with 65mm O.D. and 36" long. The brass end flanges were connected to the Vycor tube with O-ring seals. A Globar tube furnace was designed and built for heating the cell. Its chamber was 2½" I.D. by 22" long. The effective heating length of the Globars was 10" and the heated chamber was 9" long. The 120 volt-50 amp Variac power supply was operated in the on-off mode by a West Gardsman JEP proportional controller which operated a mercury relay. Power input was measured by an ammeter and voltmeter. The control thermocouple of platinum vs platinum-10% rhodium entered the heating chamber through the furnace bricks. A traverse of the furnace showed that the center of the constant temperature zone was located one inch above the center of the heating chamber. The constant temperature zone ($\pm 5C^{o}$) was 1½" long. The cell was positioned at the center of the constant temperature zone under compressive loads ranging from 20 to 380 psi. The usual load was about 200 psi.

The unit was initially operated with a gas purification train consisting of a drying column filled with anhydrous magnesium perchlorate and a reducing column containing copper shot at $300^{o}C$. The oxygen gettering agent was later changed to zirconium - 12.5 atom % titanium chips at $375^{o}C$. The chips

were obtained from the Oremet Metallurgical Corporation. A second gas purification train was constructed for later experiments. It consisted of a second drying column filled with anhydrous magnesium perchlorate followed by a pair of gettering columns. The first was filled with Zr-Ti chips and was operated at 375°C and the second was filled with tantalum foil and was operated at 600°C. The final system could be operated with either unit or the pair in series. The tantalum column in the second unit could be by-passed.

EMF measurements with the refined apparatus were made over the temperature range 600°C to 1100°C. An experiment was started by alternately roughing with a mechanical forepump and purging with argon for two cycles. The power was then turned on. The system took about one-half hour to reach 600°C and two hours to reach 1000°C. To cool from 1000°C to room temperature required about 12 hours.

The system was periodically tested for leaks by evacuating with a vacuum pumping station. The integrity of the EMF measuring circuit was tested at 900°C with the teflon lead-throughs in place. Under open circuit conditions between the platinum electrode contacts the resistance was "infinite" between the lead-throughs and along the segments of all possible parallel paths. When the platinum leads were brought into contact the resistance between the lead-throughs was 55 ohms and the resistance along the segments of all possible parallel paths was "infinite."

Among the shortcomings of the design was the very difficult process of correctly assembling and aligning three independently movable pellets in an inaccessible location. Three different procedures were used to assemble the cells. In the

first the pellets were assembled inside a sheet metal collar attached to the lower quartz rod. Once the cell was assembled the collar was removed by pulling it down along the quartz rod with attached wires. In the second method a quartz tube of 7/8" I.D. was used to position the pellets. However, this created a stagnant atmosphere around the cell which resulted in difficulties with gas-electrode interactions which by-passed the electrolyte. In the final assembly method the three pellets were lowered onto the quartz support rod by means of a mechanical pickup and the top flange was then lowered into position. The latter method required a great deal of manual dexterity and patience, but it gave the best cell alignment. Other shortcomings include the slow thermal response of the furnace during shutdown, and a tendency for the flanges to overheat. The maximum temperature for prolonged life of the fused quartz rods and Vycor tube is 1000^{o}C; for prolonged operation above 1000^{o}C a changeover to alumina rods and an alumina tube is necessary.

The results of some of the EMF measurements made with the first and second apparatus will be presented in the next section.

IV. EXPERIMENTAL RESULTS

A. Ta - Si System

Information about the tantalum-silicon system was obtained both from phase studies and from electrode preparation. The methods used in the synthesis and heat treatment of the silicide samples were described earlier. From the highest silicide phase field information about tantalum disilicide in coexistence with pentatantalum trisilicides (hereafter called "trisilicides") was obtained by X-ray studies. The data for interplanar spacings and relative intensities were substantially in agreement with the data in the ASTM Powder Diffraction File (Card 8-53) and did not vary appreciably from one sample to another. The trisilicide can exist in tetragonal and hexagonal modifications, and both forms were produced in simultaneous coexistence with tantalum disilicide. Based on the relative intensities of the strongest peaks (d = 2.21 for h - Ta_5Si_3, d = 2.34 for t - Ta_5Si_3) tetragonal Ta_5Si_3 was produced in greater quantity than the hexagonal variety. In samples which initially contained 20 weight per cent silicon the relative intensities of the strongest trisilicide peaks were tetragonal: hexagonal::2.7:1 in one sample and 1.6:1 in a second sample. Silicon losses from the surface resulted in preferential formation of tetragonal tantalum trisilicide. For example, in the latter sample the ratio tetragonal:hexagonal was about 8:1 at the surface where silicon losses occurred during sintering.

In a sample with an initial composition based on intended silicide products of 0.95 mole % Ta_5Si_3 - 0.05 mole % $TaSi_2$ the products were Ta_5Si_3 and a trace of ditantalum monosilicide, Ta_2Si, as a result of silicon loss. From the products, information about the trisilicides in coexistence with Ta_2Si were obtained. The ratio tetragonal:hexagonal tantalum trisilicide

was again about 2.7:1 based on the strongest peaks. Since the ASTM Powder Diffraction File lists intensities based only on visual observation, the data obtained in this study for the trisilicides are presented in Table 5. The data presented in the ASTM File are listed for comparison. The interplanar spacings for the trisilicides in coexistence with the disilicide and in coexistence with Ta_2Si are not very different. The interplanar spacings are in agreement with the data in the ASTM File except for a few minor discrepancies. However, the relative intensity data obtained with the diffractometer are in considerable disagreement with the data in the ASTM File. One explanation for this discrepancy is that the baseline intensity is subtracted in computing the intensities obtained with the diffractometer, whereas the baseline intensity is probably included in the intensities computed from visual observations. Relative intensities obtained with a diffractometer are preferable to relative intensities obtained by visual observations.

X-ray data for Ta_2Si in coexistence with the trisilicides were obtained from a sample with an initial composition based on the silicides of 0.95 mole % $TaSi_2$ - 0.05 mole % Ta_5Si_3. Data for Ta_2Si in coexistence with the lower silicide were obtained from a sample with an initial composition of 6.2 wt % silicon. This sample was heat treated at 1600°C for ten minutes following synthesis. It was then ground and refabricated into pellets and heat treated for an additional hour at 1600°C. Since the data for Ta_2Si listed in the ASTM File are based on visual relative intensities the results for the two samples described above are presented in Table 6. The d values are in agreement with the listings of the ASTM File and do not vary from one side of the Ta_2Si phase line to the other. The d = 1.43 line was resolved into a pair of closely spaced peaks of comparable

TABLE 5

X-RAY DATA FOR t-Ta_5Si_3

ASTM FILE (Card 9-232)		IN COEXISTENCE WITH $TaSi_2$		IN COEXISTENCE WITH Ta_2Si	
d	I/I_o	d	I/I_o	d	I/I_o
3.63	30	3.633	10	3.624	15
3.256	10				--
2.956	20	2.982	5	2.959	5
2.862	40	2.848	30	2.845	20
2.816	70	2.824	50	2.820	50
2.490	50	2.494	20	2.490	15
2.340	100	2.343	100	2.341	100
2.305	30	2.302	10	2.994	10
2.192	60	2.189	30	2.189	30
2.132	10	2.136	5	2.139	5
2.054	70	2.058	60	2.054	45
1.978	40	---	--	1.977	30
1.948	10	---	--	1.942	5
1.693	10	---	--	---	--
1.629	10	---	--	1.622	5
1.565	60	1.564	10	1.563	10
1.533	40	---	--	1.531	5
1.521	35	1.521	10	1.519	5
1.484	50	---	--	1.484	10
1.467	80	1.466	50	1.466	30
1.455	50	---	--	1.453	10
1.428	70	1.425	50	1.425	20
1.413	30	1.413	5	1.413	10
1.363	70	1.363	20	1.363	10
1.353	20	1.353	10	---	--

TABLE 5 (cont.)

X-RAY DATA FOR h-Ta_5Si_3

ASTM FILE (Card 6-0594		IN COEXISTENCE WITH $TaSi_2$		IN COEXISTENCE WITH Ta_2Si	
d	I/I_o	d	I/I_o	d	I/I_o
3.68	40	---	--	3.723	10
3.21	50	3.238	20	3.229	35
3.02	70	3.023	20	3.031	50
2.60	30	2.635	20	2.605	10
2.44	70	2.447	30	2.442	50
2.41	70	2.414	30	2.415	50
2.21	100	2.212	100	2.212	100
2.15	50	2.156	20	2.154	30
2.13	100	2.136	80	2.139	80
1.87	20	---	--	---	--
1.67	20	---	--	1.662	5
1.62	30	1.614	5	1.622	5
1.57	40	1.564	20	1.576	10
1.52	70	1.521	30	1.519	10
1.48	50	---	--	1.484	10
1.41	70	1.413	50	1.417	25
1.38	50	---	--	1.375	20
1.31	30	---	--	---	--

TABLE 6

X-RAY DATA FOR Ta_2Si

ASTM FILE (Card 6-0552)		Ta_2Si IN COEXISTENCE WITH Ta_5Si_3		Ta_2Si IN CO-EXISTENCE WITH THE LOWER SILICIDE	
d	I/I_o	d	I/I_o	d	I/I_o
4.31	30	4.337	5	4.337	5
3.06	40	3.072	5	3.074	10
2.51	40	2.518	70	2.524	40
2.41	100	2.414	100	2.417	100
2.18	40	2.180	20	2.182	20
1.94	50	1.947	30	1.947	30
1.54	40	1.541	10	1.542	10
1.45	30	1.451	10	1.452	5
1.43	80	1.435	25	1.436	25
--	--	1.432	25	1.432	25
1.38	20	1.385	5	1.377	5
1.31	30	1.314	5	1.315	5

intensity. The visual relative intensity data is again in poor agreement with relative intensities determined with the diffractometer.

The nature of the lowest silicide was determined by examining six compositions falling between pure Ta_2Si and pure "Ta_5Si". In the evaluation of the results by X-ray diffraction the line at d = 2.51 was considered representative of Ta_2Si and the line at d = 2.73 was considered representative of Ta_xSi. The compositions studied and the results are listed in Table 7. Calculated weight percentages of Ta_2Si based on initial compositions are listed in columns 2 thru 4 for various possible molecular formulas for the lower silicide. The only case where Ta_2Si would be present for all compositions studied is where the lowest silicide composition corresponds to Ta_5Si. However, X-ray diffraction analysis, in addition to detecting the presence of Ta_2Si in all samples, detected a significant quantity of unreacted tantalum in the first three and fifth samples listed. This finding precludes the conclusion that Ta_5Si is the lowest silicide on the strength of the detection of Ta_2Si in all samples. The ratio of intensities, $I(Ta_2Si)/I(Ta_xSi)$, is plotted in Figure 6 against wt % Ta_2Si present assuming that Ta_5Si is the composition of the lowest silicide. The intersection of this curve with the abcissa should represent the true composition of the lowest silicide on the Ta_2Si, Ta_5Si basis. The locations of $Ta_{4.5}Si$, Ta_4Si and Ta_3Si are marked on this abscissa. From the graph it is clear that Ta_3Si is not a possible formula for the lowest silicide. The data points from samples where a significant quantity of tantalum is present must be considered unreliable. Since a clear distinction between Ta_5Si, $Ta_{4.5}Si$ and Ta_4Si cannot be made, $Ta_{4.5}Si$ will be selected as an average value for the composition of the lowest silicide in agreement with the phase diagram of Figure 1.

TABLE 7

THE DETERMINATION OF THE COMPOSITION OF THE LOWEST SILICIDE

INITIAL SAMPLE COMPOSITION WT % Si	CALCULATED WT % Ta_2Si as Ta_2Si-Ta_5Si	CALCULATED WT % Ta_2Si AS Ta_2Si-$Ta_{4.5}Si$	CALCULATED WT % Ta_2Si AS Ta_2Si-Ta_4Si	HEAT TREATMENTS
3.03	0.7	0	0	2 of 10 min ea
3.36	8.8	3.2	3.2	"
3.75	17.7	13.1	0.7	"
4.20	28.4	24.4	13.6	"
4.20	28.4	24.4	13.6	1 of 10 min followed by 1 of 60 min.
5.00	47.0	44.3	36.6	"
6.20	75.7	74.6	71.3	"

X-RAY INTENSITY AFTER SECOND HEAT TREATMENT		INTENSITY OF STRONGEST Ta DIFFRACTION PEAK
Ta_2Si (d = 2.51)	Ta_xSi (d = 2.73)	Ta (d = 2.34)
10	17	12
15	17	10
36	6	6
42	7	3
14	8	4
49	3	0
64	1	0

FIGURE 6. Determination of the Composition of the Lowest Tantalum Silicide.

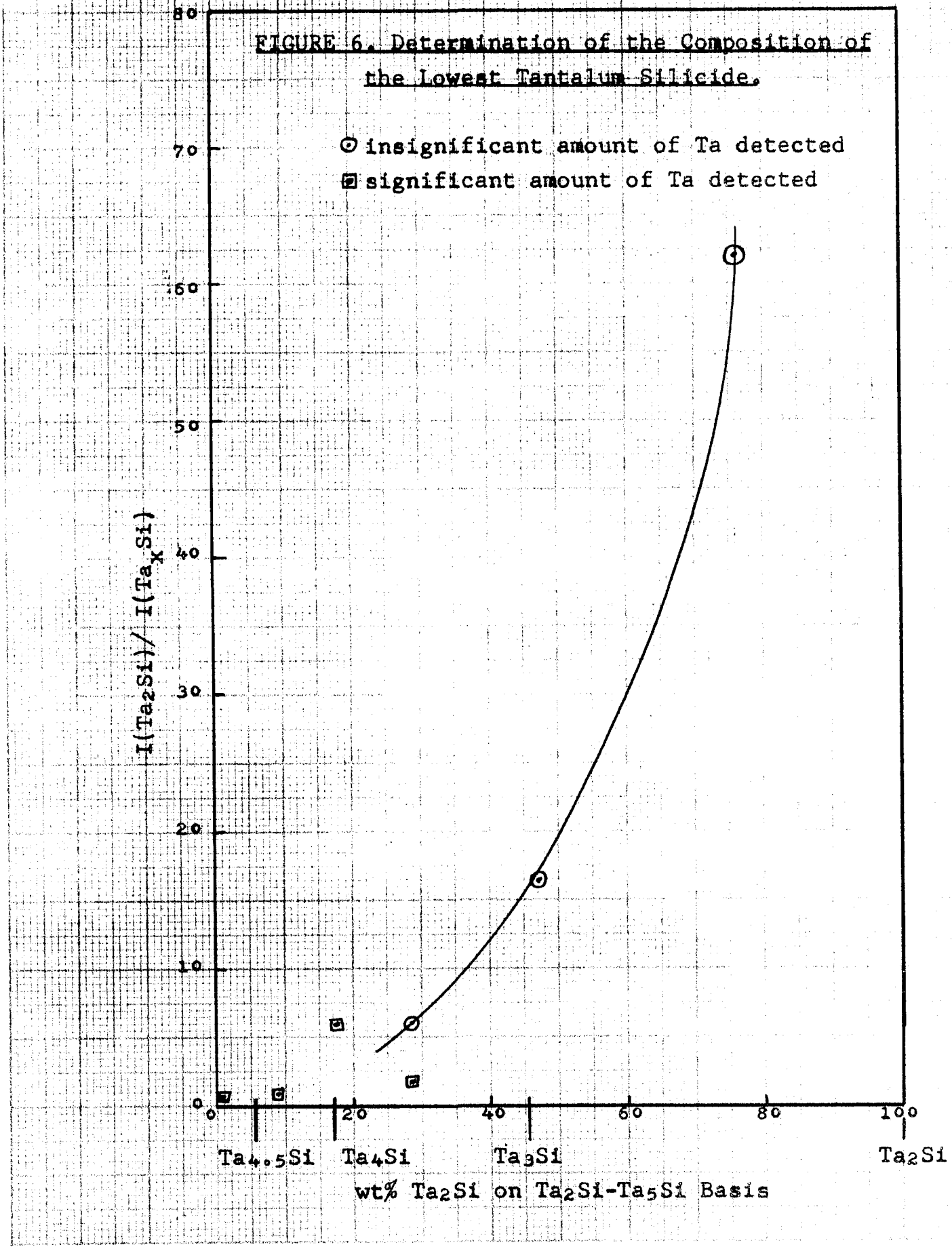

X-ray data for the lowest silicide, nominally $Ta_{4.5}Si$, were selected from the samples containing 3.03 and 3.75 wt% silicon. Interplanar spacings and relative intensities are listed in Table 8. These data are in considerable disagreement with the data listed in the ASTM File (cards 6-0569 and 8-390).

Table 8

X-ray Data for $Ta_{4.5}Si$

d	I/I_o	d	I/I_o
3.616	10	2.095	30
2.827	5	2.053	5
2.725	35	2.012	25
2.674	2	1.993	25
2.570	5	1.857	5
2.473	100	1.593	25
2.422	80	1.549	2
2.395	40	1.515	5
2.352	20	1.475	5
2.297	25	1.468	20
2.272	60	1.444	20
2.222	80	1.418	5
		1.410	30
		1.362	5

IV B. Electrode Stability Study.

The results of the electrode stability study were mentioned briefly in the development of the EMF method. The study was conducted to determine the stable oxide associated with a particular silicide pair. The experiments conducted in this study are summarized in Table 9. The composition of the sample before synthesis is listed in column II. Columns III and IV list the weight per cent of SiO_2 and Ta_2O_5 added before sintering respectively. Columns V through VIII list x-ray diffraction results. The quantities in columns V through VII indicate the relative quantities of the silicides present since the concentration of a phase is roughly proportional to the intensity of a characteristic diffraction line. The characteristic lines used and their relative intensities are as follows: $TaSi_2$, $d=3.50/I/I_o=100$; t-Ta_5Si_3, 2.34/100; h-Ta_5Si_3, 2.21/100; Ta_2Si, 2.41/100; $Ta_{4.5}Si$, 2.73/100; α-Ta_2O_5, 3.77/100 and 3.36/100, and Ta 2.34/100, 1.65/21 and 1.35/38.

The first ten samples listed had initial compositions in the $TaSi_2$-Ta_5Si_3 phase field (from 23.7 wt. % Si to 8.5 wt. % Si). Samples P and Q were initially richer in silicon than samples 1S, 2S and 3S. However the sintered P and Q samples became leaner in disilicide as can be seen from column V where the trend is clear in spite of the considerable scatter of the data. This shift in silicide composition can be explained by considering column VIII where a loss of Ta_2O_5 is evident in P and Q. The loss must occur by reaction of Ta_2O_5 with $TaSi_2$ according to the first reaction of Table III which may now be written as:

$$\frac{37}{7}\ TaSi_2 + 2\ Ta_2O_5 = 5\ SiO_2(a) + \frac{13}{7}\ Ta_5Si_3$$

$$0 > \Delta G > -87_{kcal}$$

TABLE 9

ELECTRODE THERMAL STABILITY STUDY

I Sample	II Initial Composition of Silicide wt % Si	III wt % SiC_2 added before sintering	IV wt % Ta_2O_5 added before sintering	V $\frac{I(TaSi_2)}{I(TaSi_2)+(Ta_5Si_3)}$ before sintering	V $\frac{I(TaSi_2)}{I(TaSi_2)+(Ta_5Si_3)}$ after sintering
P	23.7	6.0	13.9	0.84	0.14
Q	23.7	5.8	14.1	0.84	0.33
1S	20.0	5.0	0	-	0.57
2S	20.0	2.5	0	-	0.52
3S	20.0	0	0	-	0.64
Z	9.60	0	5.0	-	0
$2V_1^*$	8.67	3.7	5.6	-	0
$2V_2^*$	8.67	2.0	2.9	-	0
1V	8.60	2.8	6.6	-	0
2V	8.60	1.0	3.3	-	0
3W*	8.40	0	4.8	-	0
1W	8.0	4.1	0	-	0
2W	8.0	2.0	0	-	0
3W	8.0	0	7.0	-	0
4W	8.0	0	2.5	-	0
$2U_1^*$	7.40	3.7	5.5	-	0
$2U_2^*$	7.40	1.9	2.9	-	0
1U	7.30	2.4	6.1	-	0
2U	7.30	0.9	2.9	-	0
4T	6.20	0	6.6	-	0
3T	5.00	0	1.3	-	0
$3T_2$	5.00	0	1.7	-	0
2T	5.00	0	6.6	-	0
$2T_2$	5.00	0	3.4	-	0
1T	4.20	0	6.6	-	0

TABLE 9 cont.

I Sample	VI $\frac{I(Ta_5Si_3)}{I(Ta_5Si_3)+I(Ta_2Si)}$ after sintering	VII $\frac{I(Ta_2Si)}{I(Ta_2Si)+I(Ta_{4.5}Si)}$ after sintering	VIII $I(Ta_2O_5)$ before sintering	after sintering
P	1.0	-	12	0
Q	1.0	-	12	0
1S	1.0	-	-	0
2S	1.0	-	-	0
3S	1.0	-	-	0
Z	0.87	-	-	0
$2V_1^*$	0.46	1.0	-	2
$2V_2^*$	0.29	1.0	-	1
1V	0.37	1.0	-	9
2V	0.21	0.99	-	2
3W*	0.88	1.0	-	1
1W	0.32	1.0	-	3
2W	0.55	1.0	-	0
3W	0.27	1.0	-	6
4W	0.41	1.0	-	1
$2U_1^*$	0.39	1.0	-	6
$2U_2^*$	0.50	1.0	-	1
1U	0.63	1.0	-	5
2U	0.43	1.0	-	1
4T	0	0.92+Ta	-	1
3T	0	0.83+Ta	-	4
$3T_2$	0	0.99+Ta	-	0
2T	0	0.87+Ta	-	2
$2T_2$	0	0.99+Ta	-	2
1T	0	0.88+Ta	-	2

Since the above reaction is spontaneous as written, $TaSi_2$, Ta_5Si_3, SiO_2(a) is a stable electrode.

Sample Z which had an initial composition of 9.6 wt % Si did not remain in the $TaSi_2$-Ta_5Si_3 field. Assuming that all of the Ta_2O_5 reacted to form lower silicide and SiO_2 the final composition should have been 8.4 wt % Si as silicide. This composition is in the Ta_5Si_3-Ta_2Si field. Samples $2V^*_1$, $2V^*_2$, 1V and 2V also shifted from the $TaSi_2$-Ta_5Si_3 field to the Ta_5Si_3-Ta_2Si field. They also had sufficient Ta_2O_5 to cause such a shift. However, in these last four samples, the silicon losses were surprisingly large as can be seen from column VI. Hence, in addition to silicon loss by sublimation and reaction of higher silicide with Ta_2O_5, a third process which consumes the higher silicide is suspected. Such a reaction might be

$$2\ Ta_5Si_3 + SiO_2(a) \rightleftharpoons 2SiO + 5\ Ta_2Si;$$

$$\Delta G < +\ 43 \pm 54_{kcal}.$$

Since SiO is not produced at 1 atm. partial pressure, only an upper bound on ΔG can be calculated. Samples $2V^*_1$, $2V^*_2$, 1V, and 2V all contained Ta_2O_5 after sintering. The intensities of the strongest Ta_2O_5 peaks in the sintered samples were roughly proportional to the amount of Ta_2O_5 present initially.

Samples 3W*, 3W, and 4W had initial compositions in the Ta_5Si_3-Ta_2Si field (from 8.5 wt % Si to 7.2 wt % Si). The sintered materials were also in this field with column VI in qualitative agreement with the starting compositions of 92 wt % Ta_5Si_3-8 wt % Ta_2Si for 3W* and 61 wt % Ta_5Si_3-39 wt % Ta_2Si for 3W and 4W. Also, the amount of Ta_2O_5 present in the sintered material was in qualitative agreement with the amount

initially added. Since no SiO_2 was present, loss of silicon via SiO formation did not occur. From this group it appears that Ta_5Si_3, Ta_2Si, Ta_2O_5 is a stable electrode.

Samples 1W and 2W also had an initial composition of 61 wt % Ta_5Si_3-39 wt % Ta_2Si. Silica was added and the pellets were sintered. Comparison of column IV for 1W and 2W with column IV for 3W and 4W shows a possible gain of Ta_5Si_3. Also, sample 1W gained a significant amount of Ta_2O_5. This lends further support to the conclusion that Ta_5Si_3, Ta_2Si, Ta_2O_5 is a stable electrode.

Samples ($2U_1^*$, $2U_2^*$) and (1U, 2U) had starting compositions of approximately 15 wt % Ta_5Si_3 and 8 wt % Ta_5Si_3 respectively with the balance Ta_2Si. The sintered samples had Ta_2O_5 present with the intensities of the strongest peaks in qualitative agreement with the amount initially added.

To summarize, all of the evidence from samples 1Z through 2U indicates that Ta_5Si_3, Ta_2Si, Ta_2O_5 is a stable electrode and that the reaction:

$$14\ Ta_5Si_3 + 2\ Ta_2O_5 = 5\ SiO_2(a) + 37\ Ta_2Si$$

is not spontaneous. Then $180 > \Delta G > 0$ kcal. (See Table III).

Samples 4T through 1T had initial compositions in the Ta_2Si-$Ta_{4.5}Si$ field. They did not approach equilibrium after sintering. However, no evidence contradicting the predicted stability of the Ta_2Si, $Ta_{4.5}Si$, Ta_2O_5 electrode was found.

IV. C. EMF Measurements-First Apparatus

Preliminary studies were made in the first apparatus which was described earlier. To test the apparatus the following standard cell was run:

$$Pt/Cu,Cu_2O//0.85\ ZrO_2\text{-}0.15\ CaO//Ni,NiO/Pt \qquad (I)$$

The electrolyte was a 1/2" O.D. by 1/2" high crucible obtained from Zircoa. A mixture of nickel and nickel(ous) oxide powder was tamped into the crucible along with a platinum lead. Two experiments were conducted with the above cell. In the first (Cell I) the lead-wires were fed directly through the rubber stoppers and in the second (Cell Ia) the lead-wires were fed through teflon sleeves inserted in the rubber stoppers. The results of these experiments are listed in Table X. The results were in considerable disagreement with values computed from the data in Wicks and Block(6). However, the data from cell Ia deviated by no more than 2 mv from the data obtained by Steele and Alcock(48) and Kiukkola and Wagner(32). As a result of this good agreement with other investigations it was concluded that the apparatus was satisfactory for EMF measurements at high oxygen partial pressure and that the measurement circuit and technique were adequate.

The cell

$$Pt/Ni,NiO//0.85\ ZrO_2\text{-}0.15\ CaO//TaSi_2,SiO_2(a)/Pt \qquad (II)$$

was then run at 700°C as a first test of the application of oxide electrolytes to EMF measurements on the tantalum silicides. The Ni, NiO electrode was in pellet form and the $TaSi_2$, SiO_2 mixture was tamped into the electrolyte crucible. A voltage of 620 mv was observed after 15 minutes; 420 mv was observed at 30 minutes and the decline continued to 230 mv after 18 hours at 700°C. A ThO_2- 7.5 mol % Y_2O_3 crucible from Zircoa was

Table X

EMF Measurements-First Apparatus

Cell #	Cathode	Electrolyte	Anode	Temperature °C	EMF	Number of Observations
I	Cu,Cu_2O	0.85 ZrO_2- 0.15 CaO Zircoa Crucible	Ni,NiO powder	605	287	1
				698	279	1
				803	280	1
Ia	Cu,Cu_2O	0.85 ZrO_2- 0.15 CaO Zircoa Crucible	Ni,NiO powder	600	287.8	1
				700	282.0	2
				800	272.2	1
III	Ni,NiO	0.85 ZrO_2- 0.15 CaO Zircoa Crucible	Ta,Ta_2O_5 powder	550	760	1
				605	761	2
				700	662	1
				800	351	2
V	Ni,NiO	0.85 ZrO_2- 0.15 CaO Zircoa Crucible	Si,SiO_2 (a) powder	800	458	3

substituted for the ZrO_2–CaO crucible and the experiment was repeated at 700°C. The EMF rose from 275 mv after 84 minutes at temperature to 511 mv after 21 hours at temperature. When the argon was shut off an abrupt decline in EMF occurred. Resumption of the argon purge resulted in a recovery of the EMF. After 23 hours at 700°C the EMF was 531 mv. Since steady state was not yet achieved the run was discontinued. However observation of a voltage from this electrode over an extended period of time at a relatively low temperature was encouraging.

The ability of the system to handle electrodes with low oxygen partial pressures was then tested with cells of known EMF. The cell

$$Pt/Ni,NiO//0.85\ ZrO_2 - 0.15\ CaO//Ta,Ta_2O_5/Pt \qquad (III)$$

was run at temperatures ranging from 550°C to 800°C. The Ta, Ta_2O_5 mixed powder was tamped into the Zircoa crucible along with a platinum lead wire. The results are listed in Table X. The highest voltage observed (761 mv at 605°C) was 129 mv below the expected value as calculated from the data in Wicks and Block(6). Note the strong temperature dependence of the EMF. In Cell V an $Si,SiO_2(a)$ powder was substituted for Ta,Ta_2O_5. The EMF of this cell changed extremely rapidly with temperature. The EMF recorded in Table X for 800°C was 507 mv below the expected value as calculated from Wicks and Block(6). The strong temperature dependence of the EMF and the fact that the measured values were below the expected values indicated that some combination of gas leakage (a kinetic effect) and electronic conduction were causing difficulties with low oxygen partial pressure electrodes.

A final test with a silicide electrode was undertaken with the cell

$$Pt/Ni,NiO//0.925\ ThO_2 - 0.075\ Y_2O_3//TaSi_2,Ta_5Si_3,SiO_2(a)/Pt \qquad (VI)$$

The silicide electrode powder was tamped into the Zircoa crucible along with a platinum foil and lead wire. Steady values were observed for short periods, but they could not be reproduced after thermal cycling. The platinum foil was severely attacked.

From these preliminary experiments it was concluded that the method showed some promise since an EMF was observed for extended periods of time with silicide electrodes. Because of the strong temperature effects observed with the low oxygen partial pressure electrodes it was decided that purification of the argon atmosphere was required. Consequently, the second apparatus was constructed.

IV. D. EMF Measurements-Second Apparatus

1. Knowns-High Oxygen Partial Pressure

The second apparatus for EMF measurements, which was described earlier, was first tested by making measurements on standard cells with high oxygen partial pressure electrodes. In the early runs only the first two units of the gas purification train were present and the gettering agent was copper shot at 300°C. Also, the platinum lead wires were brought through the brass end flanges with ceramic vacuum lead-throughs. The first test was made with the cell

$$Pt/Cu,Cu_2O//0.85\ ZrO_2\text{-}0.15\ CaO//Ni,NiO/Pt \qquad (VII)$$

The Ni,NiO electrode consisted of the mixed powders tamped into the ZrO_2-CaO crucible which was obtained from Zircoa. The results are listed in Table XI. The data are about 1% lower than the data of Steele and Alcock(48). From the data, the value of ΔG_R (1000°K) was -12630 cal/mole of NiO compared with -11950 cal/mole of NiO computed from the data in Wicks and Block(6).

A second test of the apparatus was made with the cell

$$Pt/Ni,NiO//0.925\ ThO_2\text{-}0.075\ Y_2O_3//Fe,Fe_xO/Pt \qquad (VIII)$$

where both electrodes were in pellet form and the electrolyte was a pellet obtained from Zircoa. The results are listed in Table XI. In a later experiment (Cell VIIIa) the same reaction was run with a ThO_2-8 mol % Y_2O_3 electrolyte pellet fabricated according to the procedure described earlier and with teflon lead-throughs substituted for the ceramic lead-throughs. At this point a Zr-12.5 atom % Ti gettering agent was in use. The results are listed in Table XI. In a third cell a ThO_2-6 wt % Y_2O_3-0.2 wt % SiO_2 electrolyte was used to test the effect of SiO_2 additions on EMF measurements at high oxygen partial

Table XI

EMF Measurements On Cells with Two High Oxygen Partial Pressure Electrodes-Second Apparatus

Cell #	Cathode	Electrolyte	Anode	Temperature °C	EMFmv	Number of Observations
VII	Cu,Cu_2O	0.85 ZrO_2-0.15 CaO Zircoa Crucible	Ni,NiO powder	600	284.7	3
				650 ±4	280.8 ±1	2
				700 ±4	276.3 ±1	2
				750	272.2	1
VIII	Ni,NiO	0.925 ThO_2-0.075 Y_2O_3 Zircoa pellet	Fe,Fe_xO	600	245.2	1
				700 ±4	255.2 ±1	1
VIIIa	Ni,NiO	0.92 ThO_2-0.08 Y_2O_3	Fe,Fe_xO	600	244.6	1
				700	254.6	1
				725	257.7	1
				790 ±4	262.7 ±1	1
				825	267.8	1
				910	270.9	1
				975	276.4	1
VIIIb	Ni,NiO	0.93 ThO_2-0.07 Y_2O_3 (0.2 wt % SiO_2)	Fe,Fe_xO	700	255.7	3
				800 ±4	265.0 ±1	4
				900 ±4	275.7 ±1	3
				995	284.5	2

pressures. At this point the complete gas purification train was in operation. The results are listed in Table XI. The three sets of data are in good agreement with the data of Steele and Alcock(48), with the expected EMF values computed from the data compiled in Wicks and Block(6), and with each other.

From the results of the above experiments it was concluded that the second EMF apparatus is adequate for measurements on cells with a pair of high oxygen partial pressure electrodes with the first two units of the gas purification train as well as with the complete purification train. Also, from cells VIII, VIIIa, and VIIIb it was concluded that there is little difference between Zircoa electrolytes and electrolytes fabricated by the procedures described earlier and that SiO_2 addition has no appreciable effect upon EMF measurements at relatively high oxygen partial pressure.

IV. D. 2. Knowns-Low Oxygen Partial Pressure

The second apparatus was subsequently tested with cells of calculable EMF with one or both electrodes exhibiting low oxygen partial pressure . Successful measurements with such cells were a necessary requirement for subsequent experiments with silicide electrodes. The early measurements were made with only the first and second units of the gas purification train in operation and with the lead wires brought through ceramic lead-throughs in the brass end flanges. The gettering agent was copper shot at 300°C.

The first cell

$$Pt/Ni,NiO//0.85\ ZrO_2\text{-}0.15\ CaO//Ta,Ta_2O_5/Pt \qquad (IX)$$

where the electrolyte was a Zircoa crucible with the Ta,Ta_2O_5 powder tamped inside along with the platinum lead wire gave no steady EMF over prolonged periods of time. Disassembly of the apparatus revealed that the negative lead wire was in contact with the radiation shields and that the lower lead wire had separated from the platinum foil causing an open circuit. The system was repaired and reassembled (Cell IXa) and steady EMFs well below the expected values were observed. The results are listed in Table XII. The fairly strong temperature dependence of the EMF indicates that gas leakage at one or both electrodes was occurring in addition to possible electronic conduction.

Substitution of a ThO_2 - 15 mol % $YO_{1.5}$ crucible obtained from Zircoa resulted in improved results (Cell X). The cell was run for a period of four days with the EMFs improving from day to day with respect to the expected values. The results for the fourth day are presented in Table XII. A strong temperature effect was again noted. The average transport number at 1000°C where the strength of the temperature dependence is

Table XII

EMF Measurements On Cells with One or Two Low Oxygen Partial Pressure Electrodes-Second Apparatus

Cell #	Cathode	Electrolyte	Anode	Temperature °C	EMF	Number of Observations
IXa	Ni,NiO	0.85 ZrO_2-0.15 CaO Zircoa Crucible	Ta,Ta_2O_5 powder	600	529	1
				700	564	1
				800 ±4	576 ±9	11
				900	609	1
X	Ni,NiO	0.925 ThO_2-0.075 Y_2O_3	Ta,Ta_2O_5 powder	500	500	1
				600	554	1
				700	643	1
				800 ±4	751 ±5	1
				900	817	1
				950	840	1
				1000	851	1
Xa	Ni,NiO	0.925 ThO_2-0.075 Y_2O_3 Zircoa Disc and Crucible	Ta,Ta_2O_5 powder	900	821 ±15	3
Xb	Ni,NiO	0.925 ThO_2-0.075 Y_2O_3 Zircoa disc	Ta,Ta_2O_5	800	570	2
				900 ±4	675 ±3	2

Table XII (cont.)

Cell #	Cathode	Electrolyte	Anode	Temperature °C	EMF	Number of Observations
XI	Ni,NiO	0.925 ThO_2 - 0.075 Y_2O_3 Zircoa disc	Cr,Cr_2O_3	500 600 700 ±4 800	230 280 340 ±10 400	1 1 1 1
XII	Cr,Cr_2O_3	0.925 ThO_2 - 0.075 Y_2O_3 Zircoa disc	Ta,Ta_2O_5	890 ±4 980 ±4	158 220	1 1
XIII	Fe,Fe_xO	0.925 ThO_2 - 0.075 Y_2O_3 Zircoa disc	Ta,Ta_2O_5	600 800 900 970 ±4 990	310 510 545 ±5 562 574	1 1 2 1 1
XIIIa	Fe,Fe_xO	0.925 ThO_2 - 0.075 Y_2O_3 Zircoa disc	Ta,Ta_2O_5	800 900 ±4 1000	510 550 585	1 1 1
XIV	Ni,NiO	0.93 ThO_2 - 0.07 Y_2O_3 4 hrs, 1950°C	Cr,Cr_2O_3	600 700 ±10 900	505 620 ±10 770	2 1 1
XV	Cr,Cr_2O_3	0.93 ThO_2 - 0.07 Y_2O_3 32 hrs, 1950°C	Ta,Ta_2O_5	900 ±10	154 ±6	3

Table XII (cont.)

Cell #	Cathode	Electrolyte	Anode	Temperature °C	EMF	Number of Observations
Xc	Fe,Fe_xO	0.93 ThO_2 - 0.07 Y_2O_3 4 hrs, 1950°C	Ta,Ta_2O_5	700 ±10	337 ±10	4
				750 ±5	407 ±10	5
				800 ±5	452 ±10	6
				850 ±5	488 ±10	6
				900 ±5	512 ±20	6
				950 ±5	546 ±15	7
				1000 ±5	560 ±10	7
XIIIb	Ni,NiO	0.93 ThO_2 - 0.07 Y_2O_3 4 hrs, 1950°C	Ta,Ta_2O_5	700	595	1
				750	668	1
				800	726	1
				850 ±5	766 ±5	2
				900	792	1
				950	807	1
				1000	813	1
Xd	Fe,Fe_xO	0.925 ThO_2 - 0.075 Y_2O_3 3 hrs, 2100°C ρ = 88.5% thickness 0.181"	Ta,Ta_2O_5	720	596	1
				800 ±4	608 ±2	2
				900	606	2
				1000	604	2
Xe	Fe,Fe_xO	0.925 ThO_2 - 0.075 Y_2O_3 3 hrs, 2000°C ρ = 87.5% thickness 0.170"	Ta,Ta_2O_5	700	546 ±25	1
				750	556 ±10	2
				800	586 ±15	3
				850 ±5	589 ±2	2
				900	598 ±5	3
				950	600 ±2	3
				1000	597 ±2	3

Table XII (cont.)

Cell #	Cathode	Electrolyte	Anode	Temperature °C	EMF	Number of Observations
Xf	Fe,Fe_xO	0.925 ThO_2–0.075 Y_2O_3 3 hrs, 2100°C thickness 0.078"	Ta,Ta_2O_5	700	608	3
				750	612	2
				800	613	3
				850 ±7	611 ±4	2
				900	609	3
				950	604	2
				1000	598	2
Xg	Fe,Fe_xO	0.93 ThO_2–0.07 $YO_{1.5}$ 3 hrs, 2000°C thickness 0.133"	Ta,Ta_2O_5	700	598	2
				750	605	2
				800	605	3
				850 ±8	606 ±3	2
				900	605	2
				950	603	2
				1000	599	2
Xh	Fe,Fe_xO	0.99 ThO_2–0.01 Y_2O_3 3 hrs, 2000°C	Ta,Ta_2O_5	650	620	1
				700	613	3
				750	612	2
				800	607	4
				850 ±5	603 ±2	2
				900	601	3
				950	598	2
				1000	595	2

Table XII (cont.)

Cell #	Cathode	Electrolyte	Anode	Temperature °C	EMF	Number of Observations
Xi	Fe,Fe_xO	0.93 ThO_2-0.07 Y_2O_3 (0.2 wt % SiO_2)	Ta,Ta_2O_5	600	620	1
				650	625	1
				700	622	2
				750	617	2
				800 ±5	610 ±2	3
				850	605	2
				900	602	3
				950	602	2
				1010	599	2
Xj	Fe,Fe_xO	0.99 ThO_2—0.01 Y_2O_3	Ta,Ta_2O_5	700	619	2
				800	613	4
				900 ±5	604 ±2	4
				1010	597	2
X	Mean Values Xd through Xj			700	618	
				800	610	
				900	604 ±2	
				1000	598	

weakest was 0.957. The run was repeated with a ThO_2-7.5 mol % Y_2O_3 disc inserted between the Ni,NiO pellet and the base of the crucible (Cell Xa). The observed voltage at 900°C was not appreciably different from the voltage observed in Cell X. A slight sensitivity to argon flow rate was noted. The fact that Cells X and Xa gave the same results at 900°C leads to the conclusion that the kinetic or gas leakage effect occurred at the Ta,Ta_2O_5 electrode. A third experiment with Ni,NiO versus Ta,Ta_2O_5 (Cell Xb) where the electrolyte was a ThO_2-7.5 mol % Y_2O_3 disc obtained from Zircoa and the Ta,Ta_2O_5 electrode was porous as in Plate II gave poorer results than Cells X and Xa.

A cell (XI)

$$Pt/Ni,NiO//0.925\ ThO_2-0.075\ Y_2O_3//Cr,Cr_2O_3/Pt \qquad (XI)$$

where the electrolyte was a disc obtained from Zircoa and the Cr,Cr_2O_3 electrode was a porous pellet, did not give the expected EMFs. A strong temperature effect was observed (see Table XII).

Also, Cell XII

$$Pt/Cr,CrO_3//0.925\ ThO_2-0.075\ Y_2O_3//Ta,Ta_2O_5/Pt \qquad (XII)$$

where both electrodes were porous pellets and the electrolyte was a disc obtained from Zircoa did not exhibit the expected EMFs. In this and subsequent experiments the gettering agent was Zr 12.5 atom % Ti alloy chips at 375°C. The interactions with the inert atmosphere were strong enough to generate an EMF larger than the expected value.

Cells XIII and XIIIa,

$$Pt/Fe,Fe_xO//0.925\ ThO_2-0.075\ Y_2O_3//Ta,Ta_2O_5/Pt \qquad (XIII)$$

where the electrolyte was a Zircoa disc and the Ta,Ta_2O_5 electrode was a porous pellet similar to Plate II, did not develop the expected EMFs. The results are listed in Table XII. A strong temperature effect was again evident.

As a result of the difficulties encountered with low oxygen partial pressure electrodes it was decided that electrolytes should be fabricated as described earlier in order to have control over their purity. Zircoa electrolytes were thought to contain appreciable quantities of impurities which could have a detrimental effect upon electronic properties at low oxygen partial pressure. The first run conducted with electrolytes fabricated in our laboratory as described earlier was

$$Pt/Ni,NiO//0.93\ ThO_2 - 0.07\ Y_2O_3//Cr,Cr_2O_3/Pt \qquad (XIV)$$

The results are listed in Table XII. They were considerably better than those of Cell XI. However they were below the expected values and a strong temperature effect was still evident.

The ceramic lead-throughs were replaced with teflon lead-throughs and the cell

$$Pt/Cr,Cr_2O_3//0.93\ ThO_2 - 0.07\ Y_2O_3//Ta,Ta_2O_5/Pt \qquad (XV)$$

was run. Measurements at 900°C were close to the expected value of 152 mv calculated from the data of Wicks and Block(6). However measurements were made for short times only and a decline of the EMF with time was noted.

After this experiment the last three units of the gas purification train were built and added. The first Zr-12.5 atom % Ti getter column was operated at 425°C and the second was operated at 375°C. The Ta getter column was generally operated at 600°C.

Cells of type X and XIII were examined. The pair Xc and XIIIb employed the same electrolyte and Ta,Ta_2O_5 electrode; only the high oxygen partial pressure electrode was changed. The Ta,Ta_2O_5 electrode was similar to the porous sample shown in Plate II. The results for these cells are listed in Table XII. For Cell Xc a large number of observations were made. The data

showed considerable scatter. The data taken by cooling did not agree with the data taken by heating. The former values generally exceeded the latter. The data did not vary with variations of the Ta getter temperature between room temperature and 800°C. If the cell reaction for Xc is subtracted from the cell reaction for XIIIb, the cell reaction for Cell VIII (Ni,NiO vs Fe,Fe_xO) is obtained. The differences in EMF between XIIIb and Xc compare favorably with the results for Cells VIII through VIIIb. Therefore, it was concluded that the difficulties encountered with cells containing Ta,Ta_2O_5 electrodes lay with these electrodes. The problem was solved by producing dense Ta,Ta_2O_5 electrodes similar to the one shown in Plate III. Results for dense Ta,Ta_2O_5 electrodes versus Fe,Fe_xO are presented in Table XII (Cells Xd through Xj). Cells Xd, Xe, Xf, and Xg show a strong positive temperature coefficient at 700°C or above. However, only Cell Xe shows a strong temperature effect at 900°C. The EMFs of Cells Xd, Xe, Xf, and Xg at 900°C were compared with the relative resistances of the electrolytes. No correlation was found. The effect of gas flow rate was tested in Cell Xj. No change in EMF was noted at 800°C and 900°C when the flow rate was increased from 1CFH to 3CFH. Hence, in Cell Xj where the temperature dependence of the EMF was of the expected magnitude and sign the gas phase interaction with the Ta,Ta_2O_5 electrode was negligible. The same was true for the other cells where dE/dT had the expected magnitude and sign. Average values for cells Xd through X_j were computed using data only from those cells exhibiting the proper sign of dE/dT at a particular temperature. The results are listed in Table XII. The temperature dependence of the data is close to the expected temperature dependence. However the magnitude of the EMF values is below the expected values. Since gas flow

rate had no effect on Cell Xj it is concluded that electronic conduction was occurring. At lower temperatures in cells where dE/dT became positive both electronic conduction and a gas-electrode interaction were occurring. The expected values for Cells X and XIII are plotted in Figure 7. Data for Cells Xc and XIIIb where porous Ta,Ta_2O_5 electrodes were employed are also shown in Figure 7. Finally averaged data for Cells Xd through Xj where dense Ta,Ta_2O_5 electrodes were employed are plotted. One can see that the slope of the line fitted to the average values for Cells Xd through Xj is in excellent agreement with the slope of the line fitted to the expected values.

Several other low oxygen partial pressure standard cells were examined. In all of the following cells the teflon lead-throughs and the complete gas purification train were in place. The cell

$$\underset{\substack{\\ 1950^{\circ}C,\ 4\ hrs \\ \rho = 89.8\%}}{Pt/Ni,NiO//0.93\ ThO_2\text{-}0.07\ Y_2O_3} \underset{1150^{\circ}C,\ 10\ min}{//C,SiC,SiO_2(a)//Ni/Pt} \qquad (XVI)$$

was expected to exhibit the reaction

$$SiC + 2NiO = 2Ni + SiO_2(a) + C \qquad (52)$$

with an expected value of 917 mv at $1200^{\circ}K$. At $1000^{\circ}C$ the maximum voltage observed was approximately 570 mv. The voltage declined steadily with time.

The cell

$$\underset{\substack{\\ 1950^{\circ}C,\ 4\ hrs \\ \rho = 89.8\%}}{Pt/Ni,NiO//0.93\ ThO_2\text{-}0.07\ Y_2O_3} \underset{1350^{\circ}C,\ 5\ min.}{//Si,SiO_2(a)/Ni/Pt}$$

exhibited a maximum EMF of 320 mv at $1000^{\circ}C$ compared with an expected value of 965 mv. The cell voltage decreased with time.

FIGURE 7. EMF Data for the Cells

$$Pt \left| \begin{matrix} Fe, Fe_xO \\ or \\ Ni, NiO \end{matrix} \right| \left| \left| ThO_2\text{-}Y_2O_3 \right| \right| Ta, Ta_2O_5 \left| Pt \right.$$

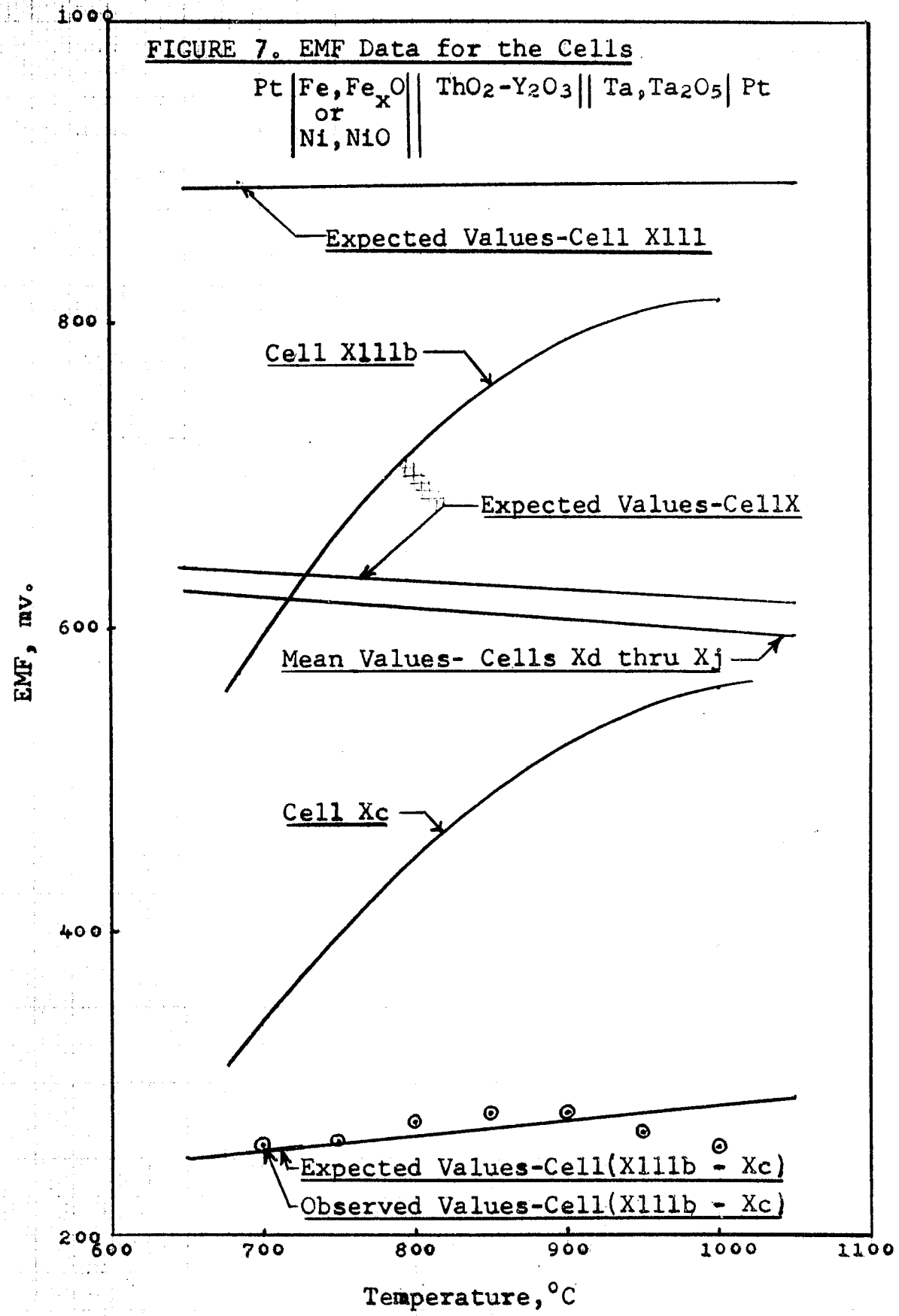

The cell

$$\underset{\text{porous}}{Pt/Ta,Ta_2O_5}//0.93\ ThO_2\text{-}0.07\ Y_2O_3//Si,SiO_2(a)/Ta/Pt \quad (XVIII)$$

$2150^{\circ}C$, 3 hrs; $\rho = 90.3\%$ — $1350^{\circ}C$, 5 min

developed a maximum EMF of 9 mv at $1000^{\circ}C$ compared with an expected value of 70 mv. The cell

$$Pt/Ni,NiO//0.93\ ThO_2\text{-}0.07\ Y_2O_3//Si,\text{Silica gel}/Ta/Pt \quad (XIX)$$

$1950^{\circ}C$, 4 hrs; $\rho = 89.3\%$ — $1325^{\circ}C$, 5 min

exhibited a maximum EMF of 510 mv at $1000^{\circ}C$ compared with the expected value of 965 mv. The voltage declined steadily with time. Finally, the cell

$$Pt/Ni,NiO//0.93\ ThO_2\text{-}0.07\ Y_2O_3//Si(\text{single crystal})/Ta/Pt \quad (XX)$$

$1950^{\circ}C$, 4 hrs; $\rho = 89.0\%$

developed a maximum EMF of 595 mv at $1000^{\circ}C$ compared to an expected value of 965 mv; and again, the EMF declined with time.

This concludes the results for EMF measurements on cells with calculable voltages with low oxygen partial pressure electrodes. The results for dense Ta,Ta_2O_5 electrodes were of good quality whereas the results for porous electrodes (Cr,Cr_2O_3; Ta,Ta_2O_5; Si,SiO_2; SiO_2, C,SiC) were poor. Similar behavior should be expected with silicide electrodes.

IV. D. 3. Transport Properties of ThO_2-Y_2O_3 Electrolytes and Kinetic Effects in Porous Ta,Ta_2O_5 Electrodes

Since the deviation of the average values from the expected values was due essentially only to electronic conduction in dense Ta,Ta_2O_5 electrodes the data may be used to compute the local and average transport numbers of thoria-yttria electrolytes. p_θ is first calculated from equation (49) with p_{O_2}'' calculated from the data for Ta_2O_5 in Wicks and Block(6) and p_{O_2}' calculated from the data for Fe_xO in Charette and Flengas(74). The calculations were done for a temperature of 1300°K with the results

$$p_\theta = 2.59 \times 10^{-29} \text{ for } m = 4$$

$$p_\theta = 8.60 \times 10^{-33} \text{ for } m = 6$$

With p_θ in hand one can calculate E and E_m as a function of p_{O_2}'' with respect to p_{O_2}' for Fe,Fe_xO at 1300°K using equations (22) and (49) respectively. The local transport number, t_i, is calculated from

$$t_i = e^{4F(E_m - E)/mRT} \tag{53}$$

and the effective or average transport number is

$$\bar{t}_i = \frac{E_m}{E} \tag{51}$$

Equation (53) is readily derived from the following equation due to Schmalzried(33)

$$t_i = \left(1 + \left(\frac{p_{O_2}}{p_\theta}\right)^{-\frac{1}{m}}\right)^{-1} \tag{48}$$

and equations (22) and (50). Using the average transport numbers and the cell model shown in Figure 8 one can estimate

the polarization current from

$$i_p = \frac{E}{R_i}(1 - \bar{t}_i) = \frac{E - E_m}{R_i} \qquad (54)$$

where R_i = the resistance of the electrolyte in the ionic mode, ohms

R_e = the resistance of the electrolyte in the electronic mode, ohms

i_p = the polarization current, amps.

and

$$R_i = \frac{\rho_i L}{A} = \frac{L}{\sigma_i A} \qquad (55)$$

where ρ_i = ionic resistivity, ohm-cm.

σ_i = ionic conductivity, mho-cm.$^{-1}$

A = cross sectional area of the electrolyte, cm.^{2}

L = thickness of the electrolyte, cm.

With an average electrolyte diameter of 3/8" (0.95 cm), average thickness of 0.1" (0.25 cm), and $\sigma_i = 2.5 \times 10^{-3}$ mho - cm^{-1} for thoria-15 mol % $YO_{1.5}$ (48) equation (54) becomes

$$i_p = 7.8(E - E_m)10^{-6} \text{ amps} \qquad (56)$$

where the EMFs are in millivolts.

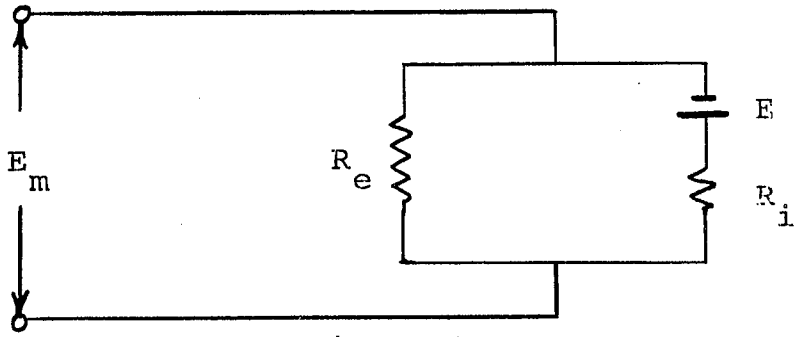

Figure 8
Equivalent Circuit

The results of all of the calculations discussed above are presented in Table XIII. The calculations were performed for m = 4 (predicted from theory) and m = 6 (since vacancy clustering tends to occur at low transport numbers). E_m vs E is plotted in Figure 9 and $\bar{t}_i, t_i$ and i_p are plotted against $(-\log p_{O_2}^{\bullet\bullet})$ in Figure 10. From these graphs corrections can be made for other cells exhibiting electronic conduction. Of course, no correction is possible for polarization effects which may be appr ciable if t_i differs appreciably from unity.

With data for a porous Ta,Ta_2O_5 electrode and a dense Ta,Ta_2O_5 electrode available, some insight into the nature of the kinetic effect in porous electrodes can be gained. The EMF produced by the dense electrode is given by equation (50). The EMF generated by the porous electrode (Cell Xc) can be represented by

$$E_m = \frac{-mRT}{nF} \ln \frac{p_{eff}^{\frac{1}{m}}}{p_{O_2}^{\bullet\ \frac{1}{m}}} \qquad (57)$$

where p_{eff} is the effective oxygen partial pressure

E_{mp} is the EMF observed for a porous electrode.

The effective oxygen partial pressure may be written as

$$P_{eff} = \left[p_\Theta^{\frac{1}{m}} + p_{O_2}^{\bullet\bullet\ \frac{1}{m}} + \left(f(t,v) p_{O_2}^{\bullet\ \frac{1}{m}} \right) \right]^m \qquad (58)$$

where f(T,v) is some function of temperature and argon flow rate.

Table XIII

Transport Properties and Polarization Current For Thoria 7 wt % Yttria Electrolytes at 1300°K With an Fe,Fe_xO Reference Electrode

		(m = 4)				(m = 6)			
$p_{O_2}^{oo}$	E	E_m	$\bar{t}_i$	t_i	i_p	E_m	$\bar{t}_i$	t_i	i_p
10^{-20}	361	361	1	1	0	361	1	1	0
10^{-21}	426	425	.998	.990	7.8×10^{-6}	424	.996	.988	1.6×10^{-5}
10^{-22}	490	488	.997	.982	1.6×10^{-5}	486	.993	.976	3.1×10^{-5}
10^{-23}	555	550	.992	.956	3.9×10^{-5}	549	.989	.965	4.7×10^{-5}
10^{-24}	619	612	.989	.939	5.5×10^{-5}	612	.989	.959	5.5×10^{-5}
10^{-25}	685	670	.979	.875	1.2×10^{-4}	673	.983	.931	9.3×10^{-5}
10^{-26}	750	726	.968	.807	1.7×10^{-4}	735	.980	.914	1.2×10^{-4}
10^{-27}	813	775	.953	.712	3.0×10^{-4}	790	.973	.871	1.8×10^{-4}
10^{-28}	878	817	.931	.580	4.8×10^{-4}	845	.963	.820	2.6×10^{-4}
10^{-29}	943	850	.902	.435	7.3×10^{-4}	895	.949	.750	3.7×10^{-4}
10^{-30}	1007	875	.869	.307	1.0×10^{-3}	943	.936	.681	5.0×10^{-4}

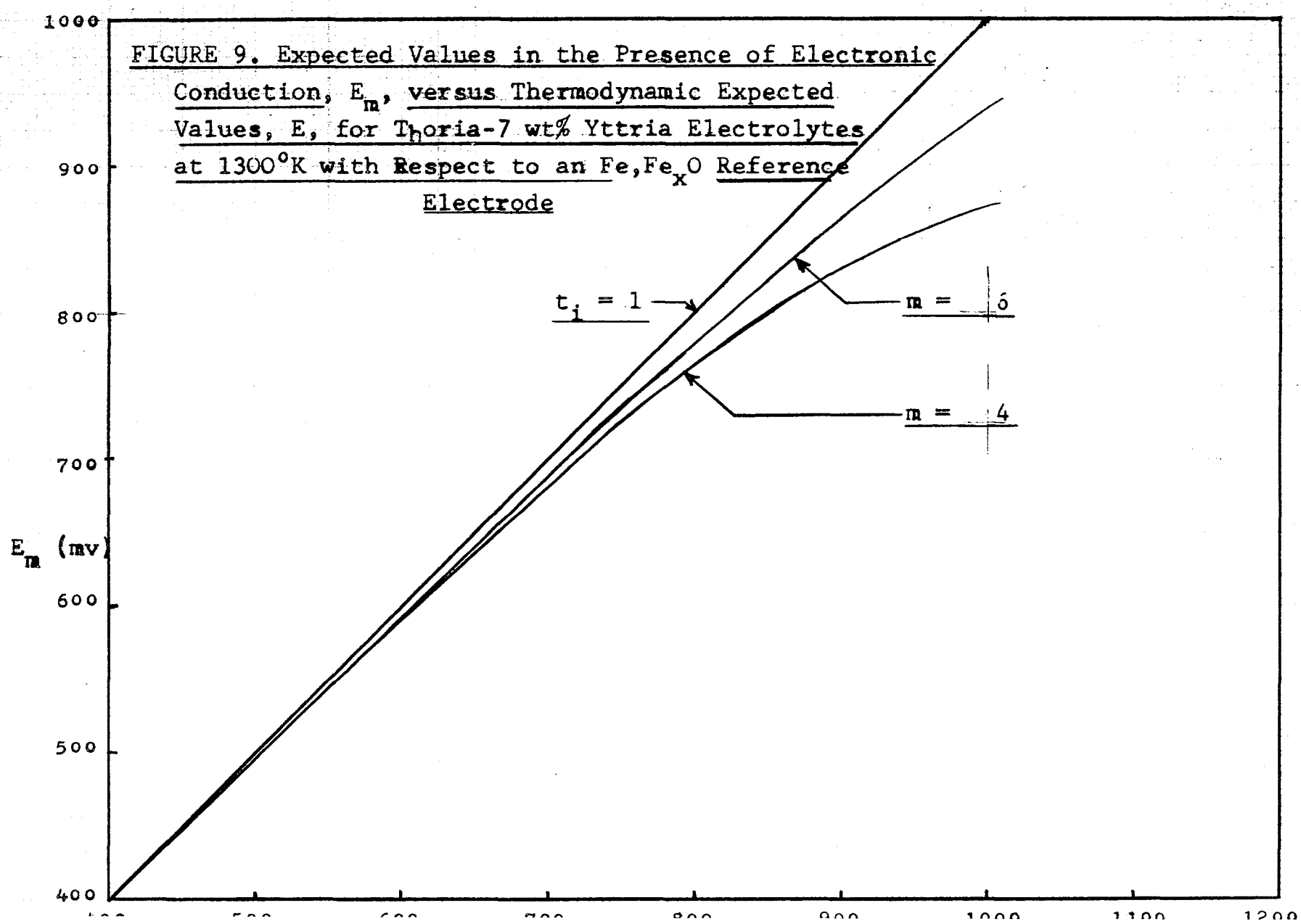

FIGURE 9. Expected Values in the Presence of Electronic Conduction, E_m, versus Thermodynamic Expected Values, E, for Thoria-7 wt% Yttria Electrolytes at 1300°K with Respect to an Fe,Fe_xO Reference Electrode

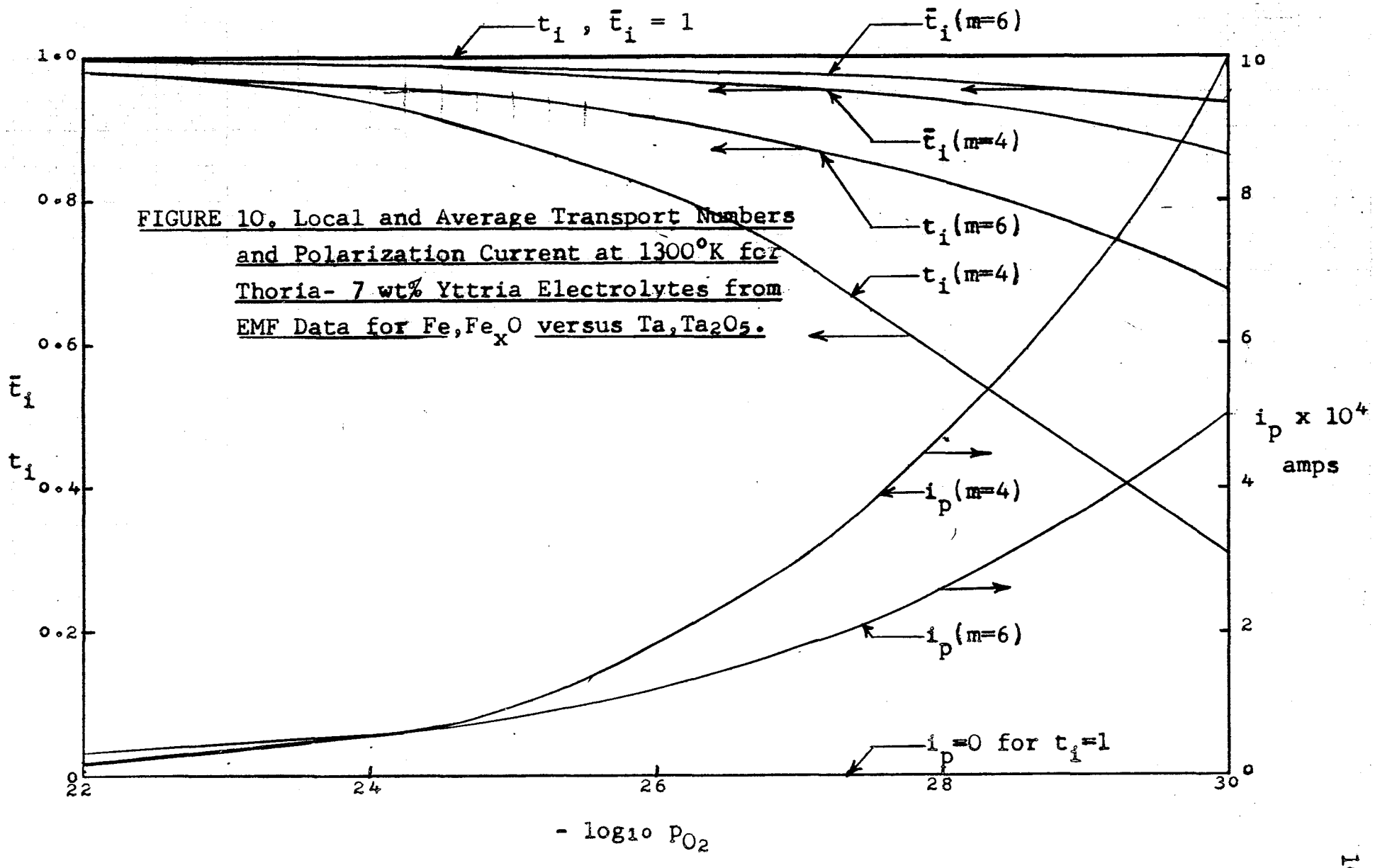

FIGURE 10. Local and Average Transport Numbers and Polarization Current at 1300°K for Thoria- 7 wt% Yttria Electrolytes from EMF Data for Fe, Fe_xO versus Ta, Ta_2O_5.

Equations (50), (57) and (58) may be combined to give

$$\left[e^{\frac{-nFEmp}{mRT}} - e^{\frac{-nFEm}{mRT}} \right]^{m} = f(T,v) \qquad (59)$$

Two forms for the excess pressure term, $f(T,v)$, that may be considered are

$$f(T,v) = \frac{k\sqrt{T}}{v} \qquad (60)$$

$$f(T,v) = \frac{ke^{+\Delta H/RT}}{v} \qquad (61)$$

The nature of the gas velocity dependence can not be established since the gas flow rate was held constant for Cell Xc. However, the nature of the temperature dependence can be established with the data for Cell Xc. The calculations are summarized in Table XIV.

Table XIV

The Effect of Temperature on Porous Ta,Ta_2O_5 Electrodes

$T^{o}K$	$\frac{1}{T} \times 10^{4}$	$\log_{10}T$	$f(T,v)$	$\log_{10}f(T,v)$
973	10.28	2.908	5.81×10^{-8}	- 7.24
1023	9.76	3.010	2.57×10^{-9}	- 8.59
1073	9.31	3.031	3.22×10^{-10}	- 9.49
1123	8.90	3.050	6.20×10^{-11}	-10.21
1173	8.52	3.069	7.51×10^{-12}	-11.13
1223	8.17	3.087	1.19×10^{-12}	-11.93
1273	7.85	3.105	3.71×10^{-13}	-12.43

The temperature dependence of equation (60) did not fit the data since a plot of $\log_{10} f(T,v)$ versus $\log_{10}(T)$ was not linear. A plot of $\log_{10} f(T,v)$ versus $1/T$ was linear. From its slope ΔH was 97.6 kcal. Such a large activation energy can not be attributed to any conductivity mode of the electrolyte or the high temperature oxidation of tantalum.

IV. D. 4. EMF Measurements on Silicide Electrodes: Ta_5Si_3-$TaSi_2$ Phase Field

The results of EMF measurements on silicide electrodes with the second apparatus will now be presented. All measurements were made with the apparatus in the final condition; lead wires were brought out of the cell through teflon lead-throughs and the complete gas purification train was in operation. The results are presented by phase fields. For the $TaSi_2$-Ta_5Si_3 phase field, from Table II, the expected electrode reaction was

$$5\ TaSi_2 + 14\ O^{=} = 7\ SiO_2(a) + Ta_5Si_3 + 28e^{-}$$

with expected values of 634 $\pm$65 mv at 1000°K and 613 $\pm$65 mv at 1300°K with respect to an Fe,Fe_xO reference electrode. Measurements were also made with Ni,NiO reference electrodes and Ta,Ta_2O_5 reference electrodes. For the above half-cell reaction, the expected values with respect to an Ni,NiO reference electrode were 890 $\pm$ 65 mv at 1000°K and 889 $\pm$65 mv at 1300°K. The expected values were 0 $\pm$65 mv at 1000°K and 3 $\pm$65 mv at 1300°K with respect to a Ta,Ta_2O_5 reference electrode.

The first column of Table XV lists the composition of the electrode as computed from the starting materials. The second column lists the heat treatments and sintering operations performed. Heat treatments (H.T.) were performed with the reacted Ta and Si after refabrication into pellets and presintering to remove the binder. Then the oxide and/or nickel powders were added and the sintering operation (S.) was performed. The third column gives X-ray results on the interface placed in contact with the electrode in terms of the intensity

Table XV

EMF Measurements Employing Half-Cells Formulated From The $TaSi_2$-Ta_5Si_3 Two-Phase Field

Silicide Electrode Composition	Heat Treatment and Sintering	$\frac{I(TaSi_2)}{I(TaSi_2)+I(Ta_5Si_3)}$	Reference Electrode	Electrolyte	Temp °C	EMF mv	Number of Observations
1)							
65 wt % $TaSi_2$	H.T. 1650°C,	0.08	Ni,NiO	0.93 ThO_2-	750	s307±10	1
	40 min.				800	s352±40	3
21 wt % Ta_5Si_3	S. 1500°C			0.07 Y_2O_3	850	s370±40	3
14 wt % SiO_2	20 min.			2050°C, 3 hrs	900 ±5	s397±40	3
				ρ = 89.7%	950	s428±45	3
					1000	s463±50	3
					1050	s495±10	1
2)							
65 wt % $TaSi_2$	H.T. 1650°C,	0.02	Fe,Fe_xO	0.93 ThO_2-	750	s173±20	2
	40 min.				800	s249±50	3
21 wt % Ta_5Si_3	S. 1650°C,			0.07 Y_2O_3	850	s276±60	4
14 wt % SiO_2	20 min			2050°C, 3 hrs	900 ±5	s313±60	6
				ρ = 89.7%	950	s363±40	5
					1000	s397±30	3
					1050	s414±15	1
3)							
$TaSi_2$	S. 1600°C,	0.70	Fe,Fe_xO	0.93 ThO_2-	900 ±5	300±15	2
	10 min.				1000	404±10	2
				0.07 Y_2O_3			
				1950°C, 4 hrs			
				ρ = 97.7%			

Table XV (cont.)

Silicide Electrode Composition	Heat Treatment and Sintering	$\frac{I(TaSi_2)}{I(TaSi_2)+I(Ta_5Si_3)}$	Reference Electrode	Electrolyte	Temp °C	EMF mv	Number of Observations
4)					800	s-0.3	4
$TaSi_2$	S. 1600°C,	0.91	Ta,Ta_2O_5	0.93 ThO_2-	850	s-0.2	1
0.5 wt % Ni	10 min.			0.07 Y_2O_3	900 ±5	s-0.2	4
				1950°C, 4 hrs	950	s-0.1	1
				ρ = 88%	1000	s+0.1	3
5)					700	s-0.2	2
39 wt % $TaSi_2$	S. 1500°C	0.10	Ta,Ta_2O_5	0.92 ThO_2-	750	s+0.9	2
54 wt % Ta_5Si_3	15 min.			0.08 Y_2O_3	800	s+1.6	1
7 wt % SiO_2				1925°C, 3 hrs	850 ±5	s+1.6	1
				ρ = 90.4%	900	s+1.4	1
					950	s+1.5	1
6)					900	550	1
67 wt % $TaSi_2$	H.T. 1600°C,	0.76	Fe,Fe_xO	0.92 ThO_2-	1000 ±5	640	1
21 wt % Ta_5Si_3	15 min.			0.08 Y_2O_3			
11 wt % SiO_2	S. 1600°C,			1925°C, 3 hrs			
0.5 wt % Ni	15 min.			ρ = 89.5%			
7)					800	s338±15	4
67 wt % $TaSi_2$	H.T. 1600°C,	0.76	Fe,Fe_xO	0.99 ThO_2-	900 ±5	s431±5	2
21 wt % Ta_5Si_3	15 min.			0.01 Y_2O_3	1000	s537±15	3
11 wt % SiO_2	S. 1600°C,			2000°C, 3 hrs			
	15 min.			ρ = 94%			

Table XV (cont.)

Silicide Electrode Composition	Heat Treatment and Sintering	$\frac{I(TaSi_2)}{I(TaSi_2)+I(Ta_5Si_3)}$	Reference Electrode	Electrolyte	Temp °C	EMF mv	Number of Observations
8) 71 wt % $TaSi_2$ 23 wt % Ta_5Si_3 5 wt % SiO_2 0.7 wt % Ni	S. 1600°C, 15 min.	0.70	Fe,Fe_xO	0.99ThO_2- 0.01 Y_2O_3 2000°C, 3 hrs ρ = 94%	1000 ±5	656	1
9) 71 wt % $TaSi_2$ 23 wt % Ta_5Si_3 5 wt % SiO_2 0.7 wt % Ni	S. 1600°C, 15 min.	0.60	Fe,Fe_xO	0.99 ThO_2- 0.01 Y_2O_3 2000°C, 3hrs ρ = 98.3%	800 900 ±5 1000	s245 585 ---	1
10) 71 wt % $TaSi_2$ 23 wt % Ta_5Si_3 5 wt % SiO_2 0.7 wt % Ni	S. 1600°C, 15 min.	0.60	Fe,Fe_xO	0.99 ThO_2- 0.01 Y_2O_3 2000°C, 3 hrs ρ = 98.3%	1000 ±5	566 ±20	4

Table XV (cont.)

Silicide Electrode Composition	Heat Treatment and Sintering	$\frac{I(TaSi_2)}{I(TaSi_2)+I(Ta_5Si_3)}$	Reference Electrode	Electrolyte	Temp °C	EMF mv	Number of Observations
11) 74 wt % $TaSi_2$ 23 wt % Ta_5Si_3 3 wt % SiO_2 0.7 wt % Ni	S. 1600°C, 15 min.	0.50	Fe,Fe_xO	0.99 ThO_2- 0.01 Y_2O_3 2000°C, 3 hrs ρ = 92%	900 ±5 1000	s472±10 s658±40	3 4
12) 74 wt % $TaSi_2$ 23 wt % Ta_5Si_3 3 wt % SiO_2 0.7 wt % Ni	S. 1600°C, 15 min.	0.67	Fe,Fe_xO	0.99 ThO_2- 0.01 Y_2O_3 2000°C, 3 hrs ρ = 94%	800 900 1000 ±5 1050 1080	~390 <500 634 651 669	1 1 1 1 1
13) 74 wt % $TaSi_2$ 23 wt % Ta_5Si_3 3 wt % SiO_2 0.7 wt % Ni	S. 1600°C, 15 min.	0.83	Fe,Fe_xO	0.99 ThO_2- 0.01 Y_2O_3 2000°C, 3 hrs ρ = 94%	1000 1050 1100	560 648 692	1 2 1

of the strongest $TaSi_2$ peak divided by the total of the intensities of the strongest $TaSi_2$ peak and the strongest Ta_5Si_3 peak. The EMF column gives average EMFs based on the number of observations indicated along with the range of these values. The letter "S" preceding an EMF value indicates that it was stable over a prolonged period of time.

The first two electrodes listed in Table XV lost considerable amounts of silicon as a result of prolonged heat treatments. These electrodes were quite porous. Their surface layers were removed and a center section was placed in contact with the electrolyte. Both gave strongly temperature dependent EMFs. Individual EMFs were stable over prolonged periods of time. However reproducibility was poor as indicated by the large spread in the mean values listed. EMFs obtained along cooling curves were greater than EMFs obtained along heating curves. The strong temperature dependence and hysteresis behavior were similar to the behavior of porous tantalum, tantalum oxide electrodes. However, with the silicide electrodes the difference in EMF between the first and second cells listed in Table XV does not correspond to the expected value for the cell Ni,NiO vs Fe,Fe_xO. Also, the difference between the expected values and the observed values were greater for the silicide electrodes than for the Ta,Ta_2O_5 electrodes. These observations indicate that the kinetics of the desired electrode reaction with the silicide electrodes are slower than the kinetics for Ta,Ta_2O_5 electrodes.

The third electrode, which was fabricated from $TaSi_2$ without nickel sintering aid did not give steady values. A center section was again used. The results of four observations are listed. They are well below the expected values. The fourth electrode was fabricated from $TaSi_2$ with 0.5 wt % Ni added as

a sintering aid. The electrode had a density greater than 95% of theoretical and was polished to a bright metallic finish. The observed EMFs were stable over prolonged periods of time and were reproducible. However the electrolyte was tested after use in the cell and was found to conduct at room temperature. A contaminant had coated the periphery of the electrolyte at some point during the experiment making the observed voltages questionable. Likewise, the results obtained with the fifth electrode are questionable because the electrode conducted at room temperature as a result of contamination during the course of the experiment. This electrode was not sintered with a sintering aid and was therefore quite porous. The surface layer was removed on emery paper and a center section was used in contact with the electrolyte. The sixth and seventh electrodes were from the same batch. This batch sintered poorly. Center reactions were placed in contact with the electrolyte. The sixth cell was poorly assembled and the results listed were not steady state values. The seventh cell gave steady values. Hysteresis and a strong temperature effect were manifest. However, the results are considerably better than the results for the second cell listed.

In an attempt to produce denser electrodes the amount of Ni sintering aid added was increased slightly and the amount of silica added was decreased further. A photomicrograph of an electrode from the group used in the eighth, ninth, and tenth cells is presented in Plate VIII. The polished surface was metallic with many very large isolated pores. The eighth electrode attained an EMF of 656 mv upon reaching the set point - 1000°C. The EMF then declined steadily. The ninth silicide electrode (Table XV) did not produce a steady EMF at 1000°C. Upon reaching the set point an EMF of 706 mv was observed. The

gas flow rate was 1 CFH. The voltage fell steadily with time. Raising the gas flow rate to 3 CFH produced a steady EMF of 727 mv over a period of 20 minutes. A further increase in the flow rate to 5 CFH resulted in an initial rise in the EMF followed by a rapid decline. At 900°C and a flow rate of 3 CFH a non-steady voltage was observed. The cell was held at 800°C over a 12 hour period. A steady voltage of 245 mv was observed at the end of this period. The ninth electrode was refinished and rerun in the tenth cell. In contrast to the other cells slowly rising EMFs were noted at 1.5 and 3 CFH with the rate of ascent declining with time. An average EMF of 566 $\pm$20 mv was observed at 1000°C. Observations were not made at other temperatures. Photomicrographs of some electrodes from this batch after use in the cells are given in Plates VII, IX, and X. Plate VII shows an almost continuous silica film grown at the center of the pellet. Plate X shows the center of an electrode surface run for a shorter period of time. Here the film is discontinuous. However at the periphery of this electrode-electrolyte interface (Plate IX) the film is more continuous and thick enough to produce interference colors (0.1μ).

Further reduction of the silica content was made in the next batch of electrodes. These electrodes were used in cells 11, 12, 13, and 15. A photomicrograph of an electrode from the batch before use in a cell is presented in Plate XII. Note the greater density compared with the electrode shown in Plate VIII. The EMF values obtained with all four cells run showed a strong temperature effect. The EMF at all temperatures generally attained a maximum value upon reaching the set point and declined thereafter. During the early part of the experiments the maximum attained values in excess of the expected value. These EMFs are attributed to conditions well removed from

equilibrium existing in the electrolyte. Later maxima, as recorded in Table XV are more representative of the cell behavior. A sensitivity to gas flow rate was noted. A photomicrograph of an electrode from the group is presented in Plate XI. A discontinuous silica film grew on the surface during the course of the experiment.

The behavior of an electrode from the final group examined (Cell 14), where silica content was reduced further, was similar in that the EMF attained an initial maximum on reaching the set point and declined thereafter and the EMF was sensitive to flow rate. Photomicrographs taken before and after the experiment (Plates XII and XI respectively) shows that a discontinuous film had grown - presumably over those regions where $TaSi_2$ was the substrate.

The results for the $TaSi_2$-Ta_5Si_3 phase field may be summarized as follows: It was not possible to obtain stable and reproducible EMFs at a series of temperatures independent of the argon flow rate. Porous electrodes such as 1, 2, 3, 6 and 7 gave stable EMFs which were strongly dependent on temperature. The behavior was similar to the behavior of porous Ta,Ta_2O_5 electrodes. Improvement in the data was noted with improvement in density. The dense metallic electrodes (8 through 15) generally gave unstable EMFs which declined with time. Exceptions were the tenth, eleventh, and thirteenth cells. Data for all cells where stable EMFs were observed with respect to Fe,Fe_xO are summarized in Figure 11. Only two points representing six observations fall within the range of expected values. These latter points may be summarized as 655 $\pm$40 mv at 1300°K. Correcting for electronic conduction by +10 mv gives an EMF of +665 $\pm$40 mv at 1300°K. This corresponds to an uncertainty of $\pm$3.7 kcal per gram atom of silicon oxidized to SiO_2.

FIGURE 11. Stable EMF Data for $TaSi_2$, Ta_5Si_3, SiO_2(a) versus Fe, Fe_xO With ThO_2-Y_2O_3 Electrolytes.

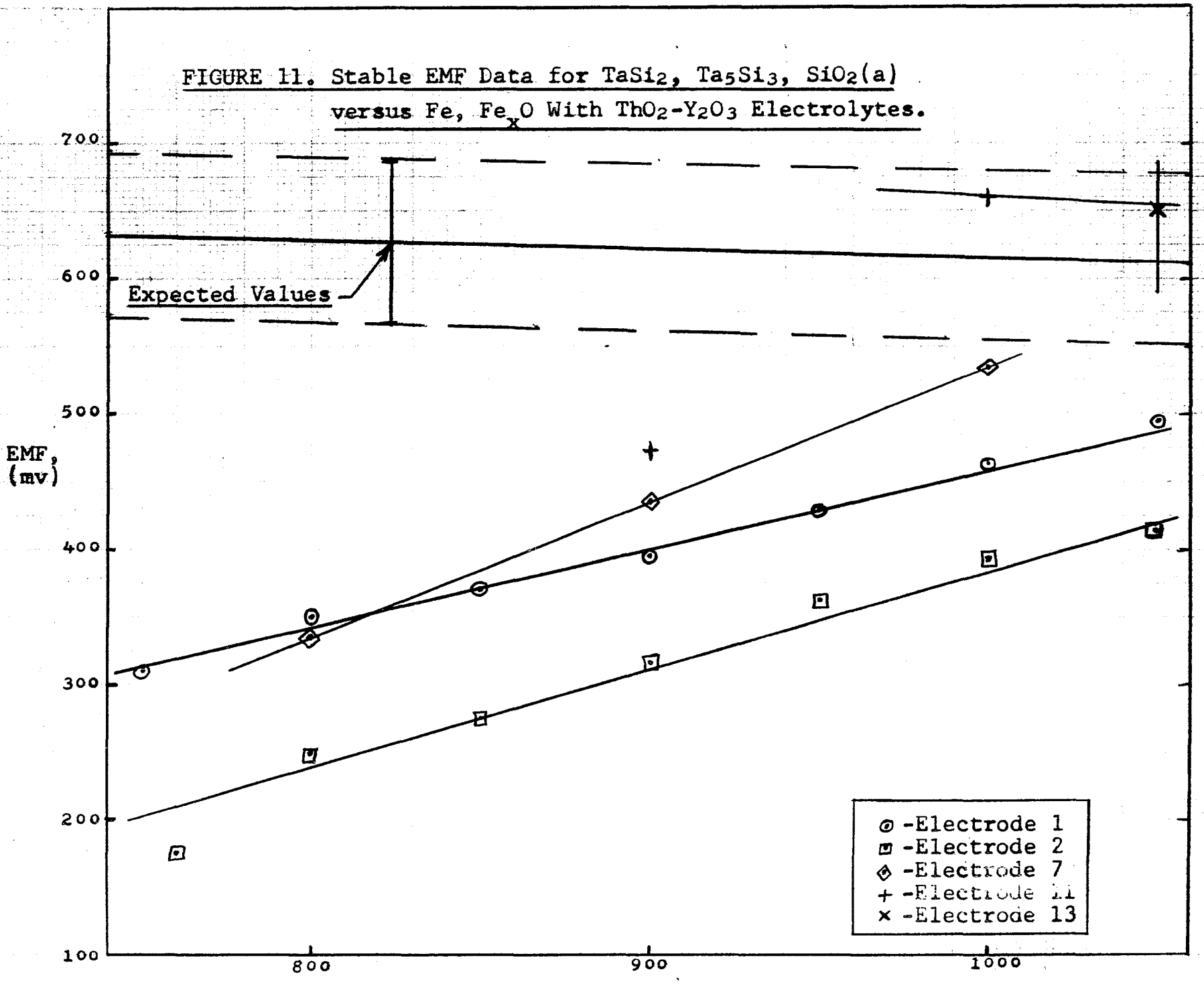

IV. D.5. EMF Measurements: Ta_5Si_3-Ta_2Si Phase Field.

In the Ta_5Si_3-Ta_2Si field three half-cell reactions were considered. Silica is the oxidation product of the first of these (see Table II, reaction A2, page 18):

$$2\ Ta_5Si_3 + 2\ O^{=} = SiO_2(a) + 5\ Ta_2Si + 4\ e^{-}$$

With an Fe,Fe_xO reference electrode values expected from thermal data are 895 $\pm$477 mv at 1000°K and 870 $\pm$477 mv at 1300°K. The expected values with respect to a Ni,NiO reference electrode are 1153 $\pm$477 mv at 1000°K and 1158 $\pm$477 mv at 1300°K; with respect to a Ta,Ta_2O_5 reference electrode the expected values are 259 $\pm$477 mv at 1000°K and 251 $\pm$477 mv at 1300°K. This half-cell, based on the results of the electrode stability study, is thermodynamically unstable but can be expected to give stable EMFs under the proper kinetic circumstances. The thermodynamically stable electrodes in this phase field are based on oxidation to tantalum oxide or complete oxidation of the trisilicide. The half-cell reaction for tantala formation is (see B5, Table II);

$$6\ Ta_2Si + 5\ O^{=} = Ta_2O_5 + 2\ Ta_5Si_3 + 10\ e^{-}$$

The expected values are: with an Fe,Fe_xO reference electrode, 475 $\pm$ 208 mv at 1000°K and 457 $\pm$208 mv at 1300°K; with an Ni,NiO reference electrode, 733 $\pm$208 mv at 1000°K and 745 $\pm$208 mv at 1300°K; with a Ta,Ta_2O_5 reference electrode, -161 $\pm$209 mv at 1000°K and -162 $\pm$208 mv at 1300°K. The half-cell reaction for complete oxidation to tantala and silica is (see C8, Table II):

$$2\ Ta_5Si_3 + 37O^{=} = 5\ Ta_2O_5 + 6\ SiO_2(a) + 74\ e^{-}$$

The expected values are: with an Fe,Fe_xO reference electrode, 577 $\pm$14 mv at 1000°K and 556 $\pm$14 mv at 1300°K; with a Ni,NiO reference electrode, 835 $\pm$14 mv at 1000°K and 844 $\pm$14 mv at 1300°K; with a Ta,Ta_2O_5 reference electrode, -59 $\pm$14 mv at

1000°K and -63 ±14 mv at 1300°K.

Measurements on electrodes formulated from the Ta_5Si_3-Ta_2Si field were conducted with the second apparatus in its final state of development; the complete gas purification train was in operation and lead wires were brought out of the cell with teflon lead-throughs. The electrode formulations and the results of the EMF measurements are presented in Table XVI. The table arrangement is the same as Table XV. The X-ray data given are for the electrode after having been used in the appropriate cell.

Data from the first five cells listed in Table XVI are in error because these early tantalum, tantalum oxide reference electrodes were porous. However, one should note that the EMFs observed were generally negative. This indicates that the oxygen partial pressure established over Ta, Ta_2O_5 electrodes is less than the oxygen partial pressure established over the silicide electrodes. Also, the temperature effect in these cells is relatively strong whereas the expected variation of voltage with temperature is very small.

Data obtained with the majority of the other electrodes examined also exhibited strong temperature dependence and sensitivity to argon flow rate. A variety of formulations were examined. The poor sintering behavior of the electrodes was at least partially overcome by using pellets in the as pressed and sintered condition in order to present the densest possible surfaces to the electrolyte. However, as a result of surface silicon losses during sintering, wide discrepencies between the compositions computed from the starting materials and those determined by X-ray diffraction were encountered.

Table XVI

EMF Measurements Employing Half-Cells Formulated From The Ta_5Si_3-Ta_2Si Two-Phase Field

Silicide Electrode Composition	Heat Treatment and Sintering	$\frac{I(Ta_5Si_3)}{I(Ta_5Si_3)+I(Ta_2Si)}$	Reference Electrode	Electrolyte	Temp °C	EMF (mv)	Number of Observations
1) 18.4wt % $TaSi_2$ 77.0wt % Ta_5Si_3 4.6wt % SiO_2	S 1600°C, 1 hr.	0.97	Ta,Ta_2O_5 1600°C,15 min porous	0.92 ThO_2- 0.08 Y_2O_3 2150°C,3 hrs ρ = 90.5%	815 870 910 ±2 1000	s-7.5 ±2 s-20.1 ±2 s-23.5 ±5 s-46.2 ±5	2 1 3 2
2) 13 wt % $TaSi_2$ 61 wt % Ta_5Si_3 26 wt % Ta_2O_5	S 1400°C, 10 min.	0.38	Ta,Ta_2O_5 1600°C,15 min porous	0.93 ThO_2- 0.07 Y_2O_3 2150°C,3 hrs ρ = 90.5%	645 700 750 810 870 ±5 900 950 995	s+7.4 ±5 s-43.7 ±5 s-128.3±5 s-150.4±20 s-198.3±5 s-181.0±20 s-186.8±5 s-169.9±5	2 1 1 2 1 2 2 2
3) 66 wt % Ta_5Si_3 12 wt % Ta_2Si 22 wt % Ta_2O	S 1400°C, 10 min.	0.83	Ta,Ta_2O_5 1600°C,15 min porous	0.93 ThO_2- 0.07 Y_2O_3 1950°C,28 hrs ρ = 90.2%	810 860 900 ±5 950 1000	s-78.6 ±50 s-131.6±6 s-138.9±20 s-139.6±2 s-122.5±4	3 2 4 2 2

Table XVI (cont.)

Silicide Electrode Composition	Heat Treatment and Sintering	$\frac{I(Ta_5Si_3)}{I(Ta_5Si_3)+I(Ta_2Si)}$	Reference Electrode	Electrolyte	Temp °C	EMF (mv)	Number of Observations	
4) 92 wt % Ta_5Si_3 5 wt % Ta_2Si 3 wt % SiO_2	S 1400°C, 10 min.	0.89	Ta, Ta_2O_5 1600°C, 15 min porous	0.93 ThO_2- 0.07 Y_2O_3 2050°C, 4 hrs ρ = 90.5%	805 900 ±5 1000±5	s-24.1 ±20 s-53.3 ±30 s-65.6 ±40	4 5 6	
5) 4 wt % Ta_5Si_3 89 wt % Ta_2Si 7 wt % SiO_2	S 1400°C, 10 min.	0.18	Ta, Ta_2O_5 1600°C, 15 min porous	0.93 ThO_2- 0.07 Y_2O_3 2150°C, 3 hrs	810 850 900 ±5 950 990	s-28.4 ±1 s-37.3 ±6 s-48.7 ±12 s-57.0 ±15 s-69.1 ±8	2 6 6 6 3	
6) 58 wt % Ta_5Si_3 38 wt % Ta_2Si 3 wt % Ta_2O_5 1 wt % Ni	S 1620°C, 10 min.	0.29	Fe, Fe_xO	0.93 ThO_2- 0.07 Y_2O_3 2000°C, 3 hrs ρ = 87.3%	900 950 1000 ±5 1050 1090	s 475 ±3 s 489 ±2 s 503 ±14 s 505 ±3 s 513 ±1	3 2 3 3 2	1.5 CFH
					900 950 1000 ±5 1050 1090	s 477 ±3 s 494 ±3 s 505 ±3 s 515 ±1 s 519 ±3	1 1 1 2 1	3 CFH

Table XVI (cont.)

Silicide Electrode Composition	Heat Treatment and Sintering	$\frac{I(Ta_5Si_3)}{I(Ta_5Si_3)+I(Ta_2Si)}$	Reference Electrode	Electrolyte	Temp °C	EMF (mv)	Number of Observations
6) cont.					1000	s 523 ±3	1
					1050 ±5	s 521 ±1	2 5
					1100	s 520 ±3	1 CFH
7) 56 wt % Ta_5Si_3 36 wt % Ta_2Si 7 wt % Ta_2O_5 1 wt % Ni	S 1620°C, 10 min.	0.18	Fe, Fe_xO	0.93 ThO_2- 0.07 Y_2O_3 2000°C, 3 hrs ρ = 89.8%	800	s 537 ±4	1
					850	s 565 ±4	2
					900 ±5	s 578 ±8	5
					950	s 583 ±4	4
					1000	s 589 ±9	6
					1045	s 585 ±4	2
8) 99 wt % Ta_5Si_3 1 wt % Ni	S 1620°C, 10 min.	0.69	Fe, Fe_xO	0.93 ThO_2- 0.07 Y_2O_3 2000°C, 3 hrs ρ = 91.3%	845	s 467 ±5	1
					900	s 470 ±20	2
					950 ±5	s 484 ±25	3 3CFH
					1000	s 503 ±20	3
					1045	s 524 ±5	1
					900	s 421	1
					950 ±5	s 443	1 1.5
					1000	s 457	1 CFH
9) 56 wt % Ta_5Si_3 36 wt % Ta_2Si 7 wt % Ta_2O_5	S 1620°C, 10 min.	0.06	Fe, Fe_xO	0.93 ThO_2- 0.07 Y_2O_3 2000°C, 3 hrs ρ = 89.3%	1000	s 360	1.5CFH
					1010	s 415	3 CFH
					1045 ±5	s 413	1.5CFH
					1045	s 452	3 CFH
					1045	s 456	5 CFH

Table XVI (cont.)

Silicide Electrode Composition	Heat Treatment and Sintering	$\frac{I(Ta_5Si_3)}{I(Ta_5Si_3)+I(Ta_2Si)}$	Reference Electrode	Electrolyte	Temp °C	EMF (mv)	Number of Observations
10)							
12 wt % Ta_5Si_3	S 1630°C,	0.02	Fe,Fe_xO	0.93 ThO_2-	895	s 458 ±5	2
					945	s 548 ±9	3
87 wt % Ta_2Si	10 min.			0.07 Y_2O_3	995 ±5	s 567 ±3	3
				2000°C, 3 hrs	1040	s 564 ±5	5
1 wt % Ni				ρ = 95.4%	1075	s 562 ±3	1
11)							
99 wt % Ta_5Si_3	S 1620°C,	0.82	Fe,Fe_xO	0.93 ThO_2-	900	s 171 ±85	3
					950	s 329 ±11	2
1 wt % Ni	10 min.			0.07 Y_2O_3	1000 ±5	s 429 ±70	4
				2000°C, 3 hrs	1050	s 470 ±35	4
				ρ = 93.3%	1090	s 510 ±5	1
12)							
85 wt % Ta_5Si_3	S 1630°C	0.85	Fe,Fe_xO	0.93 Th_2O-	895	s 315 ±100	4
					945	s 422 ±35	2
9 wt % Ta_2Si	10 min.			0.07 Y_2O_3	1000	s 455 ±30	6
5 wt % Ta_2O_5				2000°C, 3 hrs	1040 ±5	s 475 ±15	4
				ρ = 95.9%	1050	s 492	1
1 wt % Ni					1070	s 491	1
13)							
58 wt % Ta_5Si_3	S 1620°C,	0.19	Fe,Fe_xO	0.93 ThO_2-	900	s 319 ±50	2
					945	s 400 ±65	3
38 wt % Ta_2Si	10 min.			0.07 Y_2O_3	1000 ±5	s 458 ±25	2
3 wt % Ta_2O_5				2000°C, 3 hrs	1050	s 474 ±25	3
1 wt % Ni				ρ = 93.3%			

Table XVI (cont.)

Silicide Electrode Composition	Heat Treatment and Sintering	$\frac{I(Ta_5Si_3)}{I(Ta_5Si_3)+I(Ta_2Si)}$	Reference Electrode	Electrolyte	Temp °C	EMF (mv)	Number of Observations
14) 12 wt % Ta_5Si_3 88 wt % Ta_2Si	S 1650°C, 10 min.	0.04	Fe,Fe_xO	0.93 ThO_2- 0.07 Y_2O_3 2000°C,3 hrs ρ = 96.9%	900 950 1000 1040	s 468 ±25 s 369 ±85 s 498 ±40 s 530	6 3 7 1
15) 7 wt % $TaSi_2$ 87wt % Ta_5Si_3 5 wt% Ta_2O_5 1 wt % Ni	S 1600°C, 10 min.	0.90	Fe,Fe_xO	0.93 ThO_2- 0.07 Y_2O_3 2000° C,3 hrs ρ = 96.0%	895 945 995 ±5 1040	s 366 ±57 s 476 ±15 s 512 ±15 s 553 ±15	3 2 7 2
16) 99 wt. % Ta_5Si_3 1 wt % Ni	S 1620°C, 10 min.	0.94	Fe,Fe_xO	0.93 ThO_2- 0.07 Y_2O_3 2000°C,3 hrs ρ = 96.0%	950 1000 ±5 1045	s 354 s 427 ±8 s 481 ±9	1 3 3
17) 7 wt % $TaSi_2$ 87 wt % Ta_5Si_3 5 wt% Ta_2O_5 1 wt% Ni	S 1620°C, 10 min.	0.05	Fe,Fe_xO	0.93 ThO_2- 0.07 Y_2O_3 2000°C,3 hrs	900 950 1000 ±5 1025 1045	s 411 ±6 s 469 ±25 s 492 ±20 s 515 ±2 s 519 ±1	3 3 6 2 3

Table XVI (cont.)

Silicide Electrode Composition	Heat Treatment and Sintering	$\frac{I(Ta_5Si_3)}{I(Ta_5Si_3)+I(Ta_2Si)}$	Reference Electrode	Electrolyte	Temp °C	EMF (mv)	Number of Observations
18) 59 wt % Ta_5Si_3 38 wt % Ta_2Si 2 wt % SiO_2 0.8wt % Ni	S 1620°C, 10 min.	0.64	Fe,Fe_xO	0.93 ThO_2- 0.07 Y_2O_3 2000°C,3 hrs	895 955 1000±5 1045	s 383 ±6 s 449 ±8 s 477 ±2 s 499 ±3	2 2 2 3
19) 57 wt % Ta_5Si_3 38 wt % Ta_2Si 4 wt % SiO_2 0.7wt % Ni	S 1610°C, 15 min.	0.28	Fe,Fe_xO	0.93 ThO_2- 0.07 Y_2O_3 2000°C,3 hrs	900 950 1000±5 1045	s 275 ±9 s 381 ±10 s 903 ±75 s 461 ±35	2 1 7 4

Despite these difficulties, good data were obtained for the 6th and 7th, and 10th electrodes. The data for these electrodes along with expected values for the three electrode reactions for the phase field are presented in Figure 12. The three electrodes exhibited a strong temperature effect at the lower temperatures only. Furthermore, electrodes 7 and 10 were insensitive to argon flow rate over the entire range from 1.5 CFH to 5 CFH. The 6th electrode was slightly sensitive to argon flow rate. Consequently the data for this electrode are broken down according to flow rate in Table XVI and Figure 12. The curves (Figure 12) for flow rates of 1.5 CFH and 3 CFH approach the line drawn through the data for 5 CFH at the upper temperature. The data for the three electrodes fall within the range of expected values for tantala formulation via reaction 5 of Table II and within the range of expected values for silica formation via reaction 2 of Table II. The data for the tenth electrode also fall within the range of expected values for simultaneous formation of silica and tantala via reaction 8 of Table II. The corrections for electronic conduction as determined from Figure 9 are +4 mv for electrode 6, +6mv for electrode 10 and +7 mv for electrode 7. With these corrections the data for the tenth electrode fall just outside the upper limit for simultaneous silica and tantala formation via reaction 8 of Table II. None of the three sets of data fall within the range of expected values for reaction 9 of Table II. It will be recalled that this reaction was eliminated earlier. Photomicrographs of the center and periphery of electrode 10 are presented in Plates XVII and XVIII respectively. Although the relatively rough surfaces were difficult to photograph, it may be observed that the center of the surface that was in contact with

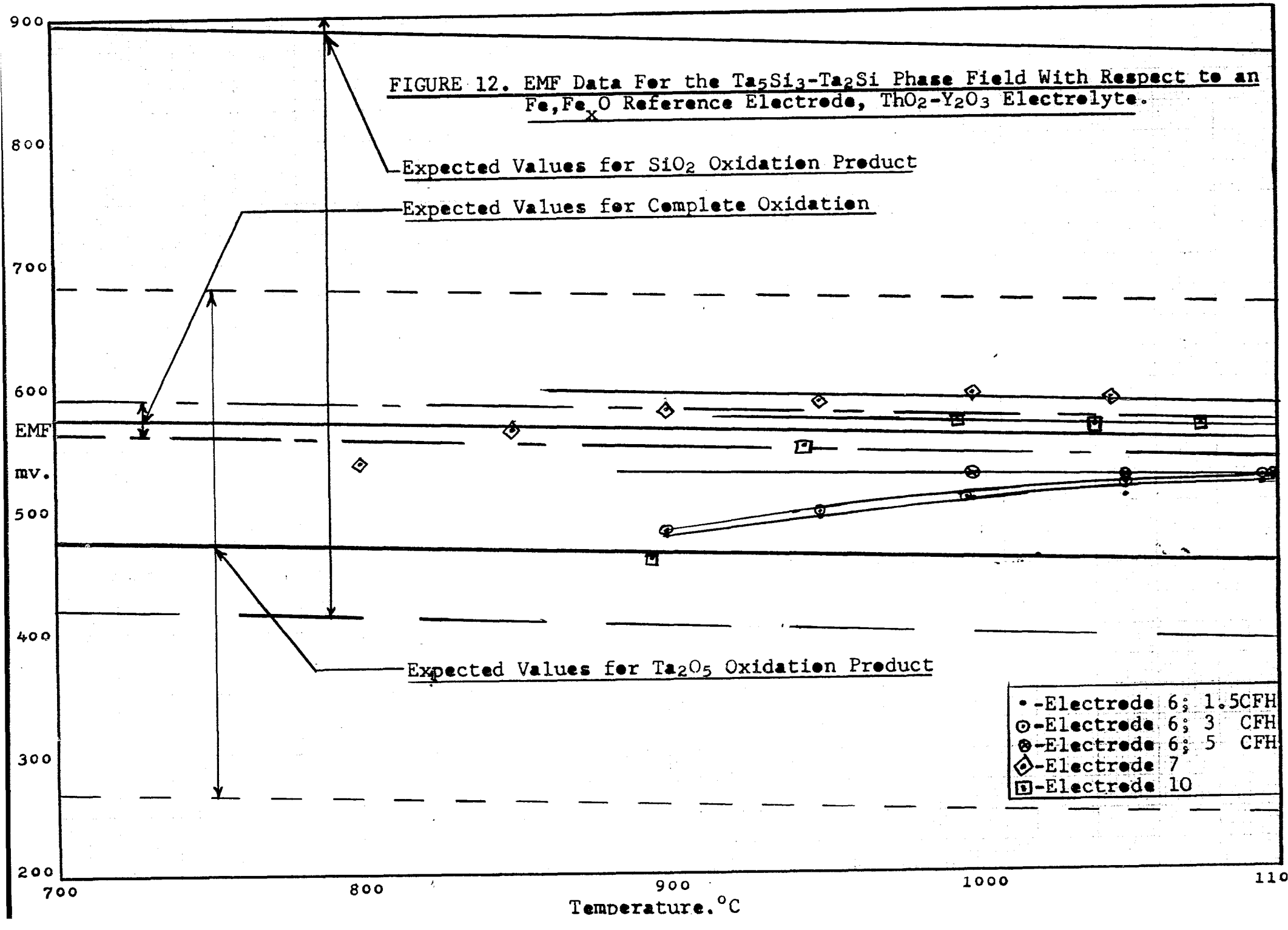

FIGURE 12. EMF Data For the Ta_5Si_3-Ta_2Si Phase Field With Respect to an Fe,Fe_xO Reference Electrode, ThO_2-Y_2O_3 Electrolyte.

the electrolyte is quite porous whereas densification occurred at the periphery as a result of oxidation. Photomicrographs of the center and periphery of electrode 6 are presented in Plates XIX and XX respectively. Porosity is again manifest. Densification at the periphery as a result of oxidation occurred.

The three sets of data are to be assigned to from one to three reactions. Because they are relatively closely spaced with respect to the range of expected values for the three possible reactions the assignments are not easily made. Micrographic and X-ray evidence are of some assistance. Micrographic examination of electrode #6 after it was used in the cell for a period of 30 hours revealed no silica film. An X-ray of the electrode from 31^{o} to 41^{o} (2θ) before use in the cell exhibited the following intensities: (Ta_2Si, d =2.41) had an intensity of 161 and (t-Ta_5Si_3, d = 2.34 + h-Ta_5Si_3, d = 2.21) had a combined intensity of 50. In a complete scan after the electrode was used in the cell the intensity of the Ta_2Si peak diminished to 135 and the combined intensity of the Ta_5Si_3 peaks increased to 56. β-Ta_2O_5 was detected. The micrographic and X-ray evidence concur and indicate that Ta_2Si was oxidized to form tantala and Ta_5Si_3 according to reaction 5 of Table II.

An X-ray scan of electrode seven before use in the cell from 31^{o} to 41^{o} (2θ) gave an intensity of 165 for the strongest Ta_2Si peak (d = 2.41) and an intensity of 60 for the intensity of the strongest t-Ta_5Si_3 peak (d = 2.34). After the electrode was used in the cell for approximately 30 hours a complete X-ray of the surface in contact with the electrolyte revealed a decrease in the quantity of Ta_5Si_3 to a combined intensity for the strongest t-Ta_5Si_3 peak (d = 2.34) and strongest h-Ta_5Si_3 peak (d = 2.21) of 39. The intensity of the strongest Ta_2Si

peak increased to 187 and β -Ta_2O_5 was again detected. Micrographic examination of the electrode detected an apparent SiO_2 film. In view of the X-ray and micrographic evidence it is concluded that Ta_5Si_3 was oxidized to silica and Ta_2Si according to reaction 2 of Table II.

X-ray examination of electrode 10 before use in the cell revealed an intensity of 204 for the strongest Ta_2Si peak (d = 2.41) and an intensity of 8 for the strongest t-Ta_5Si_3 peak (d = 2.34). An X-ray taken after the electrode was used in the cell for about 30 hours revealed a decrease in the intensity of the strongest Ta_2Si peak to 181 and a decrease in the intensity of the strongest t-Ta_5Si_3 peak to 6. β -Ta_2O_5 was also detected in this scan. The X-ray results indicate that no effective change in the relative amounts of the silicides present occurred. Micrographic examination of the electrode surface that had been in contact with the electrolyte revealed what appeared to be an SiO_2 film on the periphery of the electrode surface which had been in contact with the electrolyte. In view of the composition of this electrode, assignment of the data to reactions 2 or 8 would be unreasonable. Assignment to reaction 5 would be more reasonable. However, the EMFs observed are not appreciably different from the EMFs observed for $Ta_{4.5}Si$, Ta_2Si, Ta_2O_5 electrodes. As was shown earlier, the EMF for reaction 5 must be less than the EMF for reaction 6. Hence the EMFs observed for electrode 10 are assigned to a mixed reaction. This is not unreasonable since Ta_2O_5 was detected by X-ray diffraction and micrographic examination revealed a presumed SiO_2 film on the periphery of the electrode.

IV. D. 6. EMF Measurements: Ta_2Si-$Ta_{4.5}Si$ Phase Field.

In the Ta_2Si-$Ta_{4.5}Si$ field the expected electrode reaction was, from Table II:

$$4\ Ta_{4.5}Si + 25O^{=} = 5\ Ta_2O_5 + 4\ Ta_2Si + 50\ e^{-}$$

with expected values at 1000°K and 1300°F of 617 ±28 mv and 598 ±28 mv respectively with an Fe,Fe_xO reference electrode. The results of the experiments performed with $Ta_{4.5}Si$, Ta_2Si, Ta_2O_5 electrodes are presented in Table XVI. The Table is arranged in the same way as Table XV with heat treatment of the silicide denoted by H.T. and sintering with the oxides and nickel denoted by S. Average EMFs are tabulated. All EMFs that were stable are indicated by "s".

The data obtained with the first electrode showed a strong temperature effect similar to porous Ta,Ta_2O_5 electrodes. A center section of the electrode was used in contact with the electrolyte. The prolonged heat treatment resulted in the formation of a considerable amount of Ta. The next electrode was fabricated with less Ta_2O_5 added and the heat treatment was omitted. The sintered pellets could not be polished. Grinding on a emery disc produced a powdery surface. In order to present the densest possible surface to the electrolyte the surface of the as pressed and sintered pellets were placed in contact with the electrolyte. The data obtained with this electrode were better than those of the first cell in that the temperature effect was weaker.

The amount of Ta_2O_5, added to the $Ta_{4.5}Si$-Ta_2Si powder was reduced further in the next batch of electrodes. The sintering time was increased to 15 minutes. The surface of the pellet in the as pressed and sintered condition was again placed in contact with the electrolyte. The results for the first run with

Table XVII

EMF Measurements Employing Half-Cells Formulated From the $Ta_{4.5}Si$-Ta_2Si Two-Phase Field

Silicide Electrode Composition	Heat Treatment and sintering	$\frac{I(Ta_2Si)}{I(Ta_2Si)+I(Ta_{4.5}Si)}$	Reference Electrode	Electrolyte	Temp °C	EMF mv	Number of Observations
1)							
40.2 wt % Ta_2Si	H.T. 1600°C 70 min.	0.77 + Ta	Fe,Fe_xO	0.99 ThO_2-	800	s292	1
					850	s380	1
52.5 wt % $Ta_{4.5}Si$	S. 1600°C, 15 min.			0.01 Y_2O_3	900 ±5	s461 ±10	2
				2000°C, 3 hrs	950	s454	2
6.5 wt % Ta_2O_5				ρ = 90%	1000	s522	4
					1050	s545	1
0.8 wt % Ni							
2)							
41.5 wt % Ta_2Si	S. 1625°C, 10 min.	0.995	Fe,Fe_xO	0.93 ThO_2-	800	s414	1
					850	s436±3	2
54.4 wt % $Ta_{4.5}Si$				0.07 Y_2O_3	900	s477±24	3
				2000°C, 3 hrs	950±3	s485±16	3
3.4 wt % Ta_2O_5				ρ = 90%	1000	s494±14	4
					1050	s507±6	3
0.7 wt % Ni					1100	s516	1
3)							
42.2 wt % Ta_2Si	S.1625°C, 15 min.	0.39	Fe,Fe_xO	0.93 ThO_2-	900	s556	2
					950	s559	3
55.3 wt % $Ta_{4.5}Si$				0.07 Y_2O_3	1000±5	s559±3	3
				2000°C, 3 hrs	1050	s557	3
1.7 wt % Ta_2O_5				ρ = 88%	1100	s555	2

Table XVII (cont.)

Silicide Electrode Composition	Heat Treatment and Sintering	$\frac{I(Ta_2Si)}{I(Ta_2Si)+I(Ta_{4.5}Si)}$	Reference Electrode	Electrolyte	Temp °C	EMF mv	Number of Observations
4) 42.2 wt % Ta_2Si 55.3 wt % $Ta_{4.5}Si$ 1.7 wt % Ta_2O_5 0.8 wt T Ni	S. 1625°C, 15 min.	0.22	Fe,Fe_xO	0.93 ThO_2 - 0.07 Y_2O_3 2000°C, 3 hrs ρ = 89%	850	s554	1
					900	s567±2	4
					950 ±5	s563±2	2
					1000	s562±9	5
					1050	s560±3	4
					1090	s562±7	3

an electrode from this group were highly reproducible and displayed a weak temperature dependence of the proper sign. The majority of the observations were made at a flow rate of 1.5 CFH. Observations at 3 CFH were made at 900°C and 1000°C. At both temperatures this increase in flow rate caused a 2 mv drop in the EMF.

A second run with an electrode from this group reproduced the above data. A flow rate of 1.5 CFH was used again. An increase in flow rate to 3 CFH resulted in a 2 mv drop in EMF at 900°C and a 10 mv increase in EMF at 1000°C and 1100°C. A photomicrograph of this last electrode after use in the cell is presented in Plate XVI. The surfaces of the particles appear to be coplanar. A semicontinuous network of pores is present between the particles.

The data for this group of electrodes is summarized in Figure 13. The range of expected values is indicated by the dashed lines. Data for the last two runs are nearly colinear at the higher temperatures. At 900°C and 950°C the slope of the data from the third electrode is positive indicating that the gas-electrode interaction is becoming significant. Likewise, the data for the fourth electrode begins to show the kinetic effect at 850°C and 900°C. From Table XVII, the estimated correction for electronic conduction is +6 mv. Since an increase in gas velocity from 1.5 CFH to 3 CFH had an effect which averaged to +6 mv, an additional +6 mv correction will be applied to the data. The total correction is +12 mv. With the uncertainty in these corrections and the average variability in the data of ± 4 mv the corrected data may be considered reliable to ± 10 mv. This corresponds to an uncertainty of ± 3 kcal per gram atom of silicon for the cell reaction.

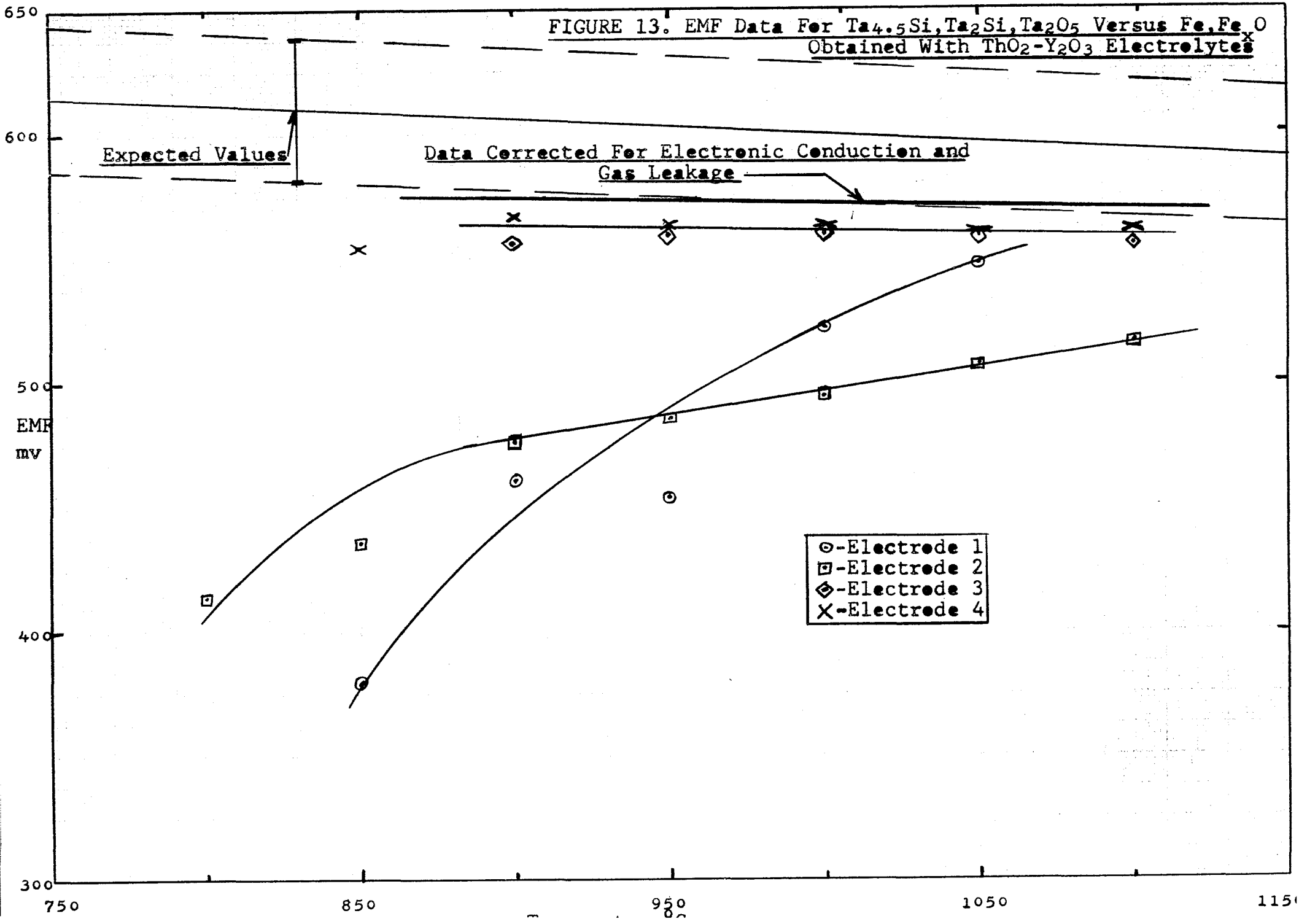
FIGURE 13. EMF Data For $Ta_{4.5}Si, Ta_2Si, Ta_2O_5$ Versus Fe, Fe_xO Obtained With ThO_2-Y_2O_3 Electrolytes
Expected Values
Data Corrected For Electronic Conduction and Gas Leakage
EMF mv
650
600
500
400
300
750
850
950
1050
1150
⊙-Electrode 1
⊡-Electrode 2
◈-Electrode 3
✕-Electrode 4

IV. E. Evaluation of Data for Silicide Electrodes.

With the data presented in Sections IV.D.4 through 6 the free energies of formation of the tantalum silicides can be evaluated. From Figures 11, 12 and 13 EMF values for 1200°K, 1300°K and 1400°K were determined. These EMF values and free energy of formation data for Fe_xO and tantala and silica were brought to equations (1), (2), (5) and (6) giving four linear equations in the free energies of formation of the silicides. The free energies of formation of Fe_xO were taken from the recent data of Charette and Flengas(74). The data for tantala and silica are from Wicks and Block(6). The calculations are presented in Table XVIII. An upper bound of 675 mv was selected for the EMF of the $TaSi_2$, Ta_5Si_3, SiO_2(a) electrode with respect to the Fe,Fe_xO reference electrode since an Si,SiO_2(a) electrode would develop an EMF of 677 mv with respect to an Fe,Fe_xO reference electrode. The results of the calculations are summarized in the last section of the Table. The results for the three lower silicides are in substantial agreement with the results of earlier investigations. An improvement of the confidence interval for Ta_5Si_3 and Ta_2Si has been achieved in this research. A similar improvement could not be achieved for the highest and lowest silicide. One should note that approximately 45% of the uncertainty in the free energy of formation data for the tantalum silicides is due to the free energy data for the oxides of iron, tantalum, and silicon. If the uncertainties in the data for the oxides are disregarded a better indication of the quality of the data obtained in this work is obtained. The confidence intervals, with uncertainties in the free energy data for the oxides disregarded, become:

Table XVIII

Evaluation of Data for Silicide Electrodes

$TaSi_2, Ta_5Si_3, SiO_2$(a): $5/7\ TaSi_2 + 2\ Fe_xO = SiO_2$(a) $+ 1/7\ Ta_5Si_3 + 2\ Fe_x$ (4 equivalents)

Temperature, °K	EMF (mv)	ΔG_R (kcal)	$\Delta G_{SiO_2(a)}$	ΔG_{Fe_xO}	$[\Delta G_{SiO_2(a)} - 2\Delta G_{Fe_xO}]$	$\frac{1}{7}(\Delta G_{Ta_5Si} - 5\Delta G_{TaSi}$
1300	665 $^{+10}_{-40}$	-61.3 $^{+3.7}_{-0.9}$	-148.1 ±.1	-42.81 ±.1	-62.5 ±.3	+1.2 $^{+4}_{-1.2}$

Ta_5Si_3, Ta_2Si, SiO_2(a): $2\ Ta_5Si_3 + 2\ Fe_xO = SiO_2$(a) $+ 5\ Ta_2Si + 2\ Fe_x$ (4 equivalents)

Temperature, °K	EMF (mv)	ΔG_R (kcal)	$\Delta G_{SiO_2(a)}$	ΔG_{Fe_xO}	$(\Delta G_{SiO_2(a)} - 2\Delta G_{Fe_xO})$	$(5\Delta G_{Ta_2Si} - 2\Delta G_{Ta_5Si}$
1200	597 ±7	-55.1 ±.6	-152.2 ±.1	-44.36 ±.1	-63.5 ±.3	+8.4 ±.9
1300	590 ±7	-54.4 ±.6	-148.1 ±.1	-42.81 ±.1	-62.5 ±.3	+8.1 ±.9
1400	583 ±7	-53.7 ±.6	-144.0 ±.1	-41.26 ±.1	-61.5 ±.3	+7.8 ±.9

Table XVIII (cont.)

$Ta_5Si_3, Ta_2Si, Ta_2O_5$: $6\ Ta_2Si + 5\ Fe_xO = Ta_2O_5 + 2\ Ta_5Si_3 + 5\ Fe_x$ (10 equivalents)

Temperature, °K Electrode 6,	EMF (mv) Table XVI	ΔG_R (kcal)	$\Delta G_{Ta_2O_5}$	ΔG_{Fe_xO}	($\Delta G_{Ta_2O_5}$ - 5 ΔG_{Fe_xO})	(2 $\Delta G_{Ta_5Si_3}$ - 6 ΔG_{Ta_2Si})
1200	528 ±5	-122 ±1.2	-363.9 ±.5	-44.31 ±.1	-142.1 ±1.0	+20.1 ±2
1300	524 ±5	-121 ±1.2	-354.2 ±.5	-42.81 ±.1	-140.1 ±1.0	+19.1 ±2
1400	520 ±5	-120 ±1.2	-344.6 ±.5	-41.26 ±.1	-138.3 ±1.0	+18.3 ±2

$Ta_2Si, Ta_{4.5}Si, Ta_2O_5$: $1/5(4\ Ta_{4.5}Si + 25\ Fe_xO = 5\ Ta_2O_5 + 4\ Ta_2Si + 25\ Fe_x)$ (10 equivalents

Temperature, °K	EMF (mv)	ΔG_R (kcal)	$\Delta G_{Ta_2O_5}$	ΔG_{Fe_xO}	($\Delta G_{Ta_2O_5}$ - 5 ΔG_{Fe_xO})	4/5(ΔG_{Ta} $\Delta G_{Ta_{4.5}Si}$
1200	578 ±10	-133 ±2.3	-363.9 ±.5	-44.36 ±.1	-142.1 ±1.0	+8.9 ±3.3
1300	573 ±10	-132 ±2.3	-354.2 ±.5	-42.81 ±.1	-140.1 ±1.0	+8.1 ±3.3
1400	568 ±10	-131 ±2.3	-344.6 ±.5	-41.26 ±.1	-138.3 ±1.0	+7.4 ±3.3

Temperature, °K	ΔG_{TaSi_2} (kcal)	$\Delta G_{Ta_5Si_3}$ (kcal)	ΔG_{Ta_2Si} (kcal)	$\Delta G_{Ta_{4.5}Si}$ (kc
1200	----	-74.5 ±9	-28.1 ±3.1	-39.2 ±7.2
1300	-16.1 $^{+3.5}_{-7.4}$	-72.1 ±9	-27.2 ±3.1	-37.3 ±7.2

$TaSi_2$ $^{+3.5}_{-6.0}$ kcal

Ta_5Si_3 ± 4.8 kcal

Ta_2Si ± 1.8 kcal

$Ta_{4.5}Si$ ± 4.7 kcal

In addition to the improvement of the data for some of the tantalum silicides, the results found in this investigation are more suitable for prediction of oxidation behavior and are thermodynamically consistent. The thermodynamic consistence of the data will be discussed first. A plot of ΔG (kcal/g-atom of silicide) versus composition is presented in Figure 14. The mean values for ΔG predict that all of the silicides are thermodynamically stable. This represents an improvement upon the enthalpy data plotted in Figure 2 (page 23).

Also a comparison of observed EMFs for the possible silicide electrodes with values calculated earlier from the Searcy and Finnie enthalpy data shows the improved consistency of the data obtained in this investigation and its value in predicting oxidation behavior. This comparison is presented in Table XIX. As was discussed earlier, EMFs for electrodes where SiO_2(a) is the oxidation product must increase as one proceeds from the lower silicide electrodes to higher silicide electrodes and EMFs for electrodes where Ta_2O_5 is the oxidation product must fall in the reverse order. Such is the case for the EMFs observed or calculated from the results of EMF measurements in this investigation. From Table XIX the oxidation behavior near equilibrium can be predicted. From the first and seventh electrodes it is evident that $TaSi_2$ oxidizes to form SiO_2(a) at near equilibrium conditions. The EMF values for electrodes 2, 4, and 8 predict that Ta_5Si_3 also oxidizes to silica and the

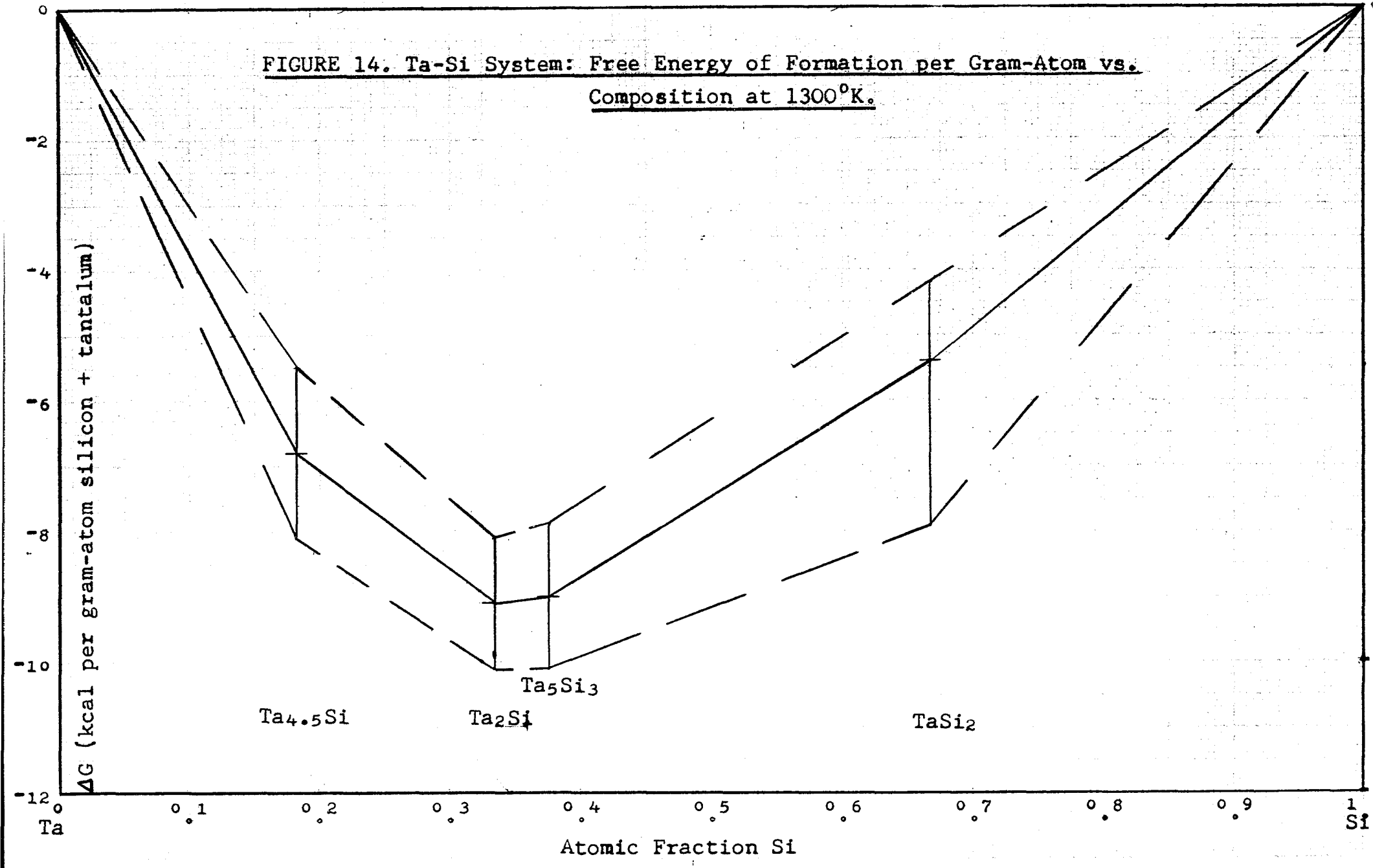
FIGURE 14. Ta-Si System: Free Energy of Formation per Gram-Atom vs. Composition at 1300°K.
0
-2
-4
-6
-8
-10
-12
ΔG (kcal per gram-atom silicon + tantalum)
Ta4.5Si
Ta2Si
Ta5Si3
TaSi2
0
0.1
0.2
0.3
0.4
0.5
0.6
0.7
0.8
0.9
1
Ta
Si
Atomic Fraction Si

Table XIX

A Comparison of Observed EMFs With Expected Values at 1300°K With Respect to an Fe,Fe_xO Reference Electrode

Electrode	Results of this Investigation (mv)	Expected Values From Searcy and Finnie
1) $TaSi_2, Ta_5Si_3, SiO_2$(a)	665 $^{+10}_{-40}$ observed	613 ±65
2) Ta_5Si_3, Ta_2Si, SiO_2(a)	590 ±7 observed	870 ±477
3) $Ta_2Si, Ta_{4.5}Si, SiO_2$(a)	468 ±123 calculated	409 ±113
4) $TaSi_2, Ta_5Si_3, Ta_2O_5$	490 $^{+50}_{-36}$ calculated	528 ±52
5) $Ta_5Si_3, Ta_2Si, Ta_2O_5$	524 ±5 observed	457 ±208
6) $Ta_2Si, Ta_{4.5}Si, Ta_2O_5$	573 ±10 observed	598 ±28
7) $TaSi_2, Ta_2O_5, SiO_2$(a)	565 $^{+12}_{-25}$ calculated	580 ±20
8) Ta_5Si_3, Ta_2O_5, SiO_2(a)	548 ±11 calculated	556 ±14
9) Ta_2Si, Ta_2O_5, SiO_2(a)	541 ±9 calculated	543 ±13
10) $Ta_{4.5}Si, Ta_2O_5, SiO_2$(a)	558 ±12 calculated	570 ±7

lower silicide. This contradicts the observations of the electrode stability study where it was concluded that the stable electrode was Ta_5Si_3, Ta_2Si, Ta_2O_5 as opposed to Ta_5Si_3, Ta_2Si, SiO_2. Examination of the EMF values for electrodes 3, 5 and 9 leads to the conclusion that the total oxidation reaction of Ta_2Si to tantala and silica should be observed in preference to oxidation to tantala and trisilicide or silica and the lowest silicide. Finally, from the EMF values for the 6th and 10th electrodes it is concluded that the lowest silicide undergoes oxidation to tantala and the higher silicide.

The disagreement between the EMF data and the electrode stability study which was pointed out above is not as strong as one might imagine at first glance. Free energies of reaction at 1300°K and 1700°K were computed for the reactions listed in Table III (page 21) using the data obtained in this study. The results were:

	ΔG_R (kcal)	
	1300°K	1700°K
Reaction I of Table III	-81^{+56}_{-36}	-56^{+56}_{-36}
Reaction II of Table III	-29 ± 231	-15 ± 231
Reaction III of Table III	$+47 \pm 73$	$+66 \pm 73$

The values at 1700°K were obtained by extrapolating the free energy data for the silicides (Table XVIII) to 1700°K. Without such an extrapolation $\Delta G_R(1700^\circ K) = \Delta G_R\ (1300^\circ K) + 6$ kcal. Then, the free energy data determined in this investigation predict that reaction I of Table III is spontaneous as was observed in the electrode stability study. The data also predict the spontaneity of reaction III, although not as clearly as do the data of Searcy and Finnie. Finally, in the stability study

reaction II was observed to be non-spontaneous as written in Table III, but the EMF data used in the above calculations predict a spontaneous reaction. However the driving force for the reaction using the data of this investigation is smaller than the driving force predicted with the data of Searcy and Finnie. Moreover, the error in the mean value of ΔG_R for reaction II above corresponds to a combined error in the free energies of formation of Ta_5Si_3 and Ta_2Si of less than 5 kcal per mole since a total of 51 moles of silicide are involved in the reaction as written. This is clearly within the uncertainties associated with the free energy data obtained in this study. Finally, the EMF measurements were made at temperatures up to 1100°C whereas the electrode stability study was conducted at approximately 1600°C. In view of the uncertainties associated with the free energy data ($\pm$6 kcal/mole of silicide on the average) a contradiction on this point is not surprising.

V. CONCLUSIONS

This work has clearly demonstrated that oxide electrolytes may be successfully employed in free energy measurements on silicide electrodes. The data obtained represent a substantial improvement over earlier enthalpy of formation data in terms of thermodynamic consistency and in their capability for predicting oxidation behavior.

Difficulties encountered in the course of this research suggest directions for future work. First, in measurements with low oxygen partial pressure electrodes, tamped electrodes and open crucible electrolytes are less advantageous than pelletized electrodes and electrolytes provided that the electrodes can be produced at densities approaching their theoretical values. Such electrodes could not be fabricated with the lower silicides using cold-pressing followed by sintering in vacuum. In future work with silicides hot-pressing is recommended since dense electrodes are a necessity. Moreover, sintering of the silicide in a closed system or in an inert gas at atmospheric pressure would reduce the problems of control of composition since silicon losses would be substantially reduced. Alternatively, future work could be directed toward the use of tamped powder electrodes in sealed electrode compartments wherein conditions approaching equilibrium could be established. Another alternative is the use of separate electrode compartments where conditions approaching the equilibrium oxygen partial pressure are produced artificially in a flowing inert gas.

EMF measurements in this work were conducted over the range from 700°C to 1100°C. At temperatures above about 950°C the kinetics of the desired electrode reactions for tantalum, tantalum pentoxide and silicide electrodes were just beginning to reach the point where the electrode-gas interaction was becoming

a small fraction of the net cell reaction. Operation at higher temperatures with dense electrodes should substantially eliminate this difficulty. The need for higher operating temperatures is particularly strong where silica is the oxidation product since the kinetic processes in these electrodes are extremely sluggish. A general indicator of electrode kinetics can be found from consideration of the diffusivity of the ionic species in the oxides involved in the electrode reaction. For example at 1000°C the diffusivity of nickel ions in nickelous oxide is about $4.4 \times 10^{-3} cm^2/sec$; the diffusivity of ferrous ions in ferrous oxide at about 1000°C is 1.18×10^{-1} cm^2/sec; at 1000°C the diffusivity of oxygen in cuprous oxide is about 6.5×10^{-3} and the diffusivity of cuprous ions is about $4.4 \times 10^{-2} cm^2/sec$(75). These values for ionic diffusivity are fairly close to the estimated ionic diffusivity, of oxygen ions in thoria-yttria electrolytes ($\sim$1 cm^2/sec at 1000°C). Hence one would not expect diffusion control in the electrodes to be significant under open circuit conditions, and no difficulties with electrode kinetics were encountered with these electrodes. On the other hand the diffusivity of oxygen in silica is reported to be about $10^{-14} cm^2/sec$ at 1000°C(76). This is many orders of magnitude smaller than the diffusivity of oxygen in the electrolyte and corresponds to a resistivity approaching that of an open circuit. Clearly then, at 1000°C, kinetic processes in the silica film are significant.

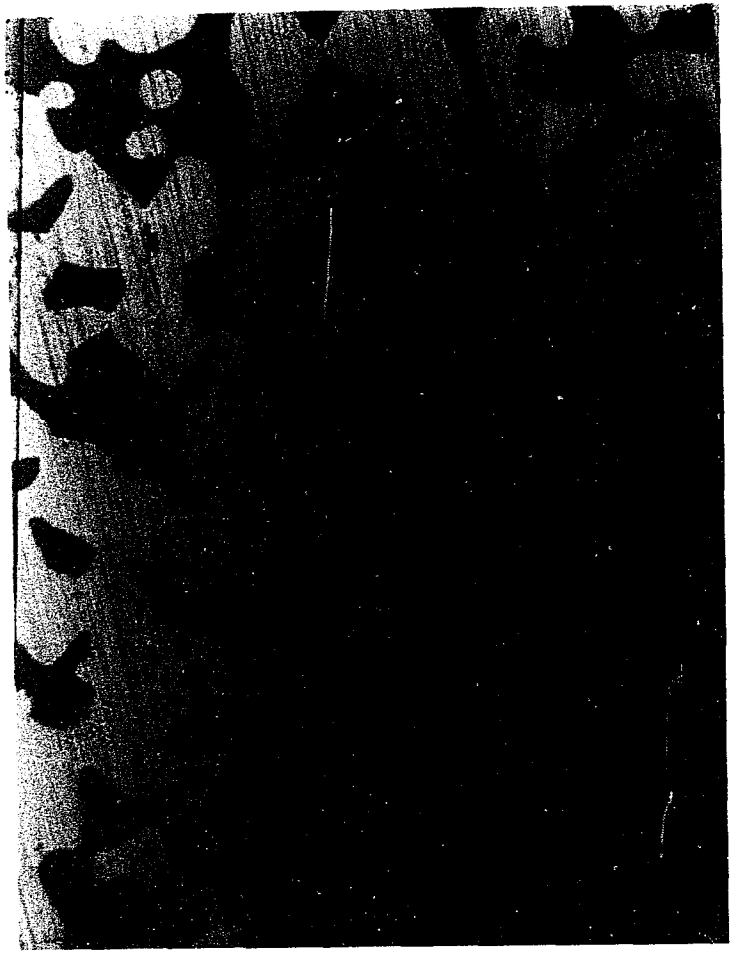

Plate I. Iron, wustite reference electrode (200X).

Plate II. Porous tantalum, tantalum pentoxide reference electrode (200X).

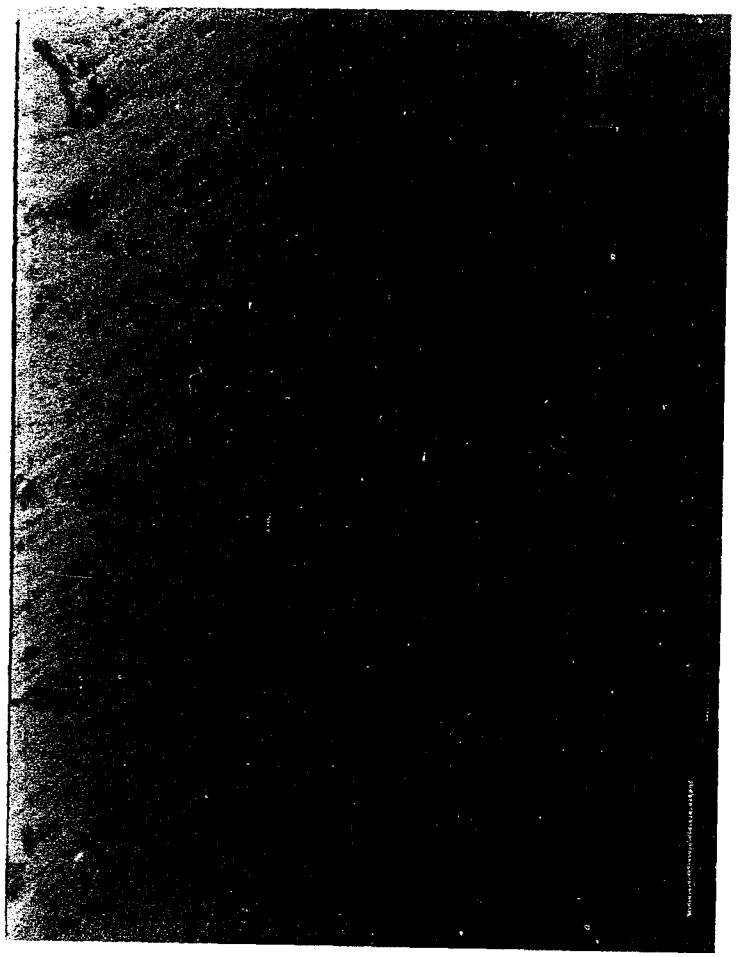

Plate III. Dense tantalum, tantalum pentoxide reference electrode (200X).

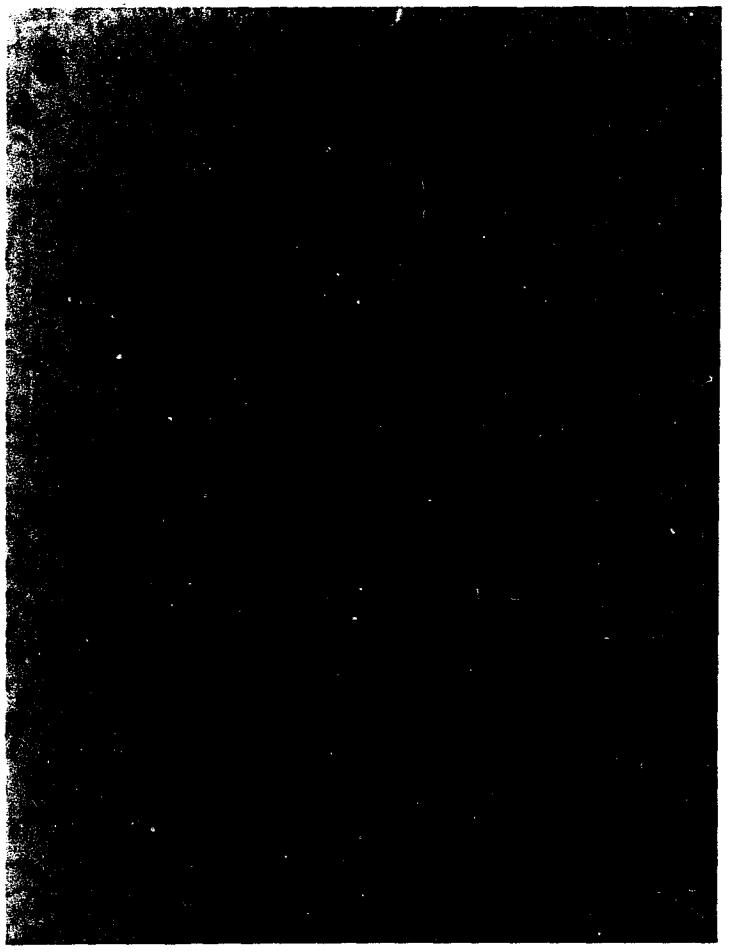

Plate IV. A Zircoa thoria-7.5 mol % yttria electrolyte. Polished and etched in concentrated sulfuric acid at 175°C for 45 min. (500X).

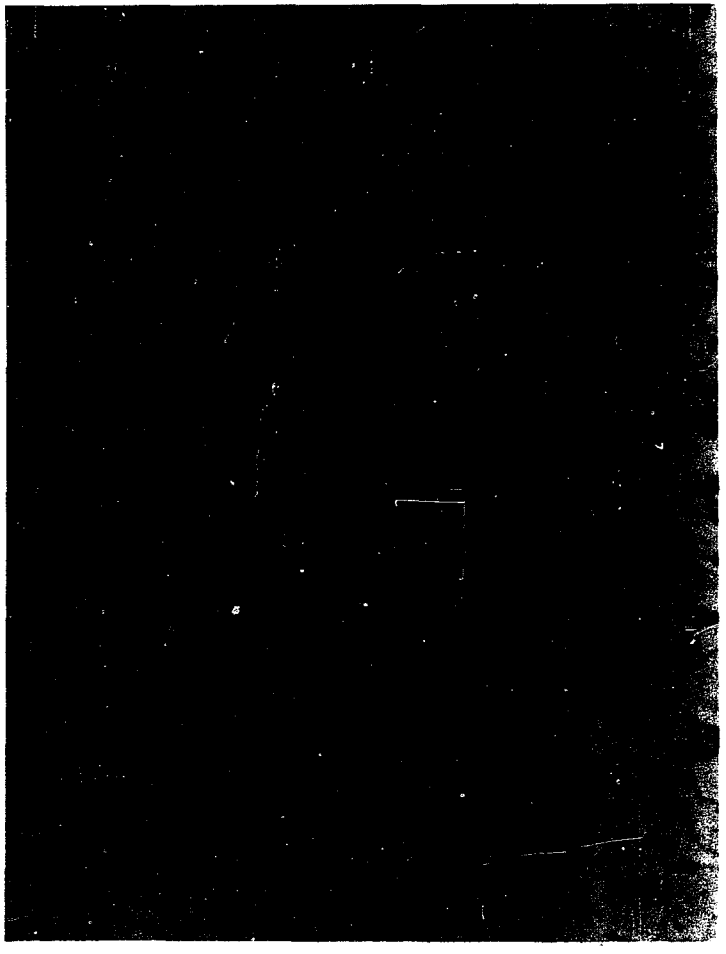

Plate V. A thoria-7 mol % yttria electrolyte sintered at 2000°C for 3 hours. Polished and etched in concentrated sulfuric acid at 175°C for 45 min. (500X).

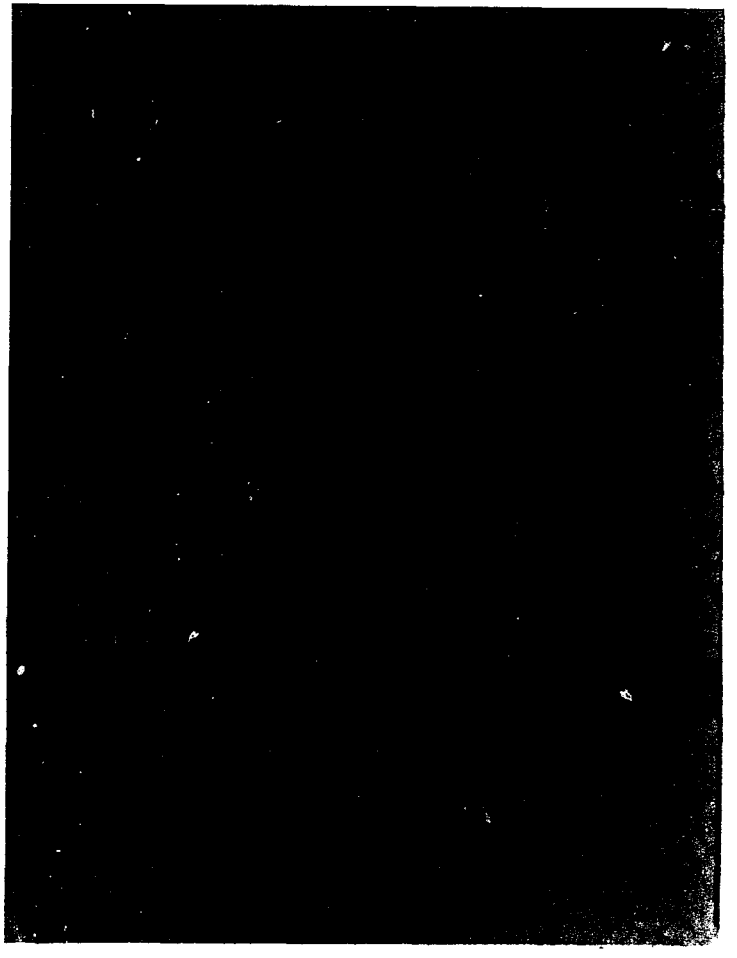

Plate VI. A thoria-7 mol % yttria (0.2 wt % SiO_2) electrolyte sintered at 2000°C for 3 hours. Polished and etched in concentrated sulfuric acid at 175° for 45 min. (600X).

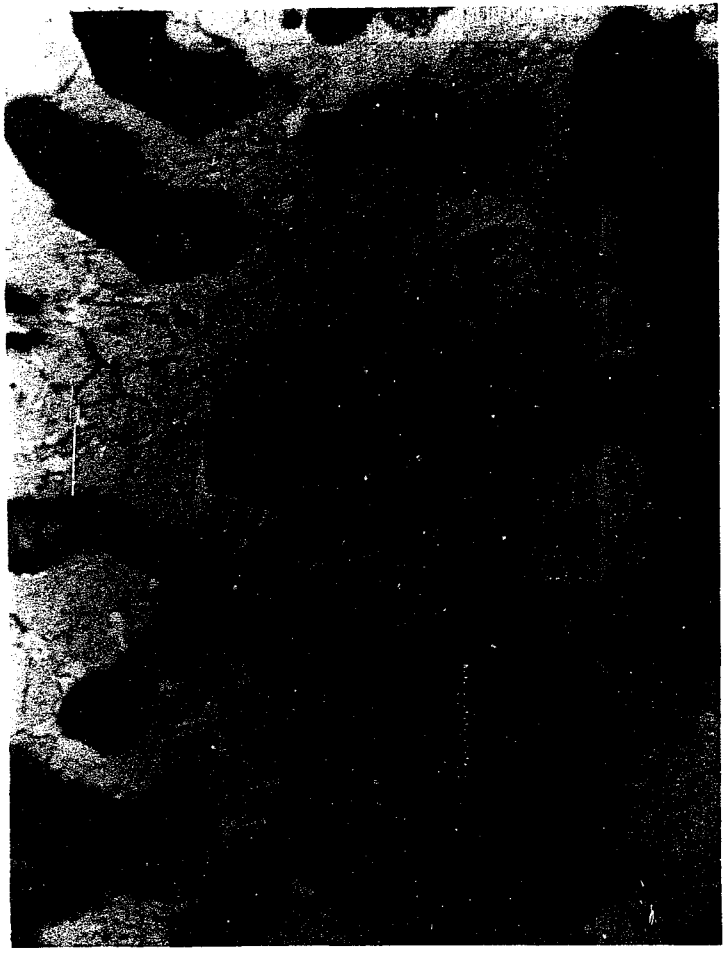

Plate VII. A $TaSi_2$-23 wt % Ta_5Si_3-5 wt % SiO_2-0.7 wt % Ni electrode after use in an electrochemical cell. The center of the surface in contact with the electrolyte is shown (500X).

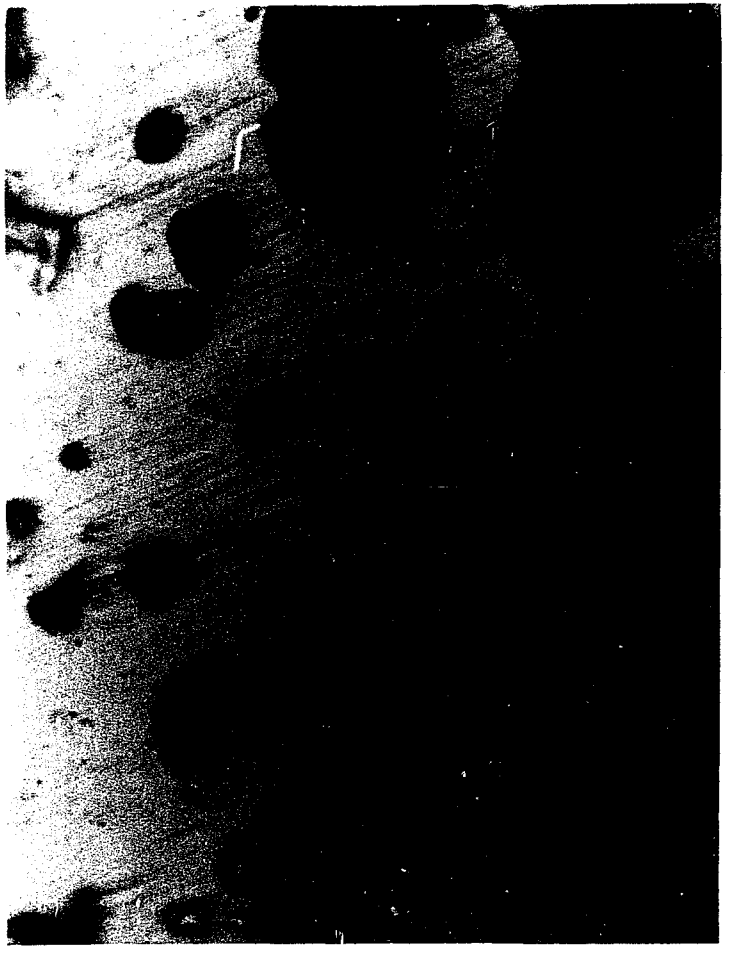

Plate VIII. A $TaSi_2$-23 wt % Ta_5Si_3-5 wt % SiO_2-0.7 wt % Ni electrode before use in an electrochemical cell (500X).

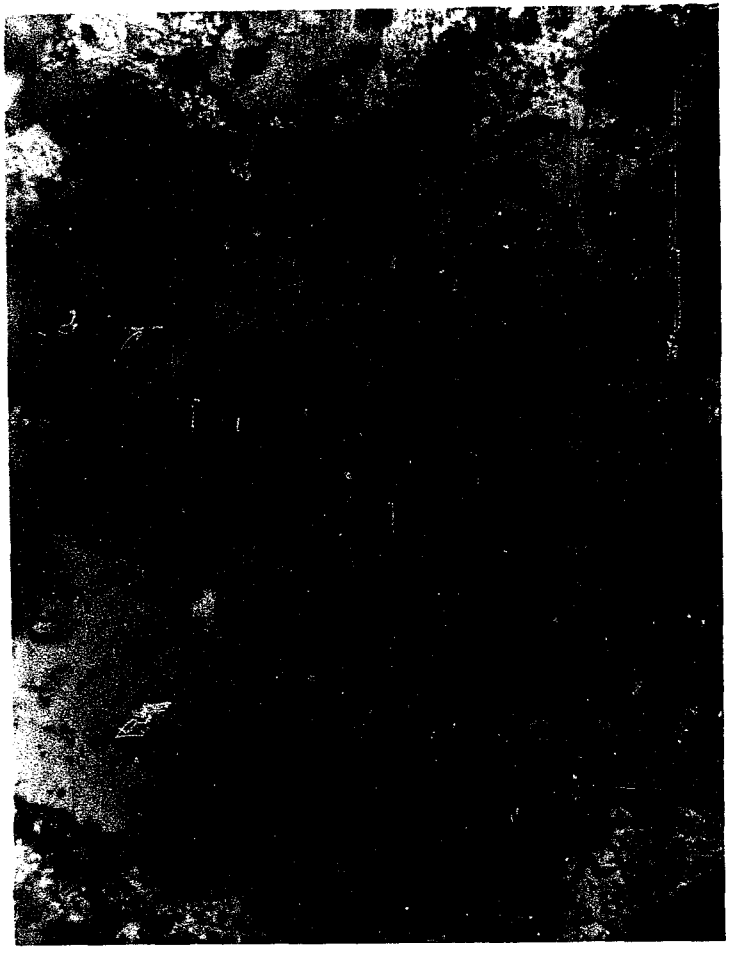

Plate IX. A $TaSi_2$-23 wt % Ta_5Si_3-5 wt % SiO_2-0.7 wt % Ni electrode after use in an electrochemical cell. The periphery of the surface in contact with the electrolyte is shown (500X).

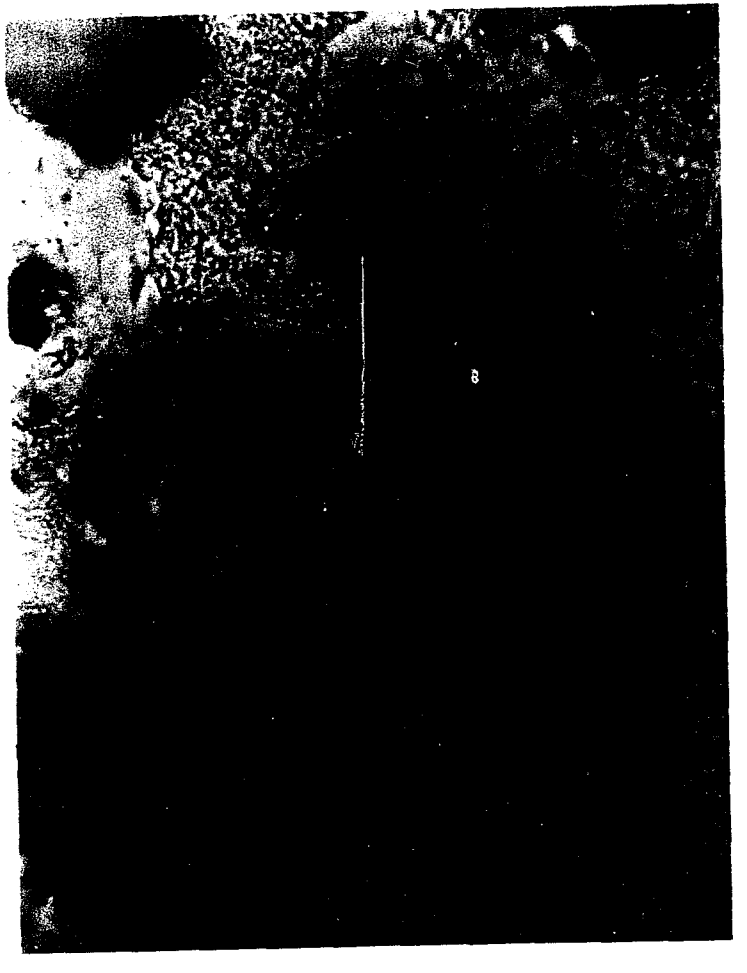

Plate X. The same electrode as in IX. The center of the surface in contact with the electrolyte is shown (500X).

Plate XI. A $TaSi_2$-23 wt % Ta_5Si_3-2.3 wt % SiO_2-0.7 wt % Ni electrode after use in an electrochemical cell. The center of the surface in contact with the electrolyte is shown (500X).

Plate XII. A $TaSi_2$-23 wt % Ta_5Si_3 2.3 wt % SiO_2-0.7 wt % Ni electrode before use in an electrochemical cell (500X).

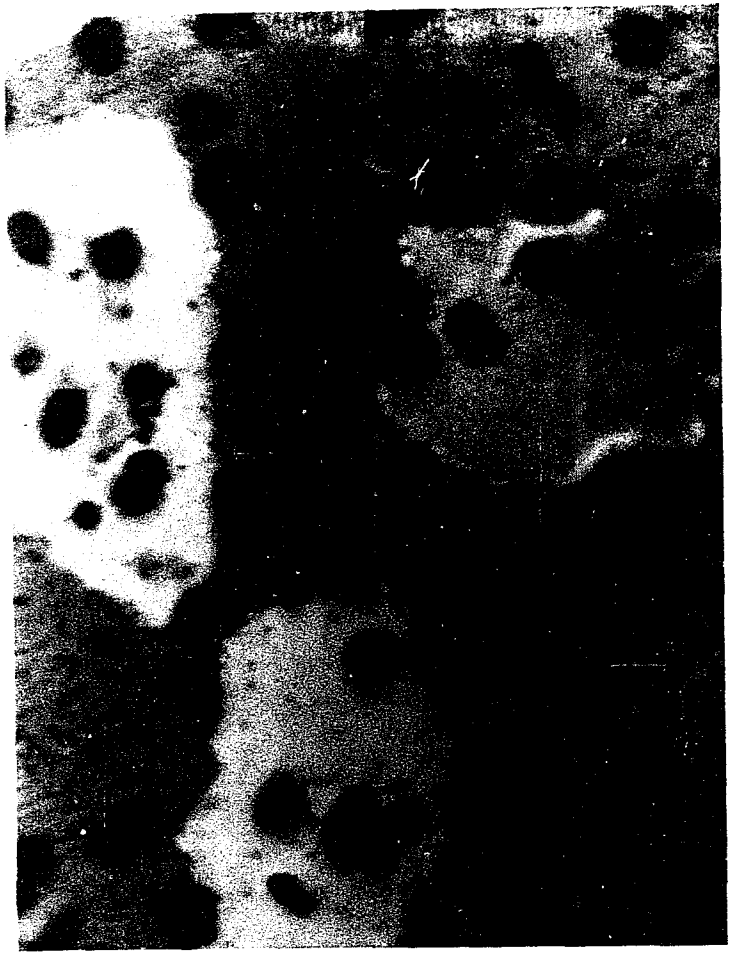

Plate XIII. A $TaSi_2$-24 wt % Ta_5Si_3-0.5 wt % Ni electrode after use in an electrochemical cell. The periphery of the surface in contact with the electrolyte is shown (500X).

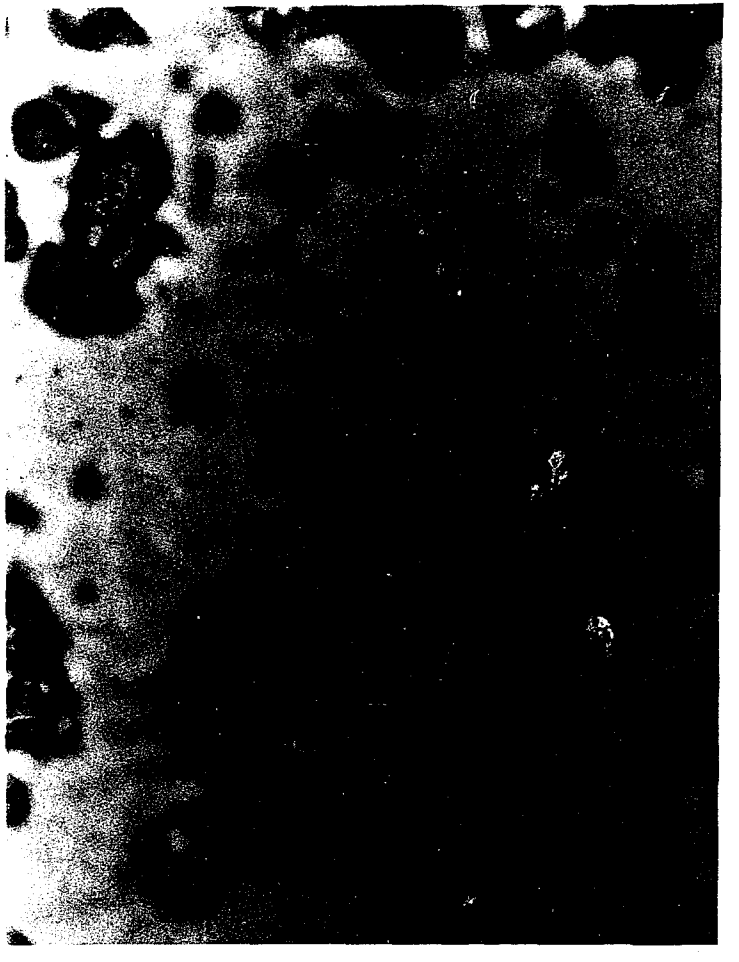

Plate XIV. A $TaSi_2$-24 wt % Ta_5Si_3-0.5 wt % Ni electrode before use in an electrochemical cell (500X).

Plate XV. The same electrode as in XIII. The center of the surface in contact with the electrolyte is shown (500X).

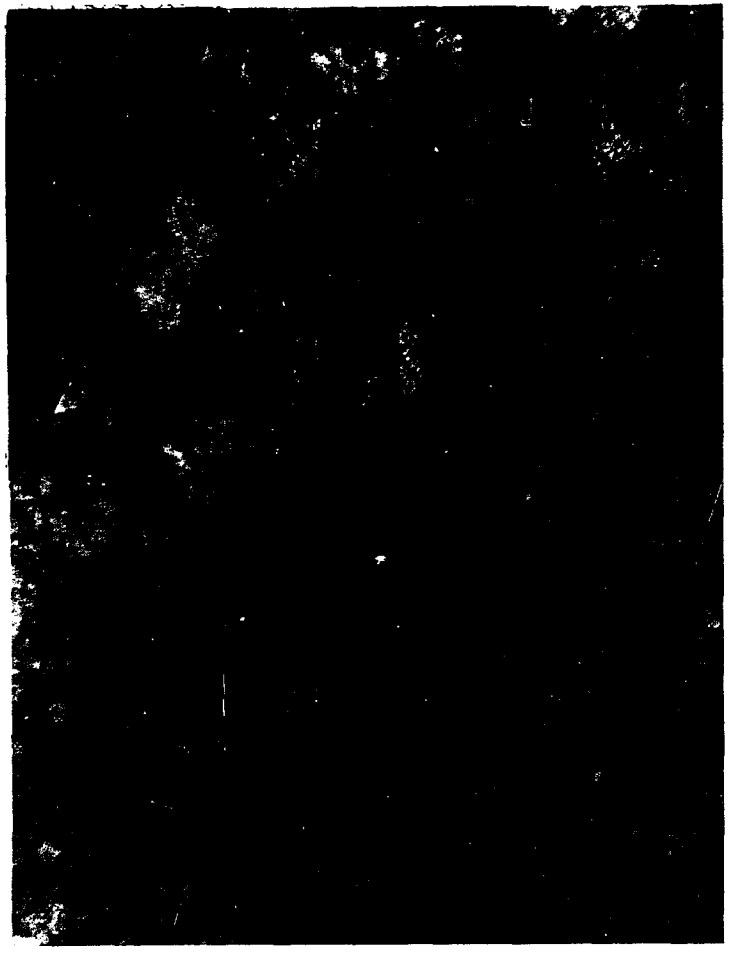

Plate XVI. A Ta_2Si-55.3 wt % $Ta_{4.5}Si$-1.7 wt % Ta_2O_5-0.8 wt % Ni electrode after use in an electrochemical cell. The center of the surface in contact with the electrolyte is shown (200X).

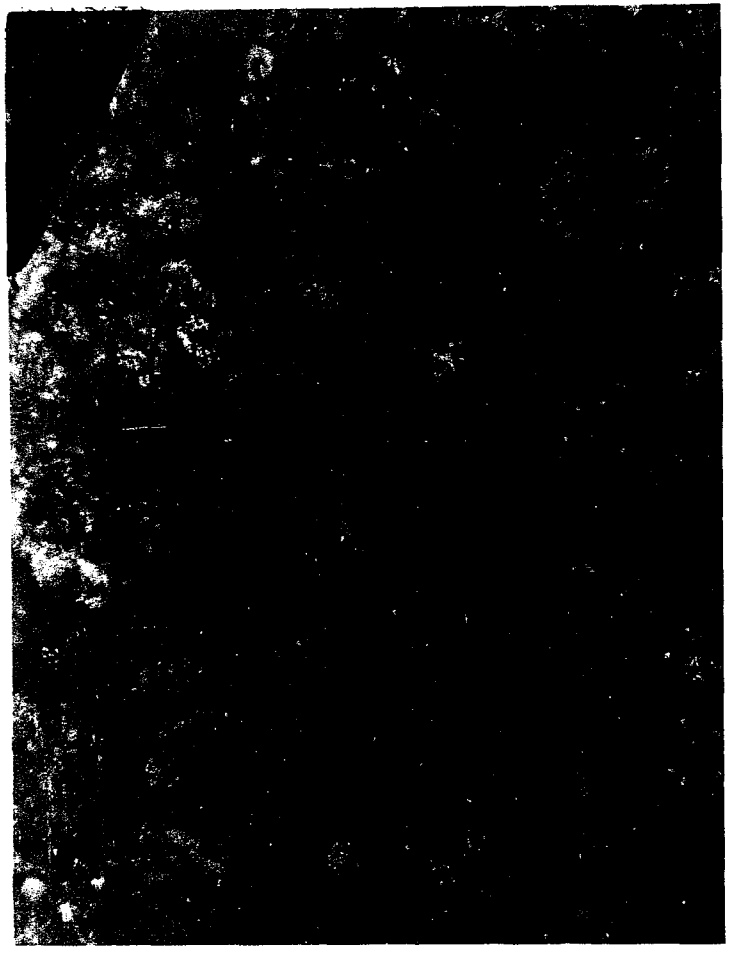

Plate XVII. A Ta_5Si_3-83.5 wt % Ta_2Si-0.1 wt % Ni electrode after use in an electrochemical cell. The center of the surface in contact with the electrolyte is shown (200X)

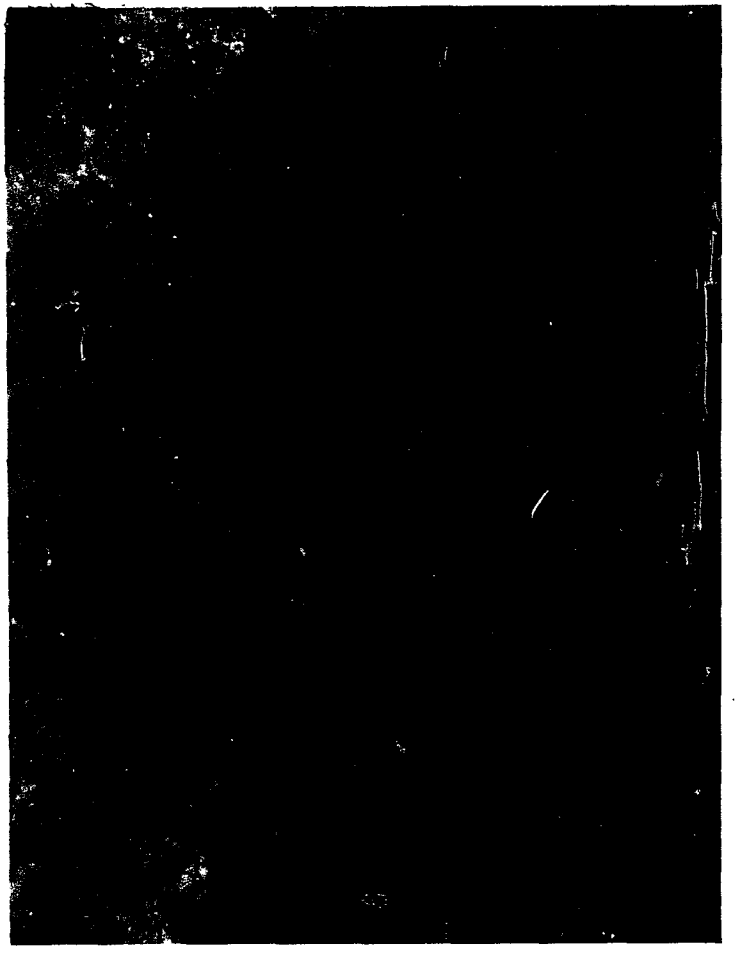

Plate XVIII. The same electrode as in XVII. The periphery of the surface in contact with the electrolyte is shown (200X).

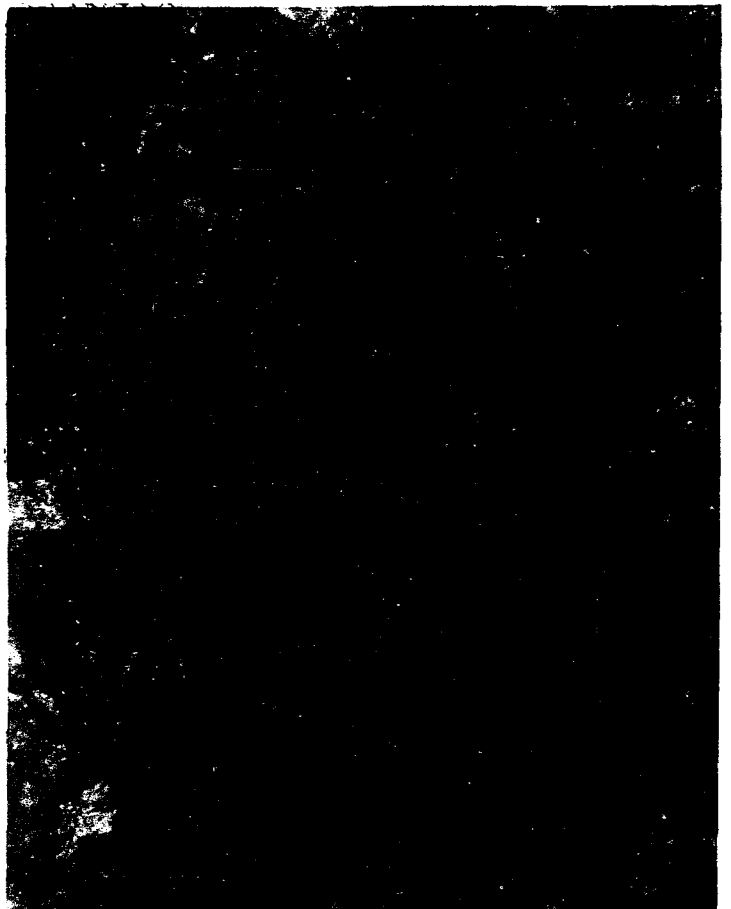

Plate XIX. A Ta_5Si_3-37 wt % Ta_2Si-2.5 wt % Ta_2O_5-1 wt % Ni electrode after use in an electrochemical cell. The center of the surface in contact with the electrolyte is shown (200X).

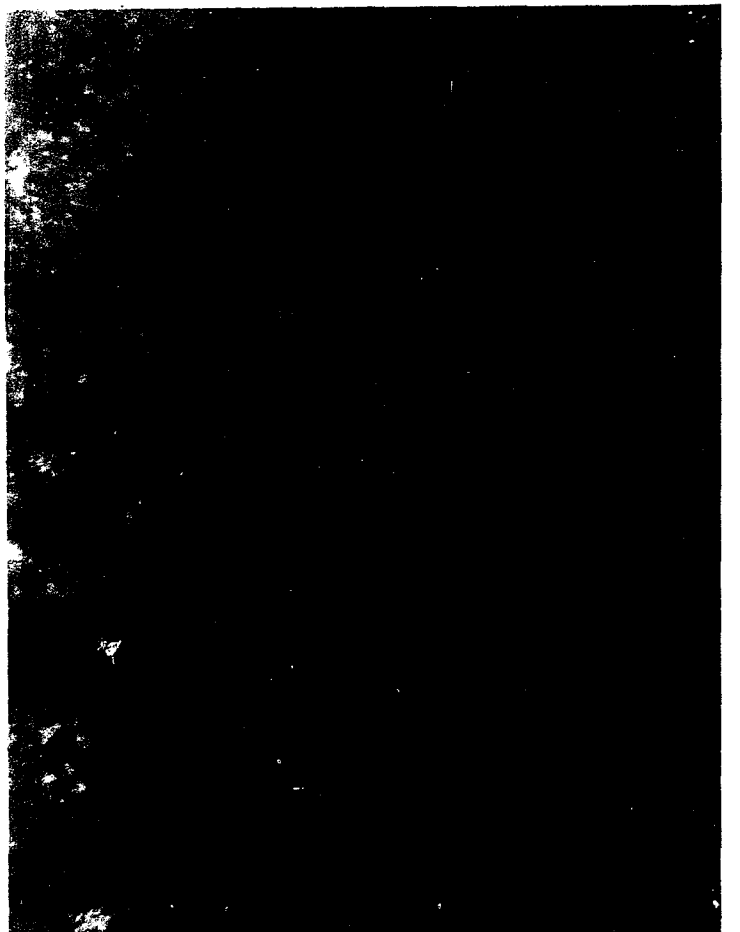

Plate XX. The same electrode as in XIX. The periphery of the surface in contact with the electrolyte is shown (200X).

Appendix II

Nomenclature

A, cross sectional area of the electrolyte, cm^2.

a_i, activity of the i^{th} component.

c_i, concentration of the i^{th} component, particles/cm^3.

c_p, heat capacity, cal/g-mol-^oK.

d, interplanar spacing, $\mathring{A}$.

D_i, diffusivity of the i^{th} species, cm^2/sec.

e, electronic charge, coulombs

E(T), thermodynamic electromotive force at null current and temperature T, volts.

$E_m(T)$, observed electromotive force at temperature T, volts.

F, the value of the Faraday (23060 cal/volt-gram-equivalent).

f, degrees of freedom of a system.

G_T^o, standard free energy at temperature T, cal/mole.

$\Delta G_i^o(T)$, standard free energy of formation of the i^{th} component at temperature T, cal/mole.

$\Delta G_R(T)$, free energy of reaction at temperature T, cal.

H_T^o, standard enthalpy at temperature T, cal/mole.

$\Delta H_i^o(T)$, standard enthalpy of formation of the i^{th} component at temperature T, cal/mole.

I, x-ray intensity.

I_∞, current at infinite time, amps.

i_p, polarization current, amps.

k, Boltzmann constant, erg/^oK. Also, a constant.

K, equilibrium constant.

L, thickness of the electrolyte, cm.

Nomenclature (cont.)

m, mole number.

n, number of equivalents transferred in an electrochemical cell. Also, a mole number.

N, number of components in a system.

P, pressure atm. Also, the number of phases in a system.

p_{eff}, effective oxygen partial pressure, atm.

p_i, partial pressure of the i^{th} component, atm.

p_θ, oxygen partial pressure at which $\sigma_\theta = \sigma_{O^=}$, atm.

q_i, charge on the i^{th} species, coulombs/particle.

R, 1.987 cal/gm-mole-^oK.

R, number of independent chemical reactions occurring in a system.

R_e, resistance of the electrolyte in the electronic mode, ohms.

R_i, resistance of the electrolyte in the ionic mode, ohms.

S^o_T, standard entropy at temperature T, eu/gram-mole.

$\Delta S^o_i(T)$, standard entropy of formation of the i^{th} component at temperature T, eu/gram-mole.

T, absolute temperature, ^oK.

t_e, electronic transport number.

t_i, local transport number for the i^{th} species. Also, ionic transport number.

$\bar{t}_i$, average transport number for the i^{th} species. Also, ionic transport number.

v, argon flow rate, SCFH.

x, mole number.

z, mole number.

Nomenclature (cont.)

η, electrochemical potential, cal/mole.

μ_i, mobility of the i^{th} species, cm^2/volt-second.

μ_{O_2}, oxygen chemical potential, cal/gram-mole.

ρ, density, gm/cm^3. Also, per cent of theoretical density.

ρ_i, resistivity due to the i^{th} species, ohm-cm.

σ_i, conductivity due to the i^{th} species, $mho\text{-}cm^{-1}$.

ϕ, electrical potential, cal/mole.

Bibliography

1. R. Speiser and G.R. St. Pierre: in "The Science and Technology of Tungsten, Tantalum, Molybdenum, Niobium and Their Alloys", N.E. Promisel, Editor; The MacMillan Company, New York, 1964.

2. G.L. Miller: "Tantalum and Columbium", Academic Press, New York, 1959.

3. J. Huminik: "High Temperature Inorganic Coatings", Reinhold Publishing Corp., New York, 1963.

4. A.W. Searcy: "Predicting the Thermodynamic Stabilities and Oxidation Resistances of Silicide Cermets", J. Am. Ceram. Soc., 40, 431 (1957).

5. R.W. Bartlett et al: "Investigation of Mechanisms for Oxidation Protection and Failure of Intermetallic Coatings for Refractory Metals", Aeroneutronic ASD-TDR 63-753, Part I, (1963); Part II, (1964), Part III, (1965).

6. C.E. Wicks and F.E. Block: "Thermodynamic Properties of 65 Elements - Their Oxides, Halides, Carbides, and Nitrides", U.S. Bur. Mines Bull. 605 (1963).

7. O. Kubaschewski and E. Evans: "Metallurgical Thermochemistry", London, 1958.

8. E.G. King and A.U. Christensen: "Low-Temperature Heat Capacity, Entropy at 298°K, and High-Temperature Heat Content of Mo_3Si", J. Phys. Chem., 62, 499 (1958).

9. L. Brewer and O. Krikorian: "Reactions of Refractory Silicides with Carbon and Nitrogen", J. Electrochem. Soc., 103, 38-51, 701-3 (1956).

10. D.A. Robins and I. Jenkins: "Heats of Formation of Some Transition Metal Silicides", Acta Met., 3, 598-604 (1955).

11. C.E. Myers and A.W. Searcy: "Dissociation Pressures of the Tantalum Silicides", J. Am. Chem. Soc., 79, 526-28 (1957).

12. A.W. Searcy and R.A. McNees: "The Silicides of Rhenium", J. Am. Chem. Soc., 75, 1578-80 (1953).

13. A.W. Searcy and A.G. Thorp: "Dissociation Pressures and the Heats of Formation of Molybdenum Silicides", J. Phys. Chem., 64, 1539-42 (1960).

14. A.W. Searcy and L.N. Finnie: "Stability of Solid Phases in the Ternary Systems of Silicon and Carbon with Rhenium and the Six Platinum Metals", J. Am. Ceram. Soc., 45, 268 (1962).

15. S.G. Davis, D.F. Anthrop, and A.W. Searcy: "Vapor Pressures of Silicon and Dissociation Pressure of Silicon Carbide", J. Chem. Phys., 34, 659-64 (1961).

16. G.V. Samsonov: "High-Temperature Materials, No. 2 - Properties Index", Plenum Press, New York, 1964.

17. O. Honigschmid: Monatsh. Chem., 28, 1017 (1907).

18. L. Brewer, A.W. Searcy, D.H. Templeton, and C.H. Dauben: "High-Melting Silicides", J. Amer. Ceramic Soc., 33, 291 (1950).

19. H. Nowotny, H. Schachner, R. Kiefer, and F.Benesovsky: Monatsh. Chem., 84, 1-12 (1953).

20. R. Kiefer, F. Benesovsky, H. Nowotny, and H. Schachner: Z. Metallkunde, 44, 242-6 (1953).

21. G.A. Geach and F.O. Jones: Plansee Proc., 80-91(1955).

22. K. Schubert, A. Raman, and W. Rossteutscher: Naturwissenschaften, 51, 506 (1964).

23. H.J. Goldschmidt, E.H. Catherall, and R.A. Taylor: "Investigation into the W-rich Region of the W-Si System and into Related Me-Si Systems", AFML-TR-65-270 (1965).

24. A.S. Berezhnoi: "Silicon and its Binary Systems", Consultants Bureau, New York, 1960.

25. S.I. Alyainovskii, P.V. Geld, and I.I. Matneenko: "Phase Components of the System Nb-Si", Tr. Uval'sk. Politekhn. Inst. Sb., 114, 149 (1961).

26. H.J. Wallbaum: Z. Metallkunde, 33, 378-81 (1941).

27. A.G. Knapton: Nature, 175, 730 (1955).

28. E. Parthé, H. Nowotny, and H. Schmid: Monatsh. Chem., 86, 385-96 (1955).

29. E. Parthé, B. Lux, and H. Nowotny: Monatsh. Chem., 86, 859-67 (1955).

30. B. Aronsson, T. Lundström, and S. Rundqvist: "Borides, Silicides and Phosphides - A Critical Review of their Preparation, Properties and Crystal Structure", John Wiley and Sons, New York, 1965.

31. G.V. Samsonov: "Silicides and Their Uses in Engineering", 1959. Translation AFSC FTD-TT-61-409, 1962.

32. K. Kiukkola and C. Wagner: "Galvanic Cells for the Determination of The Standard Molar Free Energy of Formation of Metal Halides, Oxides, and Sulfides at Elevated Temperatures", AEC·NYO·7008 (1956); and "Measurements on Galvanic Cells Involving Solid Electrolytes", AEC·NYO·7009 (1956).

33. H. Schmalzried: "On Zirconia as an Electrolyte for Electrochemical Measurements at High-Temperature", Zeitschrift für Electrochemie, 66, 572-6 (1962).

34. P. Kofstad: in "The Science and Technology of Tungsten, Tantalum, Molybdenum, Niobium and Their Alloys", N.E. Promisel, Editor; The MacMillan Co., New York, 1964.

35. P. Kofstad: J. Less-Common Metals, 5, 158 (1963).

36. ASTM Powder Diffraction File.

37. P. Kofstad: "On the Defect Structure of Ta_2O_5", J. Electrochem. Soc., 109, 776-81 (1962).

38. N.A. Toropov and V.P. Borzakovskii: "High-Temperature Chemistry of Silicates and Other Oxide Systems", Consultants Bureau, New York, 1966.

39. R.B. Sosman: "The Phases of Silica", Rutgers University Press, New Brunswick, New Jersey, 1965.

40. H. Reynolds: dissertation, University of Göttingen (1902).

41. W.D. Treadwell et al: Z. Elektrochem., 22, 415 (1916).

42. K. Hauffe, et al.: Z. Elektrochem., 46, 348 (1940).

43. C. Wagner: Naturwissenschaften, 31, 265 (1943).

44. H. Peters and G. Mann: Z. Elektrochem., 63, 244-48 (1959).

45. J. Dixon, L. LaGrange, U. Merten, C. Miller, and J. Porter: "Electrical Resistivity of Stabilized Zirconia at Elevated Temperatures", J. Electrochem. Soc., 110, 276-80 (1963).

46. D.W. Strickler and W.G. Carlson: "Electrical Conductivity in the ZrO_2-rich Region of Several M_2O_3-ZrO_2 Systems", J. Amer. Ceram. Soc., 48, 286 (1965).

47. H.A. Johansen and J.G. Cleary: "High-Temperature Electrical Conductivity in the Systems CaO-ZrO_2 and CaO-HfO_2", J. Electrochem. Soc., 111, 100-102 (1964).

48. B.C.H. Steele and C.B. Alcock: "Factors Influencing the Performance of Solid Oxide Electrolytes in High-Temperature Thermodynamic Measurements", Trans. Met. Soc. AIME, 233, 1359-67 (1965).

49. D. Singman: "Preliminary Evaluation of Ceria-Lanthana as a Solid Electrolyte for Fuel Cells", J. Electrochem. Soc., 113, 502-4 (1966).

50. R.A. Rapp: "Mixed Conduction in Solid Electrolytes", in "Thermodynamics of Nuclear Materials, 1967", IAEA, Vienna, 1968.

51. A.M. Diness and R. Roy: "Experimental Confirmation of Major Changes of Defect Type with Temperature and Composition in Ionic Solids", Solid State Comm., 3, 123 (1965).

52. E.C. Subbarao, P.H. Sutter, and J. Hrizo: "Defect Structure and Electrical Conductivity of ThO_2-Y_2O_3 Solid Solutions", J. Amer. Ceram. Soc., 48, 443 (1965).

53. F. Trombe and M. Foëx: "Study of Electrical Conduction in the System Zirconia-Calcia at High-Temperature", Comptes Rendus, 236, 1783 (1953).

54. W.D. Kingery, J. Pappis, M.E. Doty, and D.C. Hill: "Oxygen Ion Mobility in Cubic $Zr_{0.85}Ca_{0.15}O_{1.85}$", Jour. Amer. Ceram. Soc., 42, 393-8 (1959).

55. L. Simpson and R. Carter: J. Am. Ceram. Soc., 49, 199, (1966).

56. W.H. Rhodes and R.E. Carter: Bull. Am. Ceram. Soc., 41, 283 (1962).

57. W.E. Danforth and J.H. Bodine: "Polarization in Thorium Oxide Crystals". J. Franklin Inst., 260, 467 (1955).

58. R.W. Vest and N.M. Tallen: "High-Temperature Transference Number Determination by Polarization Measurements", J. Appl. Physics, 36, 2543 (1965).

59. M.H. Hebb: "Electrical Conductivity of Silver Sulfide", J. Chem. Phys., 20, 185 (1952).

60. C. Wagner: "Galvanic Cells with Solid Electrolytes Involving Ionic and Electronic Conduction", Proc. CITCE (1956).

61. J.W. Patterson, E.C. Bogren, and R.A. Rapp: "Mixed Conduction in $Zr_{0.85}Ca_{0.15}O_{1.85}$ and $Th_{0.85}Y_{0.15}O_{1.925}$ Solid Electrolytes", J. Electrochem. Soc., 114, 752-58 (1967).

62. C. Wagner: Z. physik. Chem. Abt. 1321, 25 (1930).

63. R.A. Swalin: "Thermodynamics of Solids", p. 84, John Wiley and Son, New York, 1964.

64: R.A. Rapp: "Free Energy of Formation of Molybdenum Dioxide", Trans. Met. Soc. AIME, 227, 371-74 (1963).

65. R.A. Rapp and F. Maak: "Thermodynamic Properties of Solid Copper-Nickel Alloys", Acta Met., 10, 63-69 (1962).

66. J. Weissbart and R. Ruka: "Oxygen Gauge", Review of Scientific Instr., 32, 593 (1961).

67. Y. Matsushita and K. Goto: "The Application of Oxygen Concentration Cells with the Solid Electrolyte ZrO_2-CaO to Thermodynamic Research", Thermodynamics, Vol. I, IAEA, Vienna, 1966.

68. W.L. Worrell: "Measurements of the Thermodynamic Stabilities of the Niobium and Tantalum Oxides Using a High-Temperature Galvanic Cell", Thermodynamics, Vol. I, IAEA, Vienna, 1966.

69. G.R. Fitterer: "Furtner Development of the Electrolytic Method for the Rapid Determination of Oxygen in Liquid Steels", J. Metals, page 92-6, September 1967.

70. K. Schwerdtfeger: "Measurement of Oxygen Activity in Iron, Iron-Silicon, Manganese, and Iron-Manganese Melts Using Solid Electrolyte Galvanic Cells", Trans. Met. Soc. AIME, 239, 1276-81 (1967).

71. T.C. Wilder: "Direct Measurement of the Oxygen Content in Liquid Copper; the Activity of Oxygen in Dilute Liquid Cu-O Alloys", Trans. Met. Soc. AIME, 236, 1035-40 (1966).

72. T.L. Markin and M.H. Rand: "Thermodynamic Data for Plutonium Oxides", Thermodynamics, Vol. I, IAEA, Vienna, 1966.

73. R.W. Taylor and H. Schmalzried: "The Free Energy of Formation of Some Titanates, Silicates, and Magnesium Aluminate from Measurements Made With Galvanic Cells Involving Solid Electrolytes", J. Phys. Chem., 68, 2444 (1964).

74. G.G. Charette and S.N. Flengas: "Thermodynamic Properties of the Oxides of Fe, Ni, Pb, Cu, and Mn by EMF Measurements", J. Electrochem. Soc. 115, 796-804 (1968).

75. K. Hauffe: "Oxidation of Metals", Plenum Press, New York, (1965).

76. E. W. Sucov: J. Am. Ceram. Soc. 16, 14-20 (1963).

Autobiographical Notes

Stanley R. Levine received a Bachelor of Engineering (Chemical) from the City College of New York in 1964 and was commissioned as a Second Lieutenant in the Corps of Engineers, USAR. Since that time he has been a graduate student and part-time Lecturer at the City College of The City University of New York. The author has been supported by an NSF Cooperative Fellowship, a City College Research Assistantship and as a Research Assistant on a NASA Grant. He received a Master of Engineering (Chemical) in 1966 and wrote a Masters' Thesis entitled: "Rapid Quenching of Binary Liquid Metals". Upon completion of his doctoral work, the author will enter the U.S. Army to fulfill a two-year active duty obligation. He will be assigned to the NASA Lewis Research Center, Cleveland, Ohio, for the major portion of the two-year tour.